Millimetre-wave Phased Array Antennas for Mobile Terminals

Master's Thesis

Alberto Hernández Escobar

Aalborg University

Department of Electronic Systems

Fredrik Bajers Vej 7B

DK-9220 Aalborg

Contents

Chapter 1

Introduction

1.1 Motivations

Mobile communications have improved the economic and social development of many countries over the last few decades, being now an indispensable part of millions of people's life. Bitrate necessities are expected to go up even higher in the near future and it is the fifth generation of mobile communications the one in charge of satisfy them.

The fifth generation's specifications about bitrate and capacity are so demanding that the only way to achieve them is by raising the frequency of the radio signals employed up to the millimetre wave frequencies, [1], [2], which can bring several challenges.

The first problem that comes to mind is the propagation losses, which are higher if the frequency is higher. Let us have a look at Friis Transmission Equation, which will be thoroughly analysed in this work later, when the antennas are reflection and polarization-matched:

$$P_R = P_T G_T G_R \left(\frac{\lambda}{4\pi d}\right)^2 \tag{1.1}$$

where it is clear that if the frequency goes up, the wavelength will decrease and so will the received power. However, if we pay attention to the effective area, which can be expressed as

$$A^{eff} = G\frac{\lambda^2}{4\pi} \tag{1.2}$$

then, it is possible to show the power received based on the effective area of the transmission antenna as follows:

$$P_R = P_T G_R \frac{A_T^{eff}}{4\pi d^2} \tag{1.3}$$

and this shows us that if we keep the effective area of an antenna constant, the propagation losses will not depend on the frequency. Furthermore, if the same is done with the reception antenna, it is possible to get higher received power for higher frequencies, as shown in

$$P_R = P_T \frac{A_T^{eff} A_R^{eff}}{\lambda^2 d^2}. \tag{1.4}$$

In conclusion, it seems that if it is possible to keep the effective area of the antennas as they were in previous generations then, for line-of-sight, there will be less propagation losses than at lower frequencies.

Looking at (1.2), keeping constant the effective area while decreasing the wavelength will mean that the antenna gain is higher, and so it would mean that its directivity is also higher, which leads us to an antenna radiation pattern that is very different from an isotropic one, or the traditional close to an omnidirectional one for monopole like antennas used at the lower frequencies. The key to this are beamforming arrays which would have a big area and its directivity would be high, but it would have the ability of pointing its beam to the target antenna, so it would act like an isotropic one.

Of course, these arrays would bring more problems. The size of the antennas is not an issue in base stations; however, the physical space in a cell phone is very limited. Furthermore, several arrays of antennas will be needed, since one array will not be able to point to all possible directions, and they may be obstructed by the user's hands or body. As this high number of antennas may be needed, it would be a great improvement to use a MIMO antenna system. To control the beamforming array so it points to the other end it will be needed a system or mechanics (beam sweep) which must be able to select the direction where it should point at enough speed.

1.2 Objectives

This project is a study of the design of antennas with these limitations: future 5G frequencies of operation (expected to be 6-30 GHz range), capable of delivering medium sized antenna gain (6 dBi < G < 20 dBi) on a mobile terminal. The antennas need to cover all orientations by an electronic control.

1.3 Guidelines

The organisation of this Master's Thesis is as follows: Chapter 2 will give background about antenna theory and, later, it will analyse the antenna types used in this work. Chapter 3 will study the directivity provided by different types of antenna arrays in a mobile terminal and, after, it will study the improvements made by using hybrid arrays. The objective of Chapter 4 is evaluate the losses of the different antennas employed and using two different substrates, not only with the data provided by the different simulations but also the measurements of several prototypes. Finally, Chapter 5 will state the conclusions and future work of the project.

Chapter 2

Theoretical Background

This chapter provides a review of the knowledge needed to understand the behaviour and design of antennas used in high frequency applications like mobile communications. It starts stating the electromagnetic principles and the different properties of the antennas needed to analyse the different antennas employed later in this work, which are described in detail afterwards. These are the dipole antenna, the slot antenna, the monopole antenna, the IFA antenna and the patch antenna.

2.1 Electromagnetic Analysis

The aim of this section is to obtain a solution for the problem of a radiating antenna in open space. To do so, it is needed to calculate the electric and magnetic field ($\vec{E}$ and $\vec{H}$, respectively) in each point of the space and for each instant. The source that produces these fields is the antenna, which will have an electric current density in its volume, $\vec{J}$. The geometry of the problem is shown in figure 2.1, where r' is the distance from the origin of coordinates to a point of the source, r the distance from the origin of coordinates to the point where the fields are calculated and R the distance from a point of the source to the point where the fields are calculated. In the figure 2.1 it is shown also the Cartesian (x, y, x) and (x', y', z') coordinates of these points and the spherical ones $(r, \theta,)$ and (r', θ', ϕ').

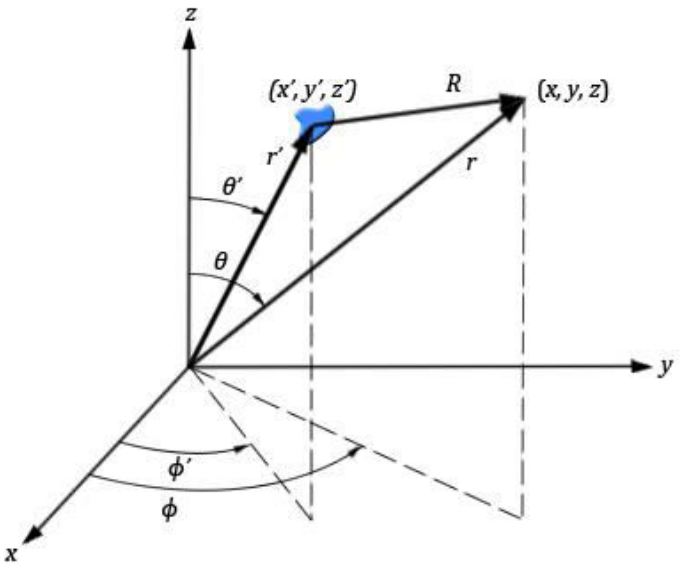

Figure 2.1: Geometry of the radiating problem.

2.1.1 Maxwell's equations

To calculate the electric and magnetic field, the basic tools employed are the Maxwell's equations, which explain the generation of the fields by the charges and currents and how they are altered by each other. They are, in their differential form:

$$\nabla \cdot \vec{D}(x,y,z;t) = \rho(x,y,z;t) \tag{2.1}$$

$$\nabla \cdot \vec{B}(x,y,z;t) = 0 \tag{2.2}$$

$$\nabla \times \vec{E}(x,y,z;t) = -\frac{\partial \vec{B}(x,y,z;t)}{\partial t} \tag{2.3}$$

$$\nabla \times \vec{H}(x,y,z;t) = \vec{J}(x,y,z;t) + \frac{\partial \vec{D}(x,y,z;t)}{\partial t} \tag{2.4}$$

where ρ is the electric charge, $\vec{D}$ is the electric flux density and $\vec{B}$ the magnetic induction. Since outside the source the medium is homogeneous we can use the medium equations to change these vectors into the electric and magnetic field vectors: $\vec{B}(x,y,z;t) = \mu_0 \vec{H}(x,y,z;t)$ and $\vec{D}(x,y,z;t) = \epsilon_0 \vec{E}(x,y,z;t)$, where ϵ_0 is the electric permittivity in free space and μ_0 the magnetic permeability in free space.

To simplify the calculation, only the periodic steady-state solution is going to be considered so it is possible to use the phasors, separating the dependence with the time, as follows:

$$\vec{E}(x,y,z;t) = \Re e\left\{\overrightarrow{E^0}(x,y,z)e^{j\omega t}\right\} \tag{2.5}$$

and the same way for the vectors $\vec{H}$ and $\vec{J}$, so in the equations 2.3 and 2.4 it is possible now to calculate the variation with the time, resulting:

$$\nabla \times \overrightarrow{E^0}(x,y,z) = -j\omega\mu_0 \overrightarrow{H^0}(x,y,z) \tag{2.6}$$

$$\nabla \times \overrightarrow{H^0}(x,y,z) = \overrightarrow{J^0}(x,y,z) + j\omega\epsilon_0 \overrightarrow{E^0}(x,y,z). \tag{2.7}$$

2.1.2 The Vector Potential $\vec{A}$

To solve the problem stated with the Maxwell's equations 2.1, 2.2, 2.6 and 2.7 the vector potential $\vec{A}$ is going to be used. This will make the solution easier, but it will consist of two steps: calculate the vector potential $\vec{A}$ and, with it, calculate the electric and magnetic fields.

Since the divergence of the curl of any vector is always zero, we can write the equation 2.2 using an arbitrary vector $\vec{A}$:

$$\nabla \cdot \left(\nabla \times \vec{A}(x,y,z)\right) = 0 \tag{2.8}$$

and then, we can define

$$\overrightarrow{B^0}(x,y,z) = \mu_0 \overrightarrow{H^0}(x,y,z) = \nabla \times \vec{A}(x,y,z) \tag{2.9}$$

substituting into equation 2.6,

$$\nabla \times \overrightarrow{E^0}(x,y,z) = -j\omega\mu_0 \overrightarrow{H^0}(x,y,z) = -j\omega\nabla \times \vec{A}(x,y,z). \tag{2.10}$$

Equation 2.10 can also be written as

$$\nabla \times \left[\overrightarrow{E^0}(x,y,z) + j\omega\vec{A}(x,y,z)\right] = \vec{0}. \tag{2.11}$$

Given an arbitrary electric scalar potential $\phi_e(x,y,z)$ and since the curl of the gradient of any twice-differentiable scalar field is always the zero vector,

$$\nabla \times \left(\nabla\phi_e(x,y,z)\right) = \vec{0} \tag{2.12}$$

and, now it is possible to write using equations 2.11 and 2.12

$$\overrightarrow{E^0}(x,y,z) + j\omega\vec{A}(x,y,z) = \nabla\phi_e(x,y,z). \tag{2.13}$$

Taking the curl of both last two sides of equation 2.9 and using the vector identity

$$\nabla \times \nabla \times \vec{A} = \nabla\left(\nabla \cdot \vec{A}\right) - \nabla^2\vec{A}, \tag{2.14}$$

it results in

$$\mu_0\nabla \times \overrightarrow{H^0}(x,y,z) = \nabla\left(\nabla \cdot \vec{A}(x,y,z)\right) - \nabla^2\vec{A}(x,y,z) \tag{2.15}$$

which, combined with the Maxwell's equation 2.7, reduces it to

$$\mu_0\overrightarrow{J^0}(x,y,z) + j\omega\epsilon_0\mu_0\overrightarrow{E^0}(x,y,z) = \nabla\left(\nabla \cdot \vec{A}(x,y,z)\right) - \nabla^2\vec{A}(x,y,z). \tag{2.16}$$

Using equation 2.13 into 2.16 nullifies the electrical field, leading to

$$\nabla^2\vec{A}(x,y,z) + \mathrm{k}_0^2 = -\mu_0\overrightarrow{J^0}(x,y,z) + \nabla\left(\nabla \cdot \vec{A}(x,y,z) + j\omega\epsilon_0\mu_0\phi_e\right) \tag{2.17}$$

where $\mathrm{k}_0^2 = \omega^2\epsilon_0\mu_0$. It is possible to define now the divergence of $\vec{A}(x,y,z)$, which is independent of its curl, as

$$\nabla \cdot \vec{A}(x,y,z) = -j\omega\epsilon_0\mu_0\phi_e(x,y,z) \tag{2.18}$$

and then, substituting 2.18 into 2.17 reduces it to

$$\nabla^2\vec{A}(x,y,z) + \mathrm{k}_0^2 = -\mu_0\overrightarrow{J^0}(x,y,z) \tag{2.19}$$

from which, finally, it is possible to determine the vector potential $\vec{A}$ given the current density of the antenna. To do this, the differential equation must be solved first. In [3] it is shown that the solution is

$$\vec{A}(x,y,z) = \frac{\mu_0}{4\pi}\iiint_V \overrightarrow{J^0}(x',y',z')\frac{e^{-jk_0R}}{R}dv' \tag{2.20}$$

where the primed coordinates (x',y',z') represent the source, and R the distance from any point on the source to the observation point, as stated in figure 2.1. If the density current is only superficial, the integral reduces to surface integral, as

$$\vec{A}(x,y,z) = \frac{\mu_0}{4\pi}\iint_S \overrightarrow{J_S^0}(x',y',z')\frac{e^{-jk_0R}}{R}ds' \tag{2.21}$$

and if the current, $\vec{I}(x,y,z)$, is limited to a line, it reduces to a line integral,

$$\vec{A}(x,y,z) = \frac{\mu_0}{4\pi}\int_C \vec{I}(x',y',z')\frac{e^{-jk_0R}}{R}dl'. \tag{2.22}$$

Once the vector potential $\vec{A}$ is calculated, the electric and magnetic fields can be derived from it. To do so, the expression 2.9 can be shown as

$$\overrightarrow{H^0}(x,y,z) = \frac{1}{\mu_0}\nabla \times \vec{A}(x,y,z) \tag{2.23}$$

to calculate the magnetic field and, then, since there is no current outside the antenna, the Maxwell's equation 2.7 to calculate the electric field:

$$\overrightarrow{E^0}(x,y,z) = \frac{1}{j\omega\epsilon_0}\nabla \times \overrightarrow{H^0}(x,y,z). \tag{2.24}$$

2.1.3 Far-Field Region

The space surrounding the antenna can be subdivided in three regions: reactive near-field, radiating near-field (Fresnel region) and far-field region (Fraunhofer region). The far-field region is going to be focused in this work, so let us see the definition of far-field region from [3]: "that region of the field of an antenna where the angular field distribution is essentially independent of the distance from the antenna. If the antenna has a maximum overall dimension D, the far-field region is commonly taken to exist at distances greater than $2D^2/\lambda$ from the antenna, λ being the wavelength. To be valid, D must also be large compared to the wavelength ($D > \lambda$)".

This simplification is essential to this work because many simplifications can be done so it is possible to calculate analytically some fields that in the near-field regions would be very difficult or unachievable. At the same time, this approximation would not have precision repercussions since in mobile communications the transmission antenna and reception antenna are usually very far away from each other. To make this easier, from now on the electric and magnetic field will be expressed in spherical coordinates instead of in Cartesian ones: $\vec{A}(r,\theta,\phi), \overrightarrow{E^0}(r,\theta,\phi), \overrightarrow{H^0}(r,\theta,\phi)$. Note that the previous results are also valid for spherical coordinates. Then, the potential vector $\vec{A}$ would take the general form of

$$\vec{A}(r,\theta,\phi) = \hat{a}_r A_r(r,\theta,\phi) + \hat{a}_\theta A_\theta(r,\theta,\phi) + \hat{a}_\phi A_\phi(r,\theta,\phi) \tag{2.25}$$

where the amplitude variations of r in all components are in the form of $1/r^n$, $n = 1, 2, ...$ [3]. In the far-field region, r is very high so it is possible to neglect higher order terms, $1/r^n = 0, n = 2, 3, ...$, then, equation 2.25 reduces to:

$$\vec{A}(r,\theta,\phi) \approx \left[\hat{a}_r A'_r(\theta,\phi) + \hat{a}_\theta A'_\theta(\theta,\phi) + \hat{a}_\phi A'_\phi(\theta,\phi)\right]\frac{e^{-jkr}}{r}. \tag{2.26}$$

Substituting this into equation 2.23, doing the curl and neglecting terms with $1/r^2$, the magnetic field results in

$$\overrightarrow{H^0}(r,\theta,\phi) \approx \mathrm{j}\frac{\omega}{\eta_0}\left[\hat{a}_\theta A'_\phi(\theta,\phi) - \hat{a}_\phi A'_\theta(\theta,\phi)\right]\frac{e^{-jkr}}{r} \tag{2.27}$$

where $\eta_0 = \sqrt{\mu_0/\epsilon_0}$ is the intrinsic impedance of the void. Then, using equations 2.27 and 2.24, the electric field results in

$$\overrightarrow{E^0}(r,\theta,\phi) \approx -\mathrm{j}\omega\left[\hat{a}_\theta A'_\theta(\theta,\phi) + \hat{a}_\phi A'_\phi(\theta,\phi)\right]\frac{e^{-jkr}}{r} \tag{2.28}$$

where both magnetic and electric fields got their radial component neglected. In summary, it is possible to state that:

$$In\ the\ Far-Field\ Region \begin{cases} E_r^0(r,\theta,\phi) \approx 0 \\ E_\theta^0(r,\theta,\phi) \approx -j\omega A_\theta(r,\theta,\phi) \\ E_\phi^0(r,\theta,\phi) \approx -j\omega A_\phi(r,\theta,\phi) \end{cases} \tag{2.29}$$

$$In\ the\ Far-Field\ Region \begin{cases} H_r^0(r,\theta,\phi) \approx 0 \\ H_\theta^0(r,\theta,\phi) \approx j\dfrac{\omega}{\eta_0}A_\phi(r,\theta,\phi) = -\dfrac{E_\phi^0(r,\theta,\phi)}{\eta_0} \\ H_\phi^0(r,\theta,\phi) \approx -j\dfrac{\omega}{\eta_0}A_\theta(r,\theta,\phi) = \dfrac{E_\theta^0(r,\theta,\phi)}{\eta_0}. \end{cases} \tag{2.30}$$

Another conclusion to this would be,

$$\overrightarrow{E^0}(r,\theta,\phi) = \overrightarrow{E'^0}(\theta,\phi)\frac{e^{jkr}}{r} \tag{2.31}$$

$$\overrightarrow{H^0}(r,\theta,\phi) = \overrightarrow{H'^0}(\theta,\phi)\frac{e^{jkr}}{r}. \tag{2.32}$$

2.1.4 Power Density, Radiation Power and Radiation Intensity

Until now, only the electric and magnetic fields have been taken into account. However, it is necessary to look at the power (and energy) associated to them to calculate some of the figures of merit of an antenna. The quantity used to describe the power density associated with these electromagnetic waves is the instantaneous Poynting vector, defined as

$$\vec{W}(r,\theta,\phi;t) = \vec{E}(r,\theta,\phi;t) \times \vec{H}(r,\theta,\phi;t) \tag{2.33}$$

which, after using the complex fields introduced in equation 2.5 and some algebra, it is concluded that

$$\begin{aligned} \overrightarrow{W}(r,\theta,\phi;t) = &\frac{1}{2}\Re e\left\{\overrightarrow{E^0}(r,\theta,\phi) \times \overrightarrow{H^0}^*(r,\theta,\phi)\right\} \\ &+ \frac{1}{2}\Re e\left\{\overrightarrow{E^0}(r,\theta,\phi) \times \overrightarrow{H^0}(r,\theta,\phi)e^{j2\omega t}\right\} \end{aligned} \tag{2.34}$$

whose first term is not dependent of the time, as it can be seen. Then let us define the average Poynting vector, which is not dependent of the time, as

$$\overrightarrow{W_{av}}(r,\theta,\phi) = \left[\vec{W}(r,\theta,\phi;t)\right]_{av} = \frac{1}{2}\Re e\left\{\overrightarrow{E^0}(r,\theta,\phi) \times \overrightarrow{H^0}^*(r,\theta,\phi)\right\}. \tag{2.35}$$

Poynting vectors represent power density. To calculate the radiated power it is necessary to integrate this vector along the surface:

$$P_{rad} = \oiint_S \overrightarrow{W_{av}}(r,\theta,\phi)\cdot d\vec{s} = \frac{1}{2}\oiint_S \Re e\left\{\overrightarrow{E^0}(r,\theta,\phi)\times \overrightarrow{H^0}^*(r,\theta,\phi)\right\}\cdot d\vec{s}. \tag{2.36}$$

To end this section, let us define the radiation intensity in a given direction: "the power radiated from an antenna per unit solid angle." This is a far-field parameter, and it is obtained by multiplying the average power density by the square of the distance, like this:

$$U(\theta,\phi) = r^2\left|\overrightarrow{W_{av}}\right|(r,\theta,\phi) \tag{2.37}$$

and because this parameter is a far-field one, we can use the equations 2.30, 2.31 and 2.32 to calculate the magnitude of the average power density:

$$\left|\overrightarrow{W_{av}}\right|(r,\theta,\phi) = \frac{1}{2r^2}\left|\overrightarrow{E'^0}(\theta,\phi)\right|\left|\overrightarrow{H'^0}(\theta,\phi)\right| = \frac{1}{2\eta_0 r^2}\left|\overrightarrow{E'^0}(\theta,\phi)\right|^2 \tag{2.38}$$

and, then, the radiation intensity in function of the magnitude of the complex electric field is

$$U(\theta,\phi) = \frac{1}{2\eta_0}\left|\overrightarrow{E'^0}(\theta,\phi)\right|^2 \tag{2.39}$$

which does not change with r, as expected. Another way to obtain the radiation power given the radiation intensity is done by integrating it over the entire solid angle of 4π. Thus

$$P_{rad} = \oiint_\Omega U(\theta,\phi)d\Omega = \int_0^{2\pi}\int_0^{\pi} U(\theta,\phi)\sin\theta\, d\theta d\phi\,. \tag{2.40}$$

2.1.5 Directivity

The directivity of an antenna is one of the most important parameters in this work, because antennas will be compared using this figure of merit. Directivity is defined as "the ratio of the radiation intensity in a given direction from the antenna to the radiation intensity averaged over all directions." Where the average radiation intensity is equal to the total power radiated by the antenna divided by 4π, which is the radiation intensity of an isotropic source. This can be expressed as:

$$D(\theta,\phi) = \frac{U(\theta,\phi)}{U_0} = 4\pi\frac{U(\theta,\phi)}{P_{rad}}, \tag{2.41}$$

to find a simpler way to compute this, let us define the radiation intensity of the antenna in another way,

$$U(\theta,\phi) = B_0 F(\theta,\phi) \tag{2.42}$$

where B_0 does not vary with the direction. Then, using equations 2.40 and 2.42 it is possible to write:

$$D(\theta,\phi) = 4\pi\frac{F(\theta,\phi)}{\int_0^{2\pi}\int_0^{\pi} F(\theta,\phi)\sin\theta\, d\theta d\phi}. \tag{2.43}$$

In summary, the directivity of an antenna permits us to determine in which directions the antenna radiates with more or less intensity compared with an isotropic

source. It is usually expressed in dBi and it is related to the gain of the antenna, as it will be stated later in this text.

2.1.6 Antenna Efficiency

Not all of the power transmitted to the feed of the antenna is radiated. Some of the power will be dissipated or reflected and thus, it is possible to define a number of efficiencies related to these losses:

- e_r: reflection (mismatch) efficiency,
- e_c: conduction efficiency,
- e_d: dielectric efficiency,
- e_0: total efficiency.

The reflection efficiency is related to the mismatch produced between the feeding line and the antenna when their impedance is different. The conduction efficiency is the ratio between the input power and the losses produced in the conductors of the antenna, and the same with the dielectric efficiency but taking into account the losses in the dielectric of the antenna instead of its conductors. Then, the total efficiency is defined as follows,

$$e_0 = e_r e_c e_d. \tag{2.44}$$

2.1.7 Gain

The gain is defined as "the ratio of the intensity, in a given direction, to the radiation intensity that would be obtained if the power accepted by the antenna were radiated isotropically." It is noted that the definition is really similar to the one of the directivity, as the difference between them is that the gain takes into account the conduction and dielectric efficiency:

$$G(\theta, \phi) = 4\pi \frac{U(\theta, \phi)}{P_{in}} = e_c e_d D(\theta, \phi). \tag{2.45}$$

Furthermore, it is possible to define the absolute gain, which also takes into account the impedance mismatches (reflection losses):

$$G_{abs}(\theta, \phi) = e_0 D(\theta, \phi). \tag{2.46}$$

2.1.8 Reciprocity Theorem

Many antenna properties are the same for both a transmitting antenna and when this one is receiving too. Gain and directivity are examples of this and since it may be easier to calculate these properties when transmitting than when receiving or vice versa, this reciprocity greatly simplifies antenna calculations and measurements. Reciprocity can be understood via Maxwell's equations, as will be stated below.

Burke & Smith state the electromagnetic case for reciprocity using the Maxell's equations as follows: "An antenna can be treated either as a receiving device, gathering the incoming radiation field and conducting electrical signals to the output terminals, or as a transmitting system, launching electromagnetic waves outward. These two cases

are equivalent because of time reversibility: the solutions of Maxwell's equations are valid when time is reversed."

So, in summary, the reciprocity theorem assures us that the directivity, gain and the following properties presented here in transmission are also valid if the antenna is receiving.

2.1.9 Effective Area (Aperture)

A receiving antenna captures the power of an incident wave in its body and carries it to its feed. Thus, it is sensible to say that the bigger the antenna the more power is captured and then there will be more received power. It is possible to define, then, the effective area (also called aperture) of an antenna in a given direction as "the ratio of the available power at the terminals of a receiving antenna to the power flux density of a plane wave incident on the antenna from that direction." This can be expressed in an equation as follows,

$$A_{eff}(\theta,\phi) = \frac{P_T}{W_{i;\theta,\phi}} \tag{2.47}$$

where P_T is the power received by the antenna and transmitted to the feed and W_i is the power density of the incident wave from the given direction.

Although the effective area and the actual total area of the antenna may not be the same, it is possible to relate them with another efficiency definition. This efficiency is called aperture efficiency and it is defined as

$$e_{ap} = \frac{A_{eff}^{max}}{A_p} \tag{2.48}$$

where A_{eff}^{max} is the maximum effective area and A_p the physical area of the antenna. It is deduced from this definition that the effective area of an antenna cannot be higher than its physical area.

Let us now assume that there are two antennas. One of them is transmitting and the other one receiving. If the transmitting antenna were isotropic, the radiated power density that reaches the receiving antenna would be:

$$W_0 = \frac{P_t}{4\pi R^2} \tag{2.49}$$

with P_t as the total radiated power. However, since the antenna is not isotropic, this density is multiplied by its directivity,

$$W_t = W_0 D_t(\theta_t,\phi_t) = \frac{P_t D_t(\theta_t,\phi_t)}{4\pi R^2} \tag{2.50}$$

where t is written to indicate that it is the directivity of the transmitter antenna. Then, using the equation 2.47 we can calculate the power received by the antenna:

$$P_r = W_t A_{eff;r}(\theta_r,\phi_r) = \frac{P_t D_t(\theta_t,\phi_t) A_{eff;r}(\theta_r,\phi_r)}{4\pi R^2} \tag{2.51}$$

which can also be expressed as

$$D_t(\theta_t,\phi_t) A_{eff;r}(\theta_r,\phi_r) = 4\pi R^2 \frac{P_r}{P_t}. \tag{2.52}$$

If the transmitter antenna is used as a the receiver one and vice versa, then

$$D_r(\theta_r, \phi_r) A_{eff;t}(\theta_t, \phi_t) = 4\pi R^2 \frac{P_r}{P_t} \tag{2.53}$$

and equating 2.52 and 2.53 reduces to

$$\frac{D_t(\theta_t, \phi_t)}{A_{eff;t}(\theta_t, \phi_t)} = \frac{D_r(\theta_r, \phi_r)}{A_{eff;r}(\theta_r, \phi_r)}. \tag{2.54}$$

If the first transmitter antenna were isotropic, then, $D_t(\theta_t, \phi_t) = 1$, and equation 2.54 would mean that its effective area would be the relation between the effective area and the directivity of any other antenna in any given direction. If we compute the directivity and the effective area of any antenna it is possible to show that the effective area of an isotropic antenna is:

$$A^i_{eff}(\theta, \phi) = \frac{\lambda^2}{4\pi} \tag{2.55}$$

which, as expected, does not vary with the direction. Equation 2.55 is also possible to be deduced from thermodynamic assumptions, but this branch of physics is far from this work.

If the antenna has losses and once the effective area of an isotropic source is found, easily it is possible to found the effective area of any antenna:

$$A_{eff}(\theta, \phi) = e_c e_d \frac{\lambda^2}{4\pi} D(\theta, \phi). \tag{2.56}$$

As shown in equation 2.56, the effective area of an antenna is directly proportional to its directivity and the square of the wavelength. Furthermore, it is possible to express the effective area in function of the gain of the antenna, as follows,

$$A_{eff}(\theta, \phi) = \frac{\lambda^2}{4\pi} G(\theta, \phi). \tag{2.57}$$

2.1.10 Polarization of an antenna

Before we define the polarization of any antenna, the polarization of a radiated wave should be described first. It can be defined as “that property of an electromagnetic wave describing the time-varying direction and relative magnitude of the electric field vector; specifically, the figure traced as a function of time by the extremity of the vector at a fixed location in space, and the sense in which it is traced, as observed along the direction of propagation.” Polarization may be classified as linear, circular o elliptical, depending on the direction taken by the vector describing the electric field at a point when time varies.

The polarization of an antenna in a given direction is defined as “the polarization of the wave radiated by the antenna.” Since the polarization of the radiated wave can vary with the direction from the centre of the antenna, a direction should be specified, if not, the direction of maximum gain is assumed.

The reciprocity theorem tells that the polarization of an antenna is the same if it is in a transmission state or a reception one but, if the polarization of the receiving antenna is not the same as the polarization of the incident wave, not all the power carried by the wave is going to be captured by the antenna. This is called a polarization

mismatch, and can be expressed as another type of efficiency, also called polarization loss factor. This will be defined as:

$$e_p = |\hat{\rho}_w \cdot \hat{\rho}_a|^2 \tag{2.58}$$

where $\hat{\rho}_w$ is the unit vector of the wave and $\hat{\rho}_a$ the polarization vector of the antenna. The case above was supposing that the transmitting and receiving antenna had the same polarization, and that is why this efficiency did not appear before.

2.1.11 Friis Transmission Equation

To study the power transmitted and received between two antennas, let us assume the scene shown in figure 2.2 if P_t is the power transmitted to the antenna by its feed, the power density which reaches the reception antenna is:

$$W_t = e_c^t e_d^t \frac{P_t D_t(\theta_t, \phi_t)}{4\pi R^2} = \frac{P_t G_t(\theta_t, \phi_t)}{4\pi R^2} \tag{2.59}$$

and, using equation 2.47, 2.56 and 2.59 to calculate the amount of power collected by the receiving antenna, it is possible to write:

$$P_r = e_c^r e_d^r \frac{\lambda^2}{4\pi} D_r(\theta_r, \phi_r) W_t = e_c^t e_d^t e_c^r e_d^r \frac{\lambda^2 D_t(\theta_t, \phi_t) D_r(\theta_r, \phi_r) P_t}{(4\pi R)^2} |\hat{\rho}_t \cdot \hat{\rho}_r|^2. \tag{2.60}$$

As can be seen, the polarization mismatch between both of the antennas has been taken into account too. If, instead of the power transmitted by the feed to the antennas, the total power transmitted to the transmission antenna and the total power received by the receiving antenna is considered, this is, including the impedance mismatch, using the equation 2.44 the ratio of the received to the input power is calculated as follows:

$$\frac{P_R}{P_T} = e_0^t e_0^r \frac{\lambda^2 D_t(\theta_t, \phi_t) D_r(\theta_r, \phi_r)}{(4\pi R)^2} e_p = \left(\frac{\lambda}{4\pi R}\right)^2 G_{abs}^t(\theta_t, \phi_t) G_{abs}^r(\theta_r, \phi_r) e_p \tag{2.61}$$

which is known as the Friis Transmission Equation and it expresses the ratio between the power of two antennas when one is transmitting and the other receiving. The term $(\lambda/4\pi R)^2$ is called the free-space loss factor because it expresses the loss of power produced by the spherical spreading of the power by the antenna.

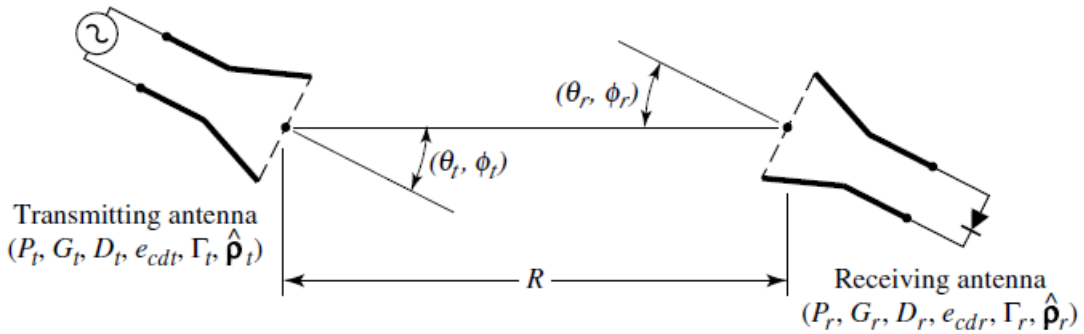

Figure 2.2: General situation of a transmitting and a receiving antenna to demonstrate Friis Transmission Equation.

2.2 Linear Arrays

One of the keys of the next generation antennas is that the will have high gain and they will be able to aim to the direction of the base station beam. To accomplish these two features it is essential the use of the arrays. As it was seen in the equation 2.57, the

larger the antenna, the more gain it has, and this is how the gain in 5G antennas is going to be produced.

Arrays are an assembly of small radiating elements, which are other antennas, so the gain increases. Furthermore, as it will be seen in this section, the direction of the maximum gain can be changed by tuning one of the controls of the array. Usually, any array has at least six parameters: geometrical configuration (we will only use linear arrays here, though), number of elements, relative distance between elements, excitation amplitude of individual elements, excitation phase of individual elements and the relative pattern of individual elements. As anyone would expect, coordinating these factors with harmony so the result is what it is desired may prove difficult, so that is why in this section the linear arrays are analysed deeply.

2.2.1 Array Factor

Since an array is an aggrupation of antennas, the total field produced by the array is determined by the vector addition of the field radiated by each of the individual elements. This way, directive patterns are achieved with constructively interference in one direction and destructive in others. To calculate this field, the coupling between each of the antennas is going to be neglected for simplicity's sake and only the far-field region is taken into account. Furthermore, all the elements are going to be identical since this simplifies the solution greatly too. So, first, let us examine the field of a single element in the far-field, determined by the equation 2.28:

$$\overrightarrow{E_{SE}^{0}}(r,\theta,\phi) \approx -\mathrm{j}\omega\frac{e^{-jkr}}{r}J^{0}e^{j\theta^{J}}\left[\hat{a}_{\theta}A''_{\theta}(\theta,\phi)+\hat{a}_{\phi}A''_{\phi}(\theta,\phi)\right] \tag{2.62}$$

where J^0, the amplitude of the current density of the single element, and its phase, θ_J, have been extracted from the potential vector $\vec{A}$ which is calculated as shown in the equation 2.20. If there were N different elements, the total field would be

$$\overrightarrow{E_{T}^{0}}(r,\theta,\phi) \approx \overrightarrow{E_{1}^{0}}(r_1,\theta_1,\phi_1)+\overrightarrow{E_{2}^{0}}(r_2,\theta_2,\phi_2)+\cdots+\overrightarrow{E_{N}^{0}}(r_N,\theta_N,\phi_N) \tag{2.63}$$

where each of the complex fields has also its own J_i^0 and θ_i^J. However, since far-field considerations are assumed, all the radiating sources are very close compared to the target point and it is clear that $\theta_1,\theta_2,\dots,\theta_N \approx \theta$ and $\phi_1,\phi_2,\dots,\phi_N \approx \phi$, where θ and ϕ are taken from coordinates origin. Also, for amplitude variations, $r_1,r_2,\dots,r_N \approx r$ but, for phase variations (for e^{-jkr} from equation 2.62), this is not valid. To study this case let us examine figure 2.3. As stated before, the array will be linear, this is, the elements will be placed along a line. The direction of the line is represented by the unity vector $\hat{a}_u$ and the observation direction by $\hat{a}_r$. Let us define then the angle γ by:

$$\cos\gamma = \hat{a}_u \cdot \hat{a}_r \tag{2.64}$$

and, using trigonometry basics in the geometry shown in figure 2.3, it is possible to state that, with far-field assumptions: $r_1 \approx r,\ r_2 \approx r - d_2\cos\gamma,\dots,\ r_N \approx r - d_N\cos\gamma$ where d_i is the distance between the element number i and the first element (situated at the origin of coordinates). Furthermore, the phase of the excitation are now expressed like $\theta_1^J = 0,\ \theta_2^J = \beta_2,\dots,\ \theta_N^J = \beta_N$. With all these considerations now and some algebra the total complex field can be calculated as:

$$\overrightarrow{E_T^0}(r,\theta,\phi) \approx -\mathrm{j}\omega\frac{e^{-jkr}}{r}J_1^0\left[\hat{a}_\theta A''_\theta(\theta,\phi)+\hat{a}_\phi A''_\phi(\theta,\phi)\right] \cdot\left[1+\frac{J_2^0}{J_1^0}e^{j(kd_2\cos\gamma+\beta_2)}+\cdots+\frac{J_N^0}{J_1^0}e^{j(kd_N\cos\gamma+\beta_N)}\right]. \tag{2.65}$$

Note that in the expression above the field is shown as two factors, one is the same as the field of a single element situated at the origin of coordinates, while the other has the different factors which composes the array (number of elements, difference between the amplitude and phase of the elements and distance between them). With this result it is possible to define the array factor, as it follows:

$$\overrightarrow{E_T^0}(r,\theta,\phi) \approx \overrightarrow{E_{SE}^0}(r,\theta,\phi)\cdot AF \tag{2.66}$$

and the normalised array factor:

$$(AF)_n = \frac{AF}{\max(AF)}. \tag{2.67}$$

Reached this point, the problem reduces to calculating the array factor of the desired array and multiplying it to the field of a single element.

2.2.2 Uniform Linear Arrays

A uniform array has all the amplitude of their elements set to the same value, and it can be shown that this configuration produces the maximum gain (directivity) of the array [3] at the expense of the side lobe level. Since this work centres its efforts in obtaining the maximum gain and it does not take into account the side lobes of the radiation pattern of the antenna, the arrays studied here will be uniforms.

To keep with the simplifications, let us consider uniform spacing and uniform difference of phase between the elements, like this: $d_1 = 0,\ d_2 = d,\ d_3 = 2d, \dots,\ d_N = (N-1)d$ and $\beta_1 = 0,\ \beta_2 = \beta,\ \beta_3 = 2\beta, \dots,\ \beta_N = (N-1)\beta$. So, the array factor reduces to:

$$AF = 1 + e^{j(kd\cos\gamma+\beta)} + e^{j2(kd\cos\gamma+\beta)} + \cdots + e^{j(N-1)(kd\cos\gamma+\beta)} = \sum_{i=1}^{N} e^{j(i-1)(kd\cos\gamma+\beta)} = \sum_{i=1}^{N} e^{j(i-1)\psi} \tag{2.68}$$

where ψ is

$$\psi = kd\cos\gamma + \beta. \tag{2.69}$$

Multiplying equation 2.68 by $e^{j\psi}$ and subtracting equation 2.68 it results as it follows:

$$AF\left(e^{j\psi}-1\right) = e^{jN\psi}-1 \Rightarrow AF = \frac{e^{jN\psi}-1}{e^{j\psi}-1} \tag{2.70}$$

and, using the sine function:

$$AF = e^{j\frac{N-1}{2}\psi}\cdot\frac{e^{j\frac{N}{2}\psi}-e^{-j\frac{N}{2}\psi}}{e^{j\frac{1}{2}\psi}-e^{-j\frac{1}{2}\psi}} = e^{j\frac{N-1}{2}\psi}\left[\frac{\sin\frac{N}{2}\psi}{\sin\frac{1}{2}\psi}\right] \tag{2.71}$$

where the expression between brackets is similar to the periodic sinc function whose maximum is N and then, the normalised array factor is

$$(AF)_n = \frac{e^{j\frac{N-1}{2}\psi}}{N}\left[\frac{\sin\frac{N}{2}\psi}{\sin\frac{1}{2}\psi}\right]. \tag{2.72}$$

To know more about the array factor of uniform arrays let us examine where are situated the maximums and minimums of the equation 2.71 and 2.72:

$$Minimums:\ \sin\frac{N}{2}\psi = 0 \Rightarrow \psi = \pm\frac{2n}{N}\pi;\ n \in \mathbb{N} - \{N, 2N, \dots\} \tag{2.73}$$

$$Maximums:\ \ sin\frac{1}{2}\psi = 0 \Rightarrow \psi = \pm 2m\pi;\ m \in \mathbb{N} + \{0\}. \tag{2.74}$$

2.2.3 Scanning Arrays

One of the more interesting feats of arrays is the ability of aiming the maximum of its gain towards any desired direction. Using equation 2.74 and 2.69 it is possible to see how this works:

$$Maximums:\ \ kd\cos\gamma + \beta = \pm 2m\pi;\ m \in \mathbb{N} + \{0\}, \tag{2.75}$$

the way the angle γ was defined in equation 2.64 means that it is possible to select a direction γ_m where the maximum is aimed if the phase difference of the excitation is set correctly, this is, using $m = 0$ (first maximum):

$$\beta = -kd\cos\gamma_m\,. \tag{2.76}$$

The array factor is represented in figure 2.3 as a function of γ, with a window which represent the actual array factor for a given value of kd and β. Tuning kd widens or stretches the window and changing β changes the centre of the window, which means that it selects where is the maximum situated.

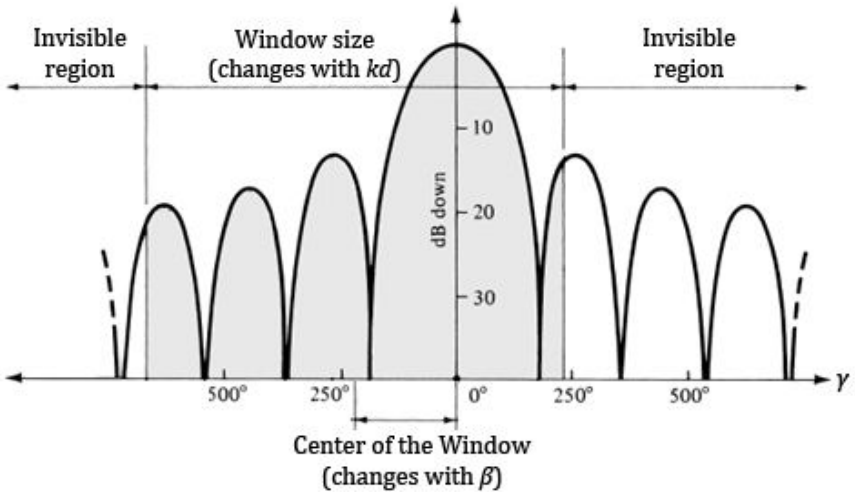

Figure 2.3: Array factor as a function of the observation angle.

If $\beta = 0$, the maximum would be located in the centre of the figure. This configuration is called broadside array, and the condition that must be satisfied so there is only one main lobe (a single maximum) is $kd < 2\pi \Rightarrow d < \lambda$. On the other hand, if $\beta = \pm kd$, the maximum would be located on the side of the array factor. This

configuration is called end-fire array and the condition to have only one main lobe is more restrictive, $kd < \pi \Rightarrow d < {}^{\lambda}/_{2}$.

2.2.4 Directivity of a Uniform Linear Array

This work centres its efforts in gain and, thus, in directivity, so the directivity of the arrays exposed here is going to be analysed. Examining the figure 2.3 it is possible to state that the directivity is going to be higher as the size of the window increases (higher kd), because the main lobe is going to has less width. However, if kd is too high others main lobes will appear and the directivity would decrease, so it is important to keep the size of the window lower than the values expressed above. Also, the maximum of the array factor increases with the number of elements of the array, N. Both of these are expected since they would mean that the area of the antenna is higher thus the directivity must rise.

Also, it is possible to compute the directivity associated to the array factor and add it (using dBi) to the directivity of the single element later. This directivity is calculated with the square of the array factor since it is done in terms of power:

$$D(\theta,\phi) = 4\pi \frac{AF(\theta,\phi)^2}{\int_0^{2\pi}\int_0^{\pi} AF(\theta,\phi)^2 \sin\theta \, d\theta d\phi}. \tag{2.77}$$

2.2.5 Coverage Efficiency

To measure the beamsteering capabilities of an array, a metric is defined in [5] called coverage efficiency (η_c) as follows:

$$\eta_c = \frac{Coverage\ Solid\ Angle}{Maximun\ Solid\ Angle}. \tag{2.78}$$

The maximum solid angle is 4π, since we want to cover all directions. To compute the coverage solid angle a minimum gain must be defined first. This gain should be the minimum to establish a link with the base station. Thus, the coverage solid angle is the solid angle where the gain of the antenna is $G(\theta,\phi) > G_{min}$, so the link can be established if the base station were in that direction.

This gain is not for a specific β, it is the directivity obtained in a direction (θ,ϕ) when the beam points in that direction, so it is the maximum directivity achievable in that direction if β is tuned properly.

2.3 Finite-length Dipole

This section initiates the analysis of different antennas used in this work. The objective of this one is to calculate the fields of a finite-length dipole in far-field conditions, however to do this, the analysis of the infinitesimal dipole must be done first. The dipole antenna is one of the simplest and most traditional antennas, but also very versatile.

2.3.1 Infinitesimal Dipole

The structure of a dipole situated along the z axis is shown in the figure 2.4. It consist of an infinitesimal diameter (a) wire with a total length of l, which in this case is very small, so: $a \ll \lambda$ and $l \ll \lambda$. The current is assumed to be constant along the length of the dipole because it is too small, thus

$$\vec{I}(z') = \hat{a}_z I_0 \tag{2.79}$$

where I_0 is constant.

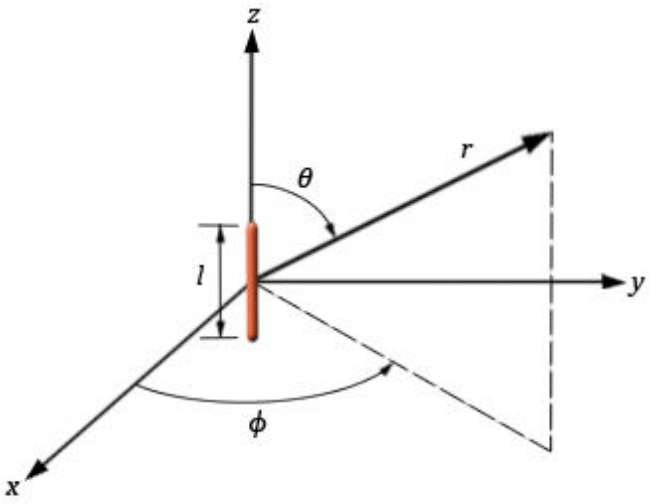

Figure 2.4: Geometrical arrangement of the dipole antenna.

The procedure to calculate the electric and magnetic fields is the same as the one explained in the first section of this chapter. First, let us calculate the potential vector $\vec{A}$ using the equation 2.22 and the current of the dipole from equation 2.79:

$$\vec{A}(x,y,z) = \hat{a}_z \frac{\mu_0 I_0}{4\pi r} e^{-jk_0 r} \int_{-l/2}^{l/2} dz' = \hat{a}_z \frac{\mu_0 I_0 l}{4\pi r} e^{-jk_0 r} \tag{2.80}$$

since the dipole is placed in the origin of coordinates, $x' = y' = z' = 0$, and then $R = r$. With the potential vector now calculated, let us find the magnetic and electric fields. To do so, first it is convenient to use spherical coordinates:

$$\vec{A}(r,\theta,\phi) = \hat{a}_r \frac{\mu_0 I_0 l}{4\pi r} \cos\theta \, e^{-jk_0 r} - \hat{a}_\theta \frac{\mu_0 I_0 l}{4\pi r} \sin\theta \, e^{-jk_0 r} \tag{2.81}$$

and, using the results from equations 2.29 and 2.30

$$E^0(r,\theta,\phi) \approx \hat{a}_\theta j \frac{\eta_0 k_0 I_0 l}{4\pi r} \sin\theta \, e^{-jk_0 r} \tag{2.82}$$

$$H^0(r,\theta,\phi) \approx \hat{a}_\phi j \frac{k_0 I_0 l}{4\pi r} \sin\theta \, e^{-jk_0 r} \tag{2.83}$$

and, thus, we have the complex electric and magnetic fields needed to calculate the ones from the finite-length dipole.

2.3.2 Finite-length Dipole Electromagnetic Analysis

The finite-length dipole has de same spatial distribution as the infinitesimal dipole, but its length is longer, not much less than the wavelength. This implies that the current is not constant in all the dipole. The current distribution along the length of the dipole is, approximately, sinusoidal with nulls at the end points, as it has been proved experimentally. Let us express this in mathematical form like this:

$$\vec{I}(x',y',z') = \begin{cases} \hat{a}_z I_0 \sin\left[k\left(\frac{l}{2}-z'\right)\right] \; when\; 0 \le z' \le \frac{l}{2} \\ \hat{a}_z I_0 \sin\left[k\left(\frac{l}{2}+z'\right)\right] \; when\; -\frac{l}{2} \le z' < 0 \end{cases} \tag{2.84}$$

since calculating the potential vector using this current distribution would lead us to a very difficult problem, it is convenient to divide the length of the dipole in infinitesimal-length dipoles and sum them afterwards using an integral. In these dipoles with such a short length, the previous result is valid. However, the position is not always $(0,0,0)$, so $R = r$ only for amplitude variations. For phase variations $R = r - z'\cos\theta$, as can be extracted from the figure 2.4. With these considerations and equation 2.82 it is possible to write:

$$dE_\theta^0(r,\theta,\phi) \approx j\frac{\eta_0 k_0 I(x',y',z')e^{-jk_0 r}}{4\pi r}\sin\theta\, e^{jk_0 z'\cos\theta}dz' \tag{2.85}$$

and, summing, we obtain

$$E_\theta^0(r,\theta,\phi) = \int_{-l/2}^{l/2} dE_\theta^0 \approx j\frac{\eta_0 k_0 e^{-jk_0 r}}{4\pi r}\sin\theta\int_{-l/2}^{l/2} I(x',y',z')\, e^{jk_0 z'\cos\theta}dz' \tag{2.86}$$

so, the next integral needs to be solved:

$$\begin{aligned} Integral = &\int_0^{l/2} I_0 \sin\left[k\left(\frac{l}{2}-z'\right)\right] e^{jk_0 z'\cos\theta}dz' \\ &+ \int_{-l/2}^{0} I_0 \sin\left[k\left(\frac{l}{2}+z'\right)\right] e^{jk_0 z'\cos\theta}dz' \end{aligned} \tag{2.87}$$

which can be solved using the next result:

$$\begin{aligned} \int e^{\alpha x}\sin(\beta x+\gamma)dx &= \frac{e^{\alpha x}}{\alpha^2+\beta^2}[\alpha\sin(\beta x+\gamma) - \beta\cos(\beta x+\gamma)] \\ with\ \alpha = jk_0\cos\theta\,, \beta &= \pm k_0, \gamma = \frac{k_0 l}{2} \end{aligned} \tag{2.88}$$

then,

$$\begin{aligned} Integral = &\frac{1}{k_0(1-\cos^2\theta)}\left[j\cos\theta\sin\left(\frac{k_0 l}{2}\right) - \cos\left(\frac{k_0 l}{2}\right) + e^{j\frac{k_0 l}{2}\cos\theta}\right. \\ &\left. - j\cos\theta\sin\left(\frac{k_0 l}{2}\right) - \cos\left(\frac{k_0 l}{2}\right) + e^{j\frac{k_0 l}{2}\cos\theta}\right] \\ &= \frac{2}{k_0}\frac{\cos\left(\frac{k_0 l}{2}\cos\theta\right) - \cos\frac{k_0 l}{2}}{\sin^2\theta} \end{aligned} \tag{2.89}$$

and, finally,

$$E^0(r,\theta,\phi) \approx \hat{a}_\theta j \frac{\eta_0 I_0}{2\pi r} e^{-jk_0 r} \left[\frac{\cos\left(\frac{k_0 l}{2}\cos\theta\right) - \cos\frac{k_0 l}{2}}{\sin\theta} \right] \tag{2.90}$$

$$H^0(r,\theta,\phi) \approx \hat{a}_\phi j \frac{I_0}{2\pi r} e^{-jk_0 r} \left[\frac{cos\left(\frac{k_0 l}{2}cos\,\theta\right) - cos\frac{k_0 l}{2}}{sin\,\theta} \right]. \tag{2.91}$$

2.3.3 Finite-length Dipole Directivity

Using the previous results from equation 2.90 and 2.39 the radiation intensity of a dipole of length *l* in the far field placed along the *z* axis is

$$U(\theta,\phi) = B_0 F(\theta,\phi) = \eta_0 \frac{{I_0}^2}{8\pi} \left[\frac{\cos\left(\frac{k_0 l}{2}\cos\theta\right) - \cos\frac{k_0 l}{2}}{\sin\theta} \right]^2 \tag{2.92}$$

where B_0 is constant. From this we can write:

$$F(\theta,\phi) = \left[\frac{\cos\left(\frac{k_0 l}{2}\cos\theta\right) - \cos\frac{k_0 l}{2}}{\sin\theta} \right]^2 \tag{2.93}$$

and, this way, compute the directivity in each direction with its definition, as in equation 2.43,

$$D(\theta,\phi) = 4\pi \frac{\left[\frac{\cos\left(\frac{k_0 l}{2}\cos\theta\right) - \cos\frac{k_0 l}{2}}{\sin\theta} \right]^2}{\int_0^{2\pi}\int_0^{\pi} \frac{\left[\cos\left(\frac{k_0 l}{2}\cos\theta\right) - \cos\frac{k_0 l}{2}\right]^2}{\sin\theta} d\theta d\phi}. \tag{2.94}$$

2.3.4 Input Impedance of a Finite-length Dipole

For a lossless antenna like this one, the radiation impedance is the same as the real part of the input impedance. Using equation 2.40 and the definition of radiation impedance, we obtain de next results:

$$P_{rad} = \int_0^{2\pi}\int_0^{\pi} U(\theta,\phi)\sin\theta\, d\theta d\phi = \frac{1}{2}{I_0}^2 R_{\text{rad}}, \tag{2.95}$$

$$R_{in} = R_{rad} = \frac{\eta_0}{2}\int_0^{\pi} \frac{\left[\cos\left(\frac{k_0 l}{2}\cos\theta\right) - \cos\frac{k_0 l}{2}\right]^2}{\sin\theta} d\theta \tag{2.96}$$

which is a function of the length of the dipole and the frequency used but must be solved numerically.

Note that to minimise the return losses it is desirable to have an input resistance close to the impedance of the line used to feed the antenna.

2.4 Slot Antenna

Another type of antenna covered in this work is the slot antenna. This antenna is popular because it is very easy to integrate and it has a radiation pattern close to omnidirectional, like the dipole antenna. The slot antenna consists of a conductor surface with a rectangular perforation, called aperture.

2.4.1 Babinet's Principle

To analyse the slot, the Babinet's principle must be known first. This principle states that "when the field behind a screen with an opening is added to the field of a complementary structure, the sum is equal to the field where there is no screen." and its results are shown in the next expressions:

$$E^0_{\theta_s}(r,\theta,\phi) = H^0_{\theta_c}(r,\theta,\phi), \qquad E^0_{\phi_s}(r,\theta,\phi) = H^0_{\phi_c}(r,\theta,\phi)$$
$$H^0_{\theta_s}(r,\theta,\phi) = -\frac{E^0_{\theta_c}(r,\theta,\phi)}{\eta^2}, \qquad H^0_{\phi_s}(r,\theta,\phi) = -\frac{E^0_{\phi_c}(r,\theta,\phi)}{\eta^2} \tag{2.97}$$

where the sub-index s indicates the field corresponding to the structure with the opening while the c the complementary structure. Note that the polarization of both structures would be reversed. Furthermore, another result of this principle states that the impedances of both structures are related to each other following the next expression:

$$Z_s Z_c = \frac{\eta^2}{4}. \tag{2.98}$$

2.4.2 Slot Antenna Analysis

In the figure 2.5 the structure of the slot antenna and its complementary antenna are shown. The complementary antenna is a dipole so, using the Babinet's principle from equation 2.97 and the results from equations 2.90 and 2.91, the results of the slot antenna are easily calculated as follows:

$$E^0(r,\theta,\phi) \approx H^0_c(r,\theta,\phi) \approx \hat{a}_\phi j \frac{I_0}{2\pi r} e^{-jk_0 r} \left[\frac{cos\left(\frac{k_0 l}{2} cos\,\theta\right) - cos\frac{k_0 l}{2}}{sin\,\theta} \right] \tag{2.99}$$

$$H^0(r,\theta,\phi) \approx -\frac{E^0_c(r,\theta,\phi)}{\eta^2} \approx -\hat{a}_\theta j \frac{I_0}{2\pi\eta_0 r} e^{-jk_0 r} \left[\frac{\cos\left(\frac{k_0 l}{2}\cos\theta\right) - \cos\frac{k_0 l}{2}}{\sin\theta} \right] \tag{2.100}$$

and, using the result from equation 2.98, it is possible to calculate the input impedance of the slot from equation 2.96:

$$R_{in} = \frac{\eta^2}{4R_{in}^c} = \frac{\eta_0}{2\int_0^{\pi} \frac{\left[\cos\left(\frac{k_0 l}{2}\cos\theta\right) - \cos\frac{k_0 l}{2}\right]^2}{\sin\theta} d\theta}. \quad (2.101)$$

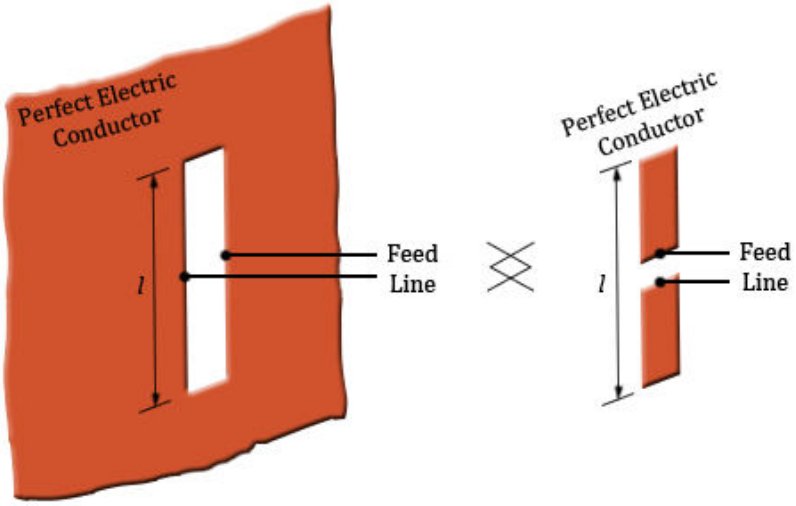

Figure 2.5: Slot antenna and its complementary antenna.

As can be seen above, the fields of the dipole antenna and the slot antenna are similar to each other. From these expressions, equation 2.99 and 2.100, it is possible to conclude that the directivity of the dipole and the slot is the same, since the maximum value of the fields does not affect the directivity.

2.5 Monopole Antenna

The monopole antenna is one of the easiest implementations of the dipole antenna, which give us similar performance in a given region of the space but it is only half long compared with the equivalent dipole. This antenna consists of two elements, the pole, which is just one of the poles from a dipole, and the infinite ground plane made of perfect electric conductor, which is necessary to make the monopole antenna work as intended, as seen in figure 2.6.

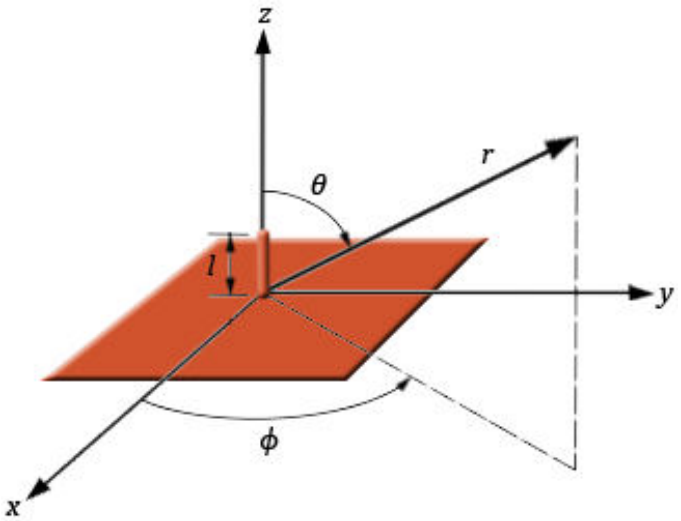

Figure 2.6: Geometry of the monopole antenna.

2.5.1 Image Theory

The analysis of the monopole antenna is made by understanding first the image theory. The image theory is thoroughly analysed in [3]. In this case, the image theory assures us that the electric and magnetic field in the region of the space outside of the ground plane is the same as if there were no ground plane and, instead, there would be another monopole situated symmetrically using the ground plane as the symmetry plane. The cause of this phenomenon is the reflection of the fields of the first monopole, which make the same effect as if there were another monopole at the other side of the ground plane. Obviously, the field of two monopoles is not the same in the region across the ground plane, which is cero in our case.

2.5.2 Monopole Antenna Analysis

When the geometry from the image theory is obtained, the result is clearly a dipole antenna with double length of the monopole antenna. So the electric and magnetic fields are the same as the ones from equations 2.90 and 2.91, but doubling the length:

$$E^0(r,\theta,\phi) \approx \hat{a}_\theta j \frac{\eta_0 I_0}{2\pi r} e^{-jk_0 r}\left[\frac{\cos(k_0 l\cos\theta)-\cos k_0 l}{\sin\theta}\right];\ 0 \le \theta < \pi/2 \tag{2.102}$$

$$H^0(r,\theta,\phi) \approx \hat{a}_\phi j \frac{I_0}{2\pi r} e^{-jk_0 r}\left[\frac{cos(k_0 l\, cos\,\theta)-cos\, k_0 l}{sin\,\theta}\right];\ 0 \le \theta < \pi/2\,. \tag{2.103}$$

The directivity of the monopole antenna is twice the directivity of a dipole antenna with double length as the monopole, since the radiated power is half of the dipole (there is no radiated power through the ground plane), as follows:

$$D(\theta,\phi) = 4\pi \frac{\left[\frac{\cos(k_0 l\cos\theta)-\cos k_0 l}{\sin\theta}\right]^2}{\int_0^{2\pi}\int_0^{\pi/2}\frac{[\cos(k_0 l\cos\theta)-\cos k_0 l]^2}{\sin\theta}\,d\theta d\phi}. \tag{2.104}$$

The input resistance, however, is half of the resistance of the dipole of double length, as it is expected of a half-length conductor material, because, again, the radiated power is half of the case of the dipole:

$$R_{in} = R_{rad} = \frac{\eta_0}{2}\int_0^{\pi/2}\frac{[\cos(k_0 l\cos\theta)-\cos k_0 l]^2}{\sin\theta}\,d\theta. \tag{2.105}$$

2.6 Inverted-F Antenna

The monopole antenna usually has good performance in mobile applications however, at lower frequencies, the monopole is too long to be integrated in a mobile terminal. That is why the monopole is sometimes folded, forming the L antenna, so it can be integrated in a reduced space but the L antenna must be matched using a lumped inductor, which is not desirable either. Substituting the lumped inductor with a line connected to the ground plane is another way of dealing with the matching, which leaves us with the inverted-F antenna (also IFA). It is called like this because it has the shape of an F on its side, as can be seen in the figure 2.7. More information about the IFA antenna can be found in [4].

Figure 2.7: Geometry of the IFA antenna.

Since this antenna is very oriented to its implementation, it has no analytics results. If an illustration of its behaviour is needed, the monopole antenna can be used. These are the results from equations 2.102, 2.103 and 2.104. The input resistance, and thus, the matching, can be tuned with its ground feed.

2.7 Patch Antenna

Microstrip antennas consist of a patch of metallic material situated on top of a dielectric substrate which is placed on a ground plane as shown in figure 2.8. This antenna has been being used in mobile communications recently since its low cost, low weight and how easily they can be fabricated. However, they provide a lower efficiency than the options above.

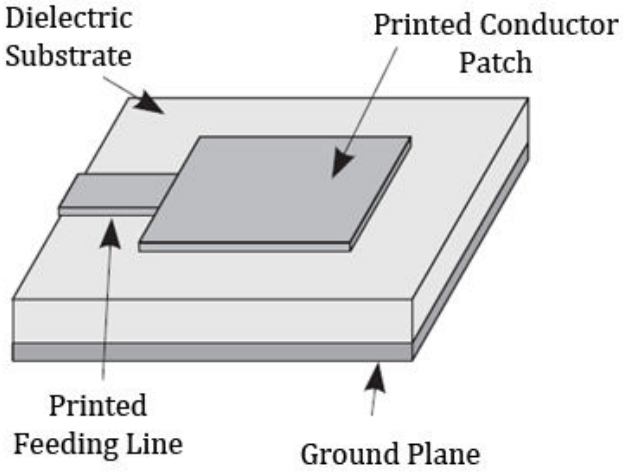

Figure 2.8: Geometry of the patch antenna.

2.7.1 Magnetic Current and the Vector Potential $\vec{F}$

Before analysing the patch antenna, it is essential to present new concepts not mentioned before in this text. In an analogue way to the electric current, there would be the magnetic current. Magnetic currents actually do not exist, because magnetic charge cannot travel separately, but it is important to define them because they are used in some mathematical formulations as equivalent magnetic currents.

From this magnetic current, $\vec{M}$, the vector potential $\vec{F}$ is defined in an analogue way to the vector potential $\vec{A}$ from equation 2.20, as

$$\vec{F}(x,y,z) = \frac{\epsilon_0}{4\pi} \iiint_V \overrightarrow{M_v^0}(x',y',z') \frac{e^{-jk_0R}}{R} dv' \tag{2.106}$$

and, also, using superficial and linear magnetic currents, analogue to equations 2.21 and 2.22:

$$\vec{F}(x,y,z) = \frac{\epsilon_0}{4\pi}\iint_S \overrightarrow{M_S^0}(x',y',z')\frac{e^{-jk_0R}}{R}ds' \tag{2.107}$$

$$\vec{F}(x,y,z) = \frac{\epsilon_0}{4\pi}\int_C \overrightarrow{M_l^0}(x',y',z')\frac{e^{-jk_0R}}{R}dl'. \tag{2.108}$$

As one would expect, it is possible to calculate the complex electric field vector $\overrightarrow{E^0}$ from the vector potential $\vec{F}$ using a similar procedure as in the section 1.1.2. Analogue to the result from equation 2.23, the electric field vector is calculated as

$$\overrightarrow{E^0}(x,y,z) = -\frac{1}{\epsilon_0}\nabla \times \vec{F}(x,y,z) \tag{2.109}$$

and, similar to equation 2.24 it is possible to calculate the magnetic field complex vector $\overrightarrow{H^0}$ using the complex electric field and

$$\overrightarrow{H^0}(x,y,z) = -\frac{1}{j\omega\mu_0}\nabla \times \overrightarrow{E^0}(x,y,z). \tag{2.110}$$

Note that these two last results are valid only in the absence of electric current.

As a last analogy between the electric and magnetic currents, the Perfect Magnetic Conductor (PMC) can be defined as a material where, in its surface, the magnetic field is always orthogonal to the surface and, thus, the electric field is always parallel to it.

2.7.2 Patch Antenna Analysis

There are several methods to analyse the patch antenna. Here the method used is the cavity model, which offers balance between precision of the results and physical insight provided. This method consists of modelling the patch as a resonant cavity, as its name suggest.

First, let us describe the electric field inside the structure. Given the properties of these types of microwave circuits, the value of the electric field inside the cavity formed by the patch and the ground plane can be approximated as

$$E^0(x,y,z) = E^0 \sin\frac{\pi y'}{L} \tag{2.111}$$

which is the TM^x_{010} mode. The radiation will be caused by this field and will occur in the four slots around the cavity. Furthermore, these four slots can be modelled as equivalent PMC material thin layers. $\overrightarrow{E^0}$ can be separated in E_x^0 and E_y^0 components and, since the length L of the patch will be close to $\lambda_g/2$, where λ_g is the wavelength inside the dielectric of the substrate, the contribution to radiation of the components E_y^0 will cancel each other for the slots situated in $y' = \pm L/2$, thus, only E_x^0 components will be taken into account for these slots. In the slots situated where $z' = \pm W/2$, the contribution to the radiation of the first half of the slot will be cancelled by the contribution of the other half, since the fields have opposites directions in those slots, as shown in figure 2.9, and, thus, we can conclude that these two slots do not radiate.

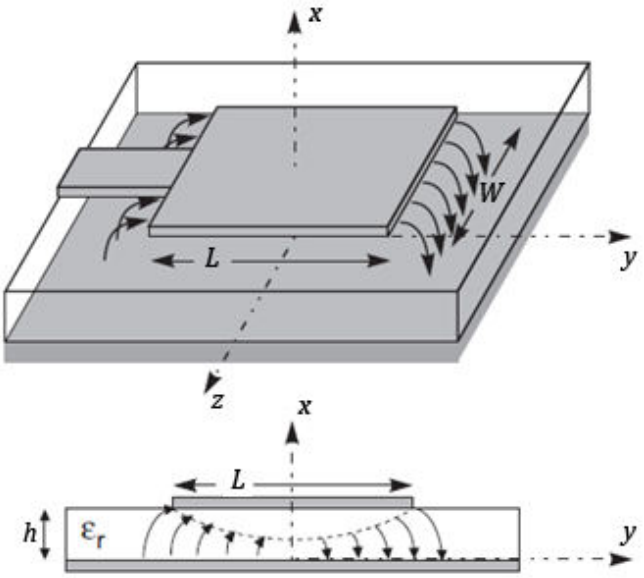

Figure 2.9: Fields direction in the patch antenna.

Once the fields that produce radiation are identified, the Huygens Principle is used to calculate the magnetic current, as follows:

$$\overrightarrow{M_S^0}(x', y', z') = -\hat{n} \times \overrightarrow{E^0}(x, y, z). \tag{2.112}$$

The Huygens Principle is thoroughly described in [3], it let us present the contribution to radiation of an electric field as an equivalent magnetic current, where $\hat{n}$ is the vector normal to the surface where the field is located. Also, to take into account the contribution of the ground plane, the image theory is applied, resulting in duplicating the contribution of these equivalent magnetic currents. In this particular case, the equivalent magnetic currents are then

$$\overrightarrow{M_S^0}(x', y', z') = 2E^0\hat{z} \quad when \quad \begin{matrix} -\frac{W}{2} \le z' \le \frac{W}{2} \\ -\frac{h}{2} \le x' \le \frac{h}{2} \end{matrix} \tag{2.113}$$

and which are situated in $y' = \pm\frac{L}{2}$, and so, using equations 2.107 to obtain the potential vector $\vec{F}$ and the equations 2.109 and 2.110 to calculate the electric and magnetic fields, they reduce to

$$E_\phi^0(r, \theta, \phi) = j\frac{k_0 hWE^0 e^{-jk_0 r}}{2\pi r}\sin\theta\frac{\sin\left(\frac{k_0 h}{2}\sin\theta\cos\phi\right)}{\frac{k_0 h}{2}\sin\theta\cos\phi}\frac{\sin\left(\frac{k_0 W}{2}\cos\theta\right)}{\frac{k_0 W}{2}\cos\theta} \tag{2.114}$$

$$E_r^0(r, \theta, \phi) \approx E_\theta^0(r, \theta, \phi) \approx 0$$

$$H_\theta^0(r, \theta, \phi)$$

$$= -j\frac{k_0 hWE^0 e^{-jk_0 r}}{2\pi\eta_0 r}sin\,\theta\frac{sin\left(\frac{k_0 h}{2}sin\,\theta\,cos\,\phi\right)}{\frac{k_0 h}{2}sin\,\theta\,cos\,\phi}\frac{sin\left(\frac{k_0 W}{2}cos\,\theta\right)}{\frac{k_0 W}{2}cos\,\theta} \tag{2.115}$$

$$H_r^0(r, \theta, \phi) \approx H_\phi^0(r, \theta, \phi) \approx 0.$$

With the last result, it is possible to extract the value of the directivity of the patch antenna using the equations 2.39, 2.42 and 2.43, as follows

$$D(\theta,\phi) = 4\pi \frac{\left[\frac{\sin\left(\frac{k_0 h}{2}\sin\theta\cos\phi\right)}{\cos\phi}\frac{\sin\left(\frac{k_0 W}{2}\cos\theta\right)}{\cos\theta}\right]^2}{\int_0^{2\pi}\int_0^{\pi}\left[\frac{\sin\left(\frac{k_0 h}{2}\sin\theta\cos\phi\right)}{\cos\phi}\frac{\sin\left(\frac{k_0 W}{2}\cos\theta\right)}{\cos\theta}\right]^2 \sin\theta\, d\theta d\phi}. \quad (2.116)$$

2.7.3 Patch Antenna Design

Even though the patch antenna has been analysed, the way of choosing the geometry of the patch has not been stated yet. This section aims to give an insight of how these dimensions should be chosen.

Once the substrate is chosen, the design follows computing the width of the patch, which, to obtain a good value of efficiency, can be [3]

$$W = \frac{\lambda_0}{2}\sqrt{\frac{2}{\varepsilon_r + 1}} \quad (2.117)$$

where λ_0 is the wavelength in free space and ε_r is the relative permittivity of the dielectric inside the substrate.

To compute the length of the patch the effective relative permittivity of the patch must be calculated first. This is the equivalent relative permittivity if the patch was submerged in a dielectric instead of having air on its top, and so, it must be lower than the dielectric constant of the substrate. When the frequency goes up, the value of the effective dielectric constant approximate the one of the dielectric constant of the substrate. At lower frequencies, the effective dielectric constant can be calculated as [1]

$$\varepsilon_{reff} = \varepsilon_r \frac{\varepsilon_r + 1}{2} + \frac{\varepsilon_r - 1}{2}\left(1 + 12\frac{h}{W}\right)^{-1/2}. \quad (2.118)$$

Electrically, the length of the patch seems longer than its physical size due to the fringing effects of the microstrip structure, so the ideal length of the patch, which should be $\lambda_g/2$, must be shorted. The final length of the patch is expressed as follows, using a popular expression for this shortening [3]:

$$L = \frac{\lambda_0}{2\sqrt{\varepsilon_{reff}}} - 0.824h\frac{\left(\varepsilon_{reff} + 0.3\right)\left(\frac{W}{h} + 0.264\right)}{\left(\varepsilon_{reff} - 0.258\right)\left(\frac{W}{h} + 0.8\right)}. \quad (2.119)$$

There are several ways of feeding the patch antenna [3] but, in any case, the position of the feeding can be tuned slightly to optimise the obtained efficiency.

Chapter 3

Coverage Efficiency

The aim of this chapter is to compute the approximated directivity of a scanning array in a mobile terminal at the desired frequency to obtain the coverage efficiency defined in the section 2.2.5. This will be repeated for different types of antennas and configurations to form a study and conclude which types of antennas are best suited to the fifth generation of mobile communications in terms of coverage efficiency. The chapter finalises with a design using the information obtained along the chapter which is able to be fabricated.

3.1 Introduction

To have an insight in how these antennas work and a starting point to use a commercial electromagnetic simulator, a MATLAB simulation will be done first. To do this, two arrays are going to be used so they fit in a mobile terminal. Using MATLAB and the theoretical expressions of the type of antenna and the array from the previous chapter, the directivity of both arrays will be calculated and plotted in each direction and thus computing the coverage efficiency. After that, a CST Microwave Studio simulation will be done to obtain more precise results.

The minimum physical size of the mobile terminal used is 100 mm of height and 40 mm of width and the frequency used in this work is 28 GHz, which is one of the expected frequencies to be used in 5G. The array will be placed in a line along the height and length of the terminal, as shown in figure 3.1. Usually, the other side of the terminal (right part of the figure 3.1) should have another array. However, to simplify and speed up the numerous simulations, only two arrays will be used. This is made this way so the results are valid for wider mobile terminals and of course translatable to when all three arrays are used, since the configuration preserves the symmetry. The bottom part of the terminal should be reserved for previous technology antennas and will not be used.

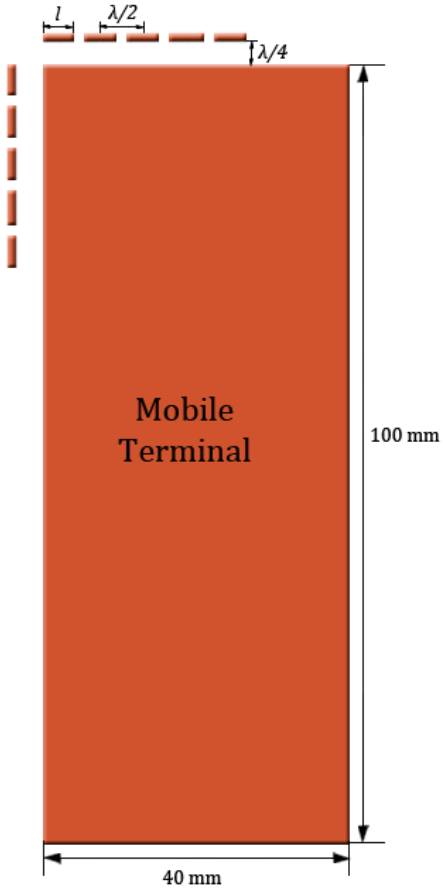

Figure 3.1: Geometry of the mobile terminal and arrays.

3.2 Fixed-length dipole

This section will show step-by-step how the coverage efficiency is computed using the simulations previously cited. These steps will be repeated for the following antennas but will not be shown here to avoid redundancy.

3.2.1 Directivity of a single element

In equation 2.94, when the dipole was analysed, the directivity of a dipole of length l in the far field placed along the z axis was calculated. Using MATLAB and this expression the directivity (dBi) of a single dipole with $l = \lambda_0/4$ has been computed and it is shown in figure 2, where we can see the expected directivity from a dipole: there is no change with ϕ, when $\theta = 90$ º the directivity takes its maximum value, 2.15 dBi, and when $\theta = 0$ º and $\theta = 180$ º there is no radiation. The MATLAB scripts employed along this chapter are shown in Appendix A. The script of the main code refers to sections A.1 and the script for the dipole is placed in section A.2.

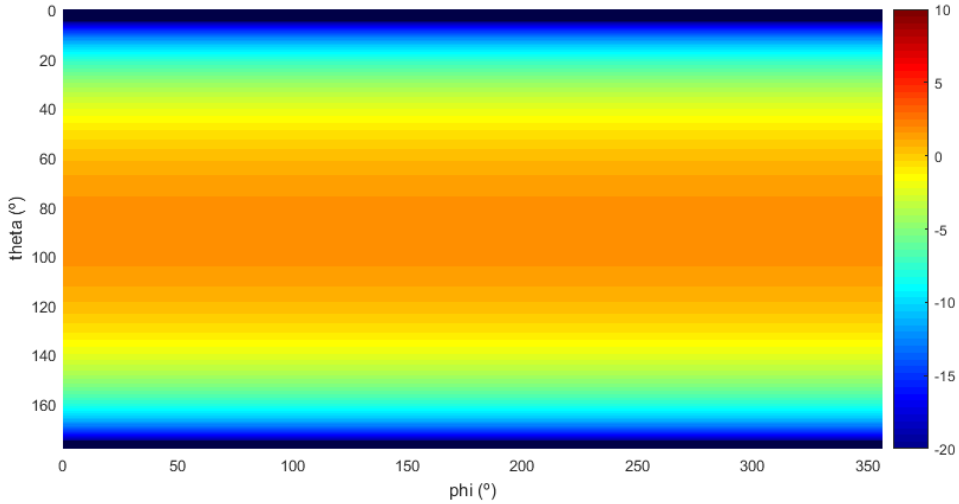

Figure 3.2: Directivity in each direction for a single dipole in dBi.

3.2.2 Array factor

Once the directivity of a dipole is computed, the next step is to introduce the array factor and its scanning ability. The normalised array factor of an array which N elements are placed along the z axis and with uniform current amplitude is shown in equation 2.72. It was shown that changing β it is possible to modify the direction of the main lobe of the radiation pattern of an array and thus, the desired aim angle, θ_0.

In the section 2.2.4, equation 2.77, the directivity taking into account only the array factor (as if the antennas were isotropic), was defined. Using this expression with MATLAB we obtain the results shown in figures 3.3 and 3.4, using $N = 5, d = \lambda_0/2$, and $\theta_0 = 90$ º (broadside) for figure 3.3 and $\theta_0 = 0$ º (end-fire) for figure 3.4. As it can be seen, the directivity in each direction is controlled with β. In this case, the maximum directivity is 7 dBi. Since the separation between the elements is $\lambda_0/2$, the end-fire array has two main lobes.

The objective of this work is to maximise the directivity and, thus, the gain. From equation 2.77, we know that the directivity of an array is proportional to the number of elements and the separation between them, however, if the separation is more or equal than $\lambda_0/2$, two or more main lobes may appear, so a distance between elements of $\lambda_0/2$ has been chosen to maximise gain without letting additional main lobes appear. The two main lobes of the end-fire array is not relevant, since dipoles have a null in their radiation pattern when $\theta_0 = 0$ º and $\theta_0 = 180$ º, so the pointing direction should never be those. In any case, both distance between elements and number of them are restricted by the available physical space in the mobile.

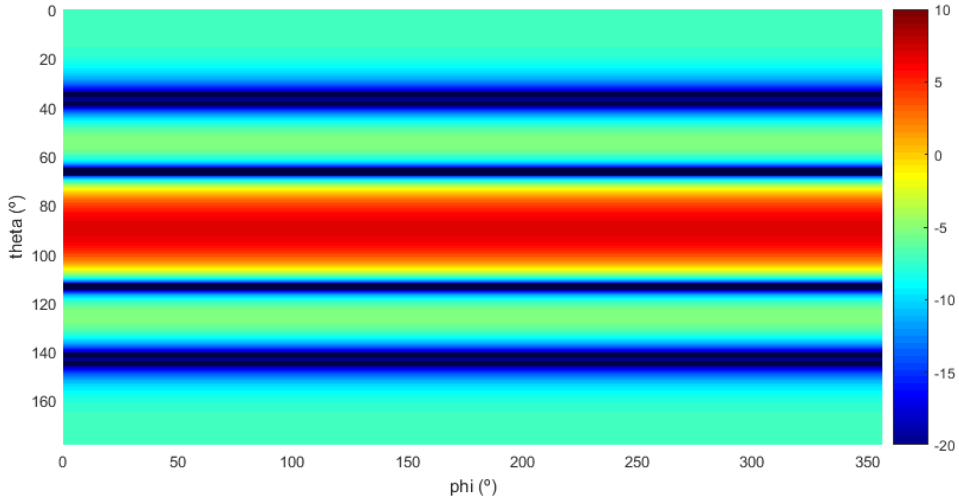

Figure 3.3: Directivity of a broadside array of isotropic antennas.

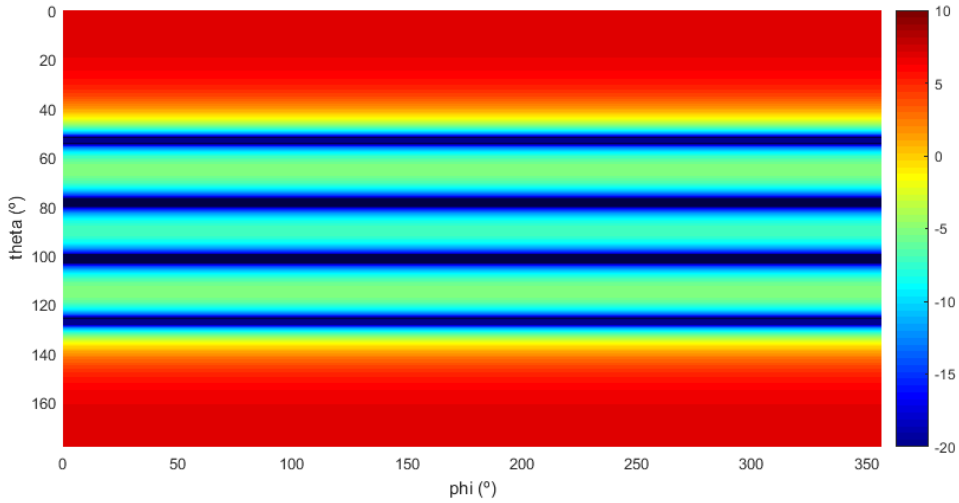

Figure 3.4: Directivity of an end-fire array of isotropic antennas.

3.2.3 Array of dipoles

Combining the two previous cases, the computation of the directivity is done for an array of dipoles placed along the z axis. To do this the same parameters has been employed and the results are shown in figures 3.5 and 3.6. Figure 3.5 shows a broadside configuration and figure 6 shows a pointing direction of 30º. The maximum directivity of these configurations is 7.1 dBi. In figure 3.7 the maximum directivity is shown for this array, which is the one used to compute the coverage efficiency. This maximum directivity is computed by taking the maximum of the directivity between all the configurations (changing β) for each direction (θ, ϕ).

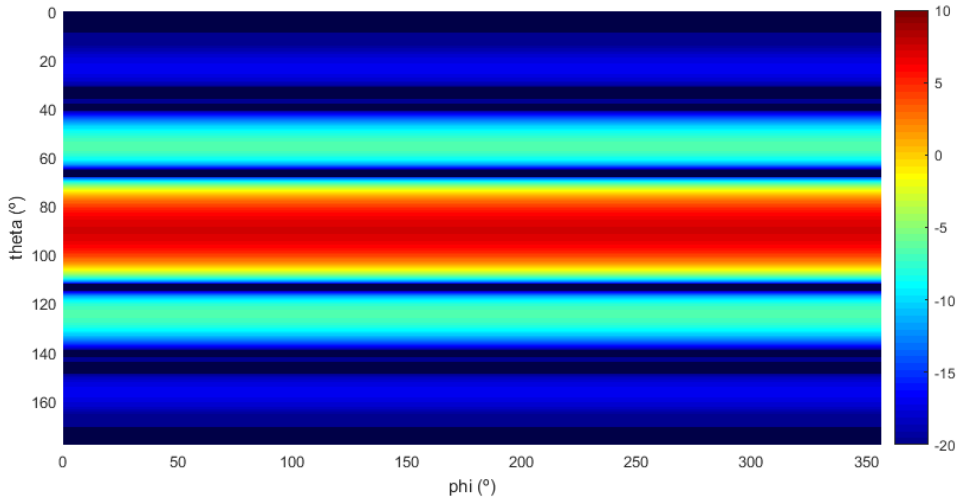

Figure 3.5: Directivity of a broadside array of dipoles.

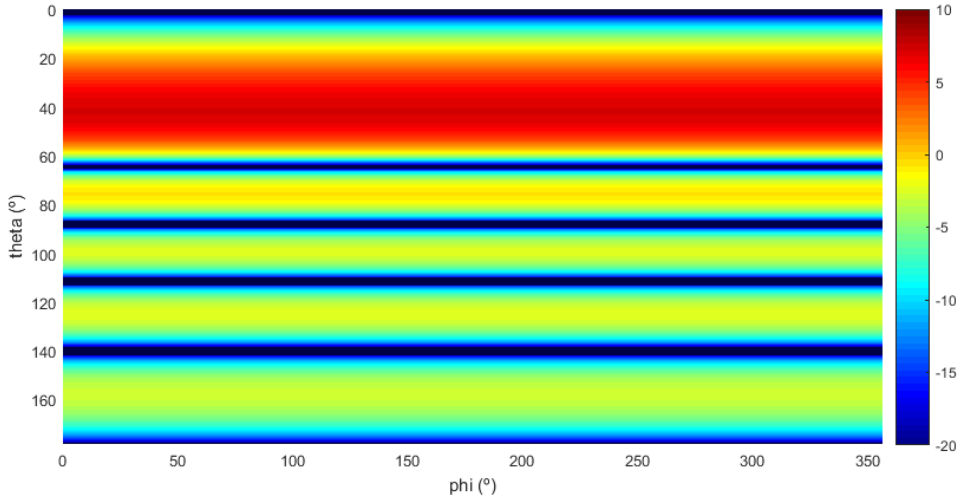

Figure 3.6: Directivity of an array of dipoles pointing to 30º.

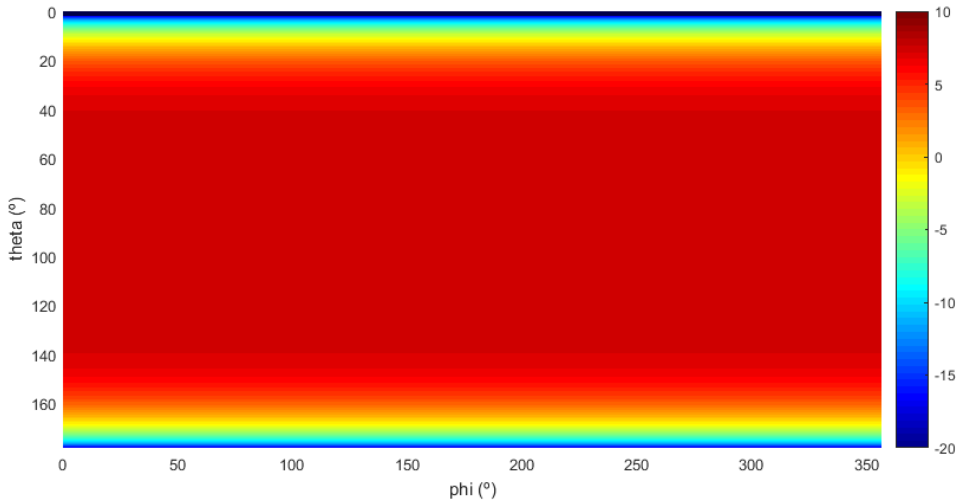

Figure 3.7: Maximum directivity in each direction obtained by changing the pointing angle of a dipole array.

3.2.4 Addition of the horizontal array

Until now the only array which has been analysed is the one placed in the side of the terminal, without the one on the top. In this section the results of the addition of the other array, placed horizontally on the top of the terminal.

However, there is other factor which has not been considered in this text. The mobile terminal is made of metal so all results here are valid for a ϕ angle from 90 º to 270 º, and they are only an approximation since the distance from the dipoles to the metal have a relevant influence in the directivity. The inclusion of this metal in the analysis has been considered but due to the difficult analytic solution that could have an antenna plus a metallic surface of finite dimensions they will be included later in an electromagnetic simulation.

To include another array, placed on the top of the terminal, the expressions 2.94 and 2.72 must be modified so they correspond to a dipole and an array placed along the *x* axis, as follows:

$$D(\theta,\phi) = 4\pi \frac{\left[\frac{\cos\left(\frac{k_0 l}{2}\sin\theta\cos\phi\right) - \cos\frac{k_0 l}{2}}{\sqrt{1-\sin\theta^2\cos\phi^2}}\right]^2}{\int_0^{2\pi}\int_0^{\pi}\left[\frac{\cos\left(\frac{k_0 l}{2}\sin\theta\cos\phi\right) - \cos\frac{k_0 l}{2}}{\sqrt{1-\sin\theta^2\cos\phi^2}}\right]^2 sin\,\theta\, d\theta d\phi} \tag{3.1}$$

$$(AF)_n = \frac{e^{j\frac{N-1}{2}\psi}}{N}\left[\frac{sin\frac{N}{2}\psi}{sin\frac{1}{2}\psi}\right] \quad with\ \ \psi = k_0 d\sin\theta\cos\phi + \beta \tag{3.2}$$

The results are fairly optimistic, since all angles are covered with a directivity close to the maximum one (7.3 dBi) and so the coverage efficiency is 100 % for minimum directivities lower than this value and 0% for higher minimum directivities. Note again, this result does not take into account the fact that the mobile terminal is made of conductor material.

3.2.5 Gain and efficiency

Antenna efficiency is not being considered in this chapter, so here we have used the directivity as the main metric. The input impedance varies with the length of the dipole as shown in equation 2.96 and, thus, it must be tuned to obtain low return losses so the efficiency is high. If the efficiency is too low, even if the directivity is higher we can face less gain than expected.

Since there is no evaluation of this efficiency in this procedure, the length of the dipole has been set to $\lambda/4$. This is a smaller value than the usual $\lambda/2$ but it may be closer to the final value of this length when the material or substrate had been chosen (the wavelength is shorter if the dielectric is not vacuum). In any case, the length of the dipole does not affect excessively its directivity.

3.2.6 CST simulation

To get more realistic results, an electromagnetic simulation has been done using the software CST STUDIO SUITE. This simulation has included the physical body of the mobile terminal made of PEC with dimensions of 40 mm x 100 mm x 1 mm. Furthermore, the dipoles have now a radius of $\lambda/50$ and each pole is separated from the other with a distance of $\lambda/50$. The distance between the arrays of dipoles and the mobile terminal is $\lambda/4$ to improve the directivity of the antennas. Others parameters are left as the previous cases (total length of each dipole is $\lambda/4$ and the separation between them is $\lambda/2$, the position and orientation are the same as in figure 1 and each array has 5 elements).

The results have been obtained from the CST simulation of each element of the array and combining each radiation pattern in MATLAB to obtain the radiation pattern of each array using several phase differences, the script used to do this can be seen in Appendix A, section A.6. In the figure 3.8 it is shown the maximum directivity achievable using this configuration as we change the phase difference of the feed of the arrays. As can be seen, the body of the mobile terminal plays a fundamental role in the radiation pattern of the antennas and now there is not possible to cover all angles with such a high directivity, near $\theta = 180º$ the radiation of the horizontal array is blocked by the mobile terminal and the vertical dipole array cannot radiate in that direction, and a similar situation occurs for angles near $\phi = 0º$. However, the overall directivity has improved, and now the maximum is 10.4 dBi. In the figure 3.9 it is possible to see the coverage efficiency as a function of minimum received gain and compare it with the previous case.

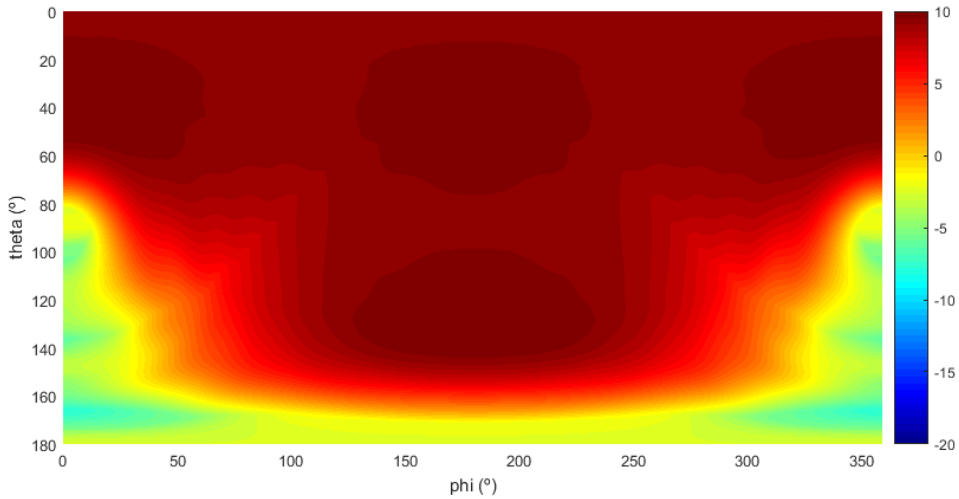

Figure 3.8: Maximum directivity in each direction using the CST simulation results.

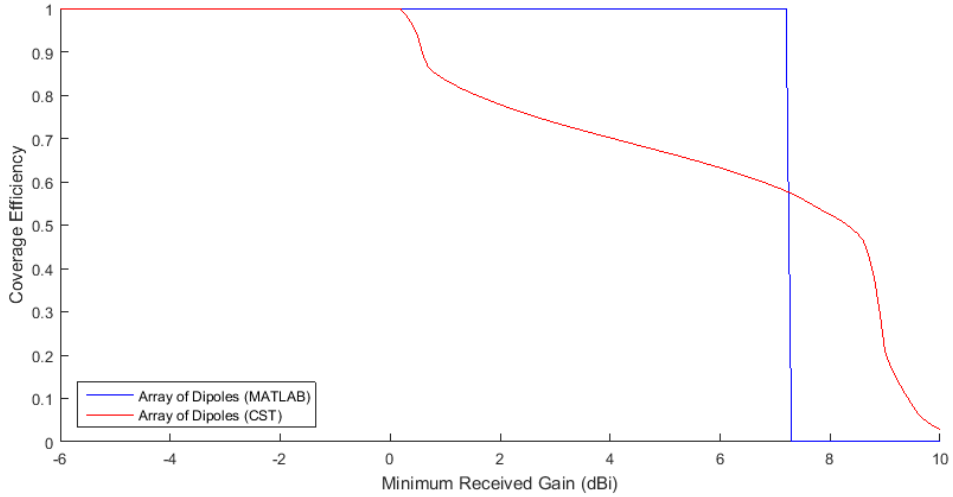

Figure 3.9: Comparison of the coverage efficiency as a function of minimum received gain between the MATLAB and CST simulation results.

3.3 Coverage Efficiency using different types of Antennas

This section has as objective to illustrate the coverage efficiency as it was done in the section 3.2, but using others antennas with different radiation patterns. It does not, however, explain the procedure step-by-step as it was done before and it shows the new antenna and its results.

3.3.1 Rotated Dipole

To explore a different solution without changing the previous configuration too much, let us study the performance of the same arrays when the orientation of the elements is rotated 90º in the *z* axis, keeping the rest of the dimensions and distances as before. The figure 3.10 shows the geometry of this new case of study.

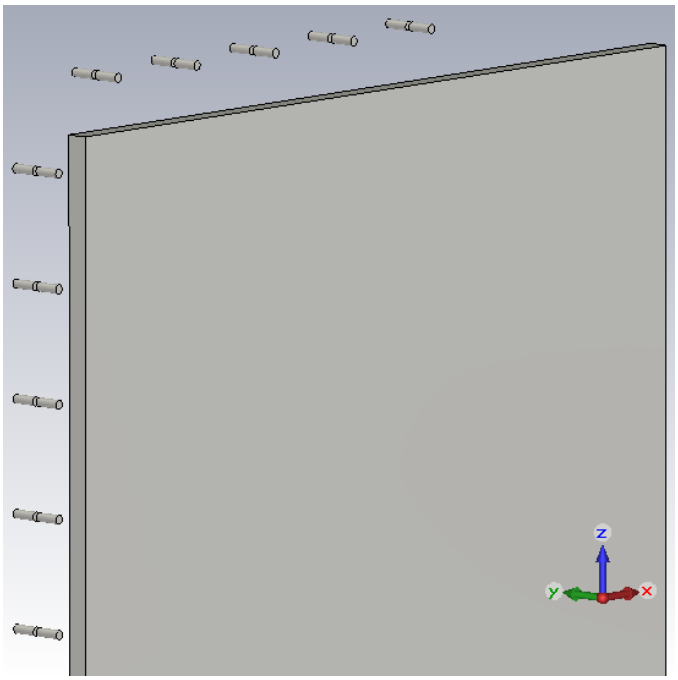

Figure 3.10: Geometry of the problem when the orientation of the dipoles is changed.

To follow the previous cases, a MATLAB simulation has been done first using the scrip from the Appendix A (see section A.3). These results do not take into account the body of the mobile terminal made of conductor material. However, in this new case, this conductor has less influence in the problem (because the dipoles are longer than its thickness) and so the MATLAB results may be more useful. The figure 3.11 shows the maximum directivity achievable for each direction using the MATLAB results and the figure 3.12 uses the CST simulation results. Finally, a comparison of the coverage efficiency between all previous cases is shown in figure 3.13.

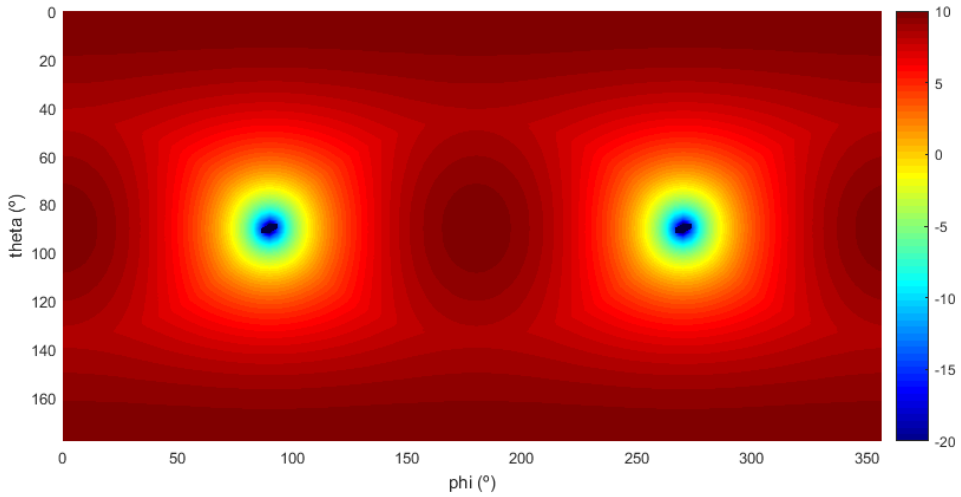

Figure 3.11: Maximum directivity in each direction changing the orientation of the dipoles in the MATLAB simulation.

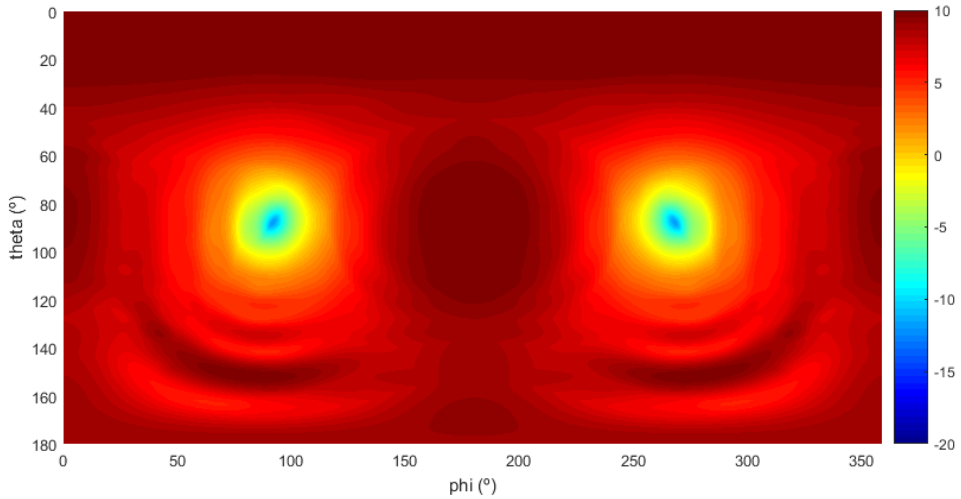

Figure 3.12: Maximum directivity in each direction changing the orientation of the dipoles using the CST simulation results.

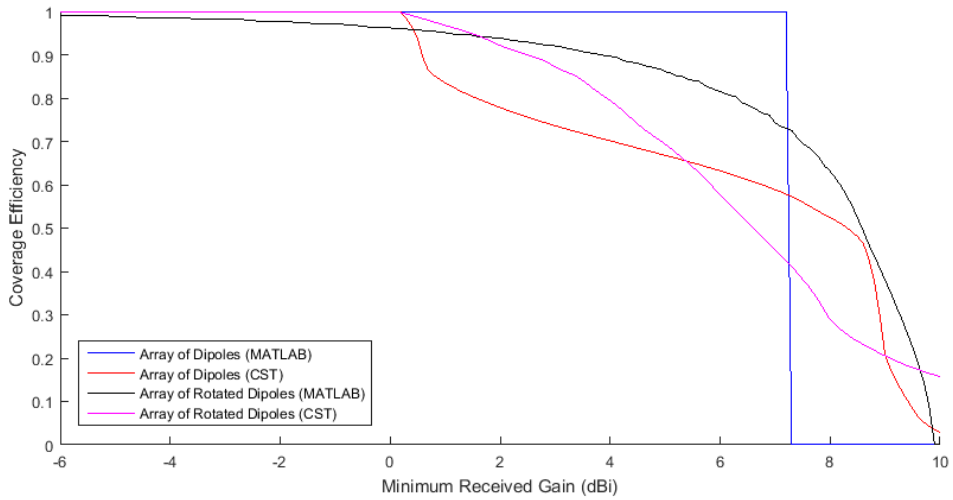

Figure 3.13: Comparison between the coverage efficiency as a function of the minimum received gain of all previous cases.

3.3.2 Slot Antenna

To do a comparison of different types of antenna, now the slot antenna will be used. The slot antenna is one of the most employed antennas due to its simplicity and compactness. On top of this, its radiation pattern is similar to the dipole so it is easy in this point of the study to evaluate another type of antenna.

The Babinet's principle shows that, for a thin slot, the far-zone electric field of the slot antenna is the same as the far-zone magnetic field of the dipole antenna so the results of the radiation pattern of the slot are the same as the rotated dipole, at least, theoretically, as was shown in the previous chapter, section 2.4. So that is why a new MATLAB simulation is not needed. The result of this simulation would be the same as the one of figure 3.11 and figure 3.13.

To make this case as similar to the dipoles one as possible, some parameters employed are the same: the distance between the body of the mobile phone and the antennas is quarter wavelength and the distance between each element of the array is half wavelength. However, if we used the same length of the dipole, the efficiency would be very low. To improve the efficiency the slot must be longer. If the slot is longer than half wavelength then the distance between each slot could not be half wavelength. That is why a substrate had to be used, with a dielectric with a relative permittivity of 3.55 and a height of 0.305 mm. The thickness of the slot is 0.035 mm. As a dielectric is used, the electric length of the slot is bigger and then it is possible to make it physically shorter so it fits in half wavelength. To maximise the efficiency, the length of the slot is 4.7 mm, its width is 0.2 mm, and the position of the port has been shifted 0.9 mm from the centre of the slot. In this case the efficiency was tuned because it could have a higher impact in the directivity of the antennas and to illustrate the need of the substrate.

In the figure 3.14 the geometry of this new case is shown. After computing the maximum directivity for each direction of both arrays and for each phase difference, the results can be seen in the figure 3.15, which resembles the figure 3.12 as expected. The maximum directivity achieved is 13 dBi. In the figure 3.16 the results of the coverage efficiency are compared to the previous cases.

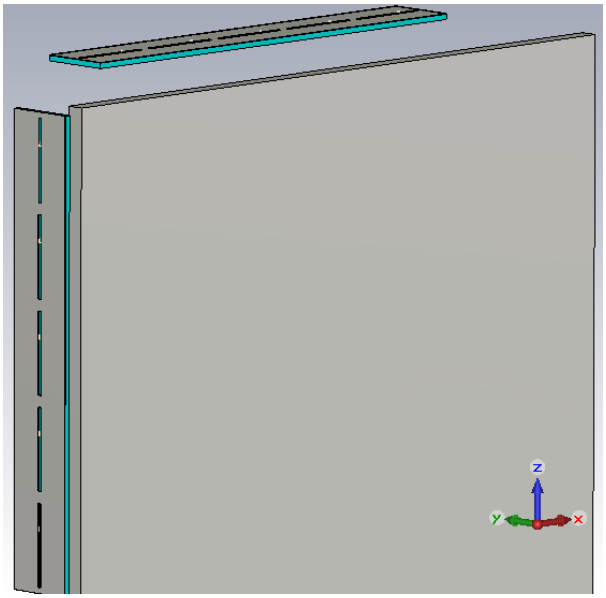

Figure 3.14: Geometry of the slot antenna array in the CST simulation.

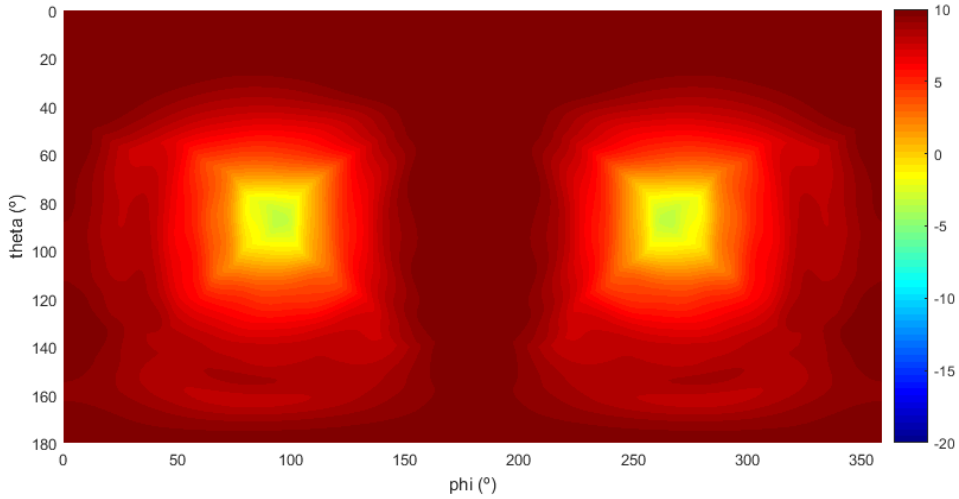

Figure 3.15: Maximum directivity in each direction of the slot antenna array using the CST simulation results.

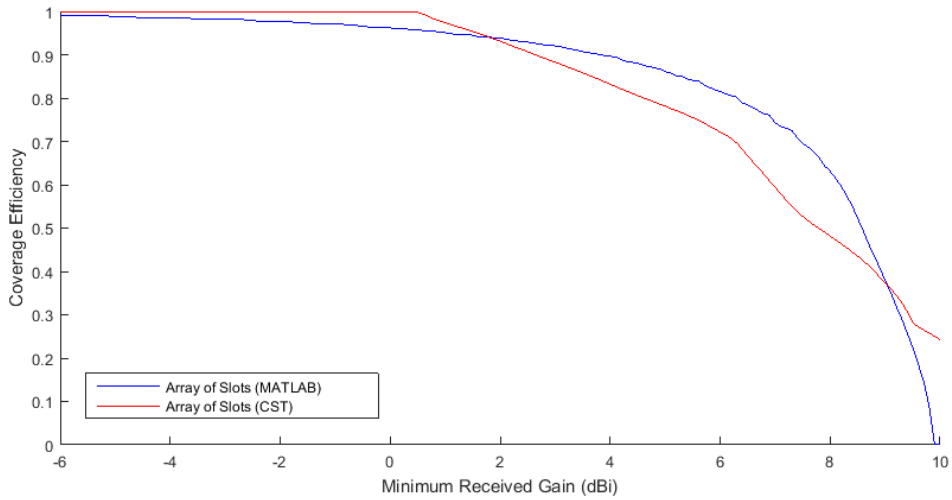

Figure 3.16: Comparison between the coverage efficiency as a function of the minimum received gain of the slot array.

3.3.3 Monopole Antenna

To continue with alternative antenna types let us study the case of the monopole antenna using the body of the mobile terminal as the ground plane. If the ground plane were endlessly large, the behaviour of the antenna would be the one shown in the section 2.5. However, the terminal would provide a rather small ground plane so the results may be very different.

Anyway, a MATLAB estimation using the dipole formula has been done, this is, as if the ground plane were infinitely large (See Appendix A, section A.4 to see the script). These results are shown in the figures 3.17 and 3.19, using the same length for the dipole as before and with them placed orthogonally to the surface of the edge of the terminal. It is possible to appreciate that there are two sections that are impossible to cover due the ground plane and antennas position and so the coverage efficiency is never more than 75%.

A CST simulation has been done next, with the radius of the monopoles set to 0.02 mm and the distance between the dipoles and the ground plane, where the port is situated, of 0.05 mm. The length of the monopole has been tuned slightly to minimise the return losses. It is clear in the results shown in figures 3.18 and 3.19 that the MATLAB simulation was not accurate at all, and it can be appreciated that the mobile terminal has a very significant impact in the results, not only because the ground plane is not as big as it should be, but also because of the surface field which appeared on the mobile terminal.

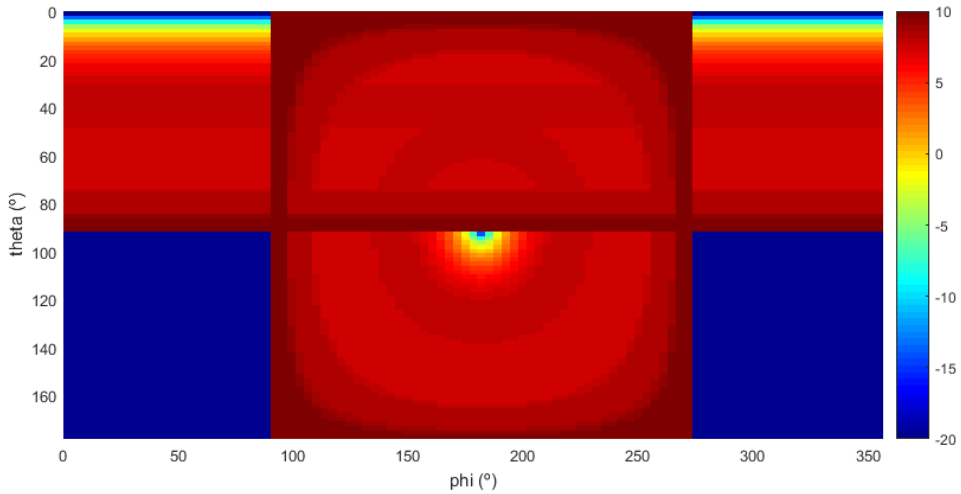

Figure 3.17: Maximum directivity in each direction using arrays of monopoles in the MATLAB simulation.

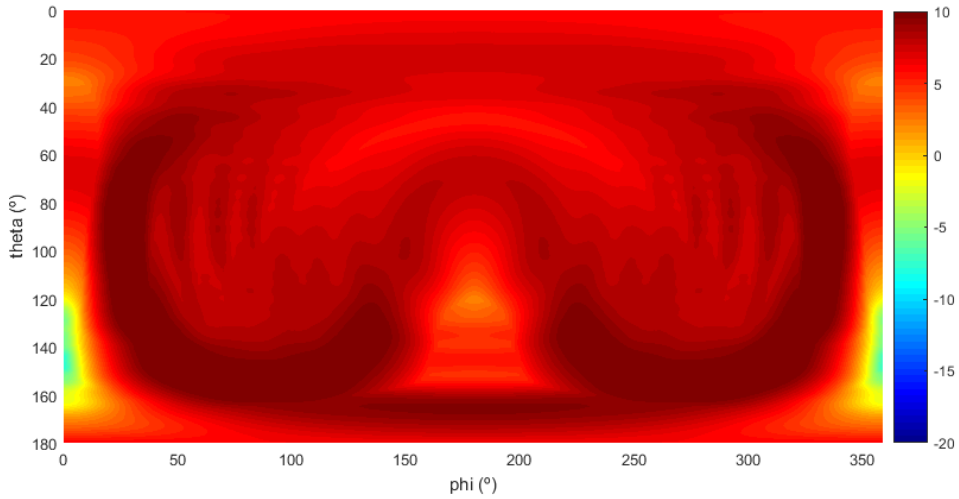

Figure 3.18: Maximum directivity in each direction of the monopole antenna array using the CST simulation results.

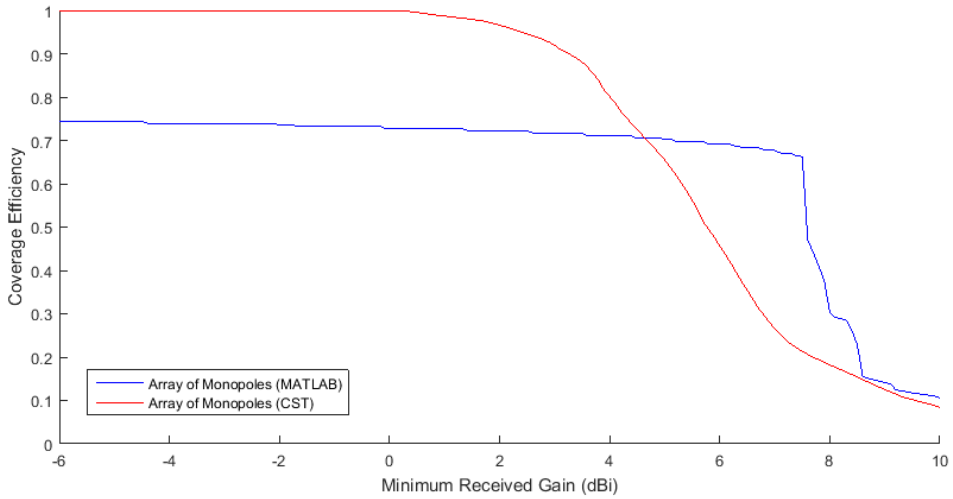

Figure 3.19: Comparison between the coverage efficiency as a function of the minimum received gain of the monopole array.

3.3.4 IFA Antenna

The next antenna studied is the Inverted-F Antenna (IFA) which is similar to the monopole antenna but folded so its length is shorter and it is easier to integrate. Its electromagnetic behaviour is also similar to the monopole so the MATLAB simulation would be the same as that one. The CST simulation has been done using the geometry of the antenna shown in the figure 3.20, where the distances have been tuned to obtain low return losses, as usual. The figures 3.21 and 3.22 show the obtained results, which are slightly different than the ones from the monopole.

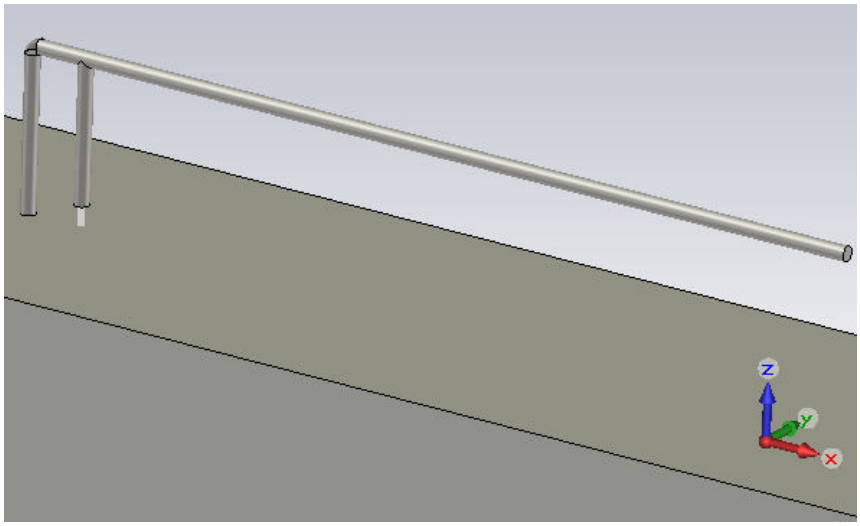

Figure 3.20: Geometry of the IFA in the CST simulation.

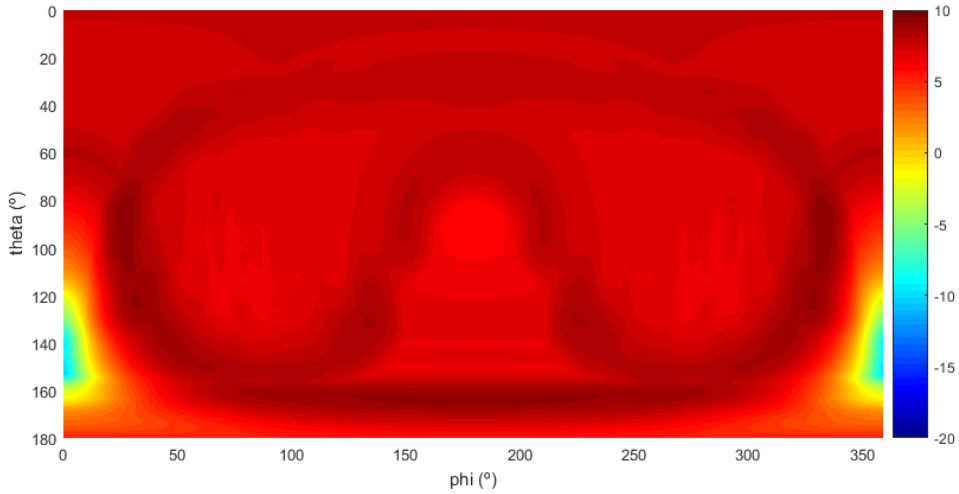

Figure 3.21: Maximum directivity in each direction of the IFA array using the CST simulation results.

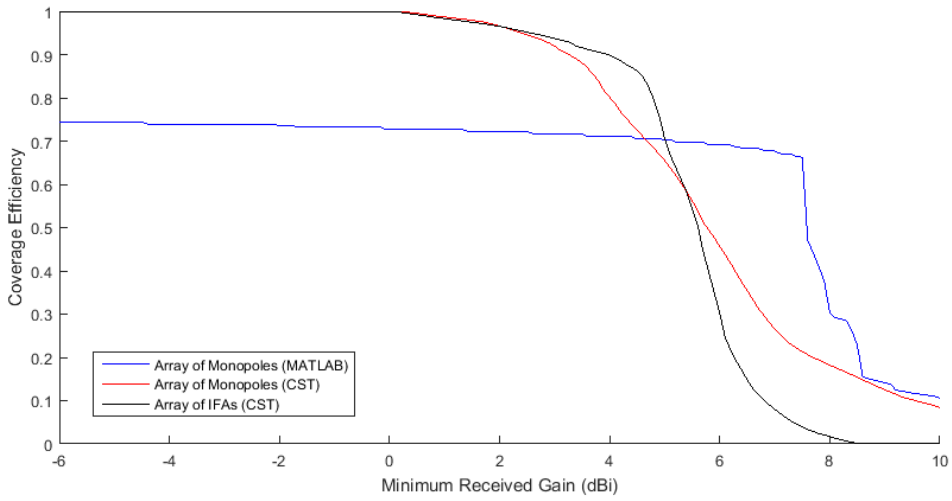

Figure 3.22: Comparison between the coverage efficiency as a function of the minimum received gain of the monopole and IFA arrays.

3.3.5 Rectangular Patch Antenna

In this section another type of antenna will be analysed and simulated to continue with the comparison. Microstrip antennas have been being used lately in communication applications because they are very inexpensive, simple and their performance is sufficient in most cases. Given its popularity, it is crucial to compare the performance of an array of patches with the ones of dipoles of the previous cases. The first microstrip antenna that is dealt with here is the rectangular patch, the most simple of them.

In a microstrip antenna design the chosen substrate plays a significant role. However, since some of the previous cases (dipole antennas, monopole, IFA) did not use any substrate, we will not know exactly how much this changes the results when they are compared to the previous ones. The substrate used here will have a dielectric with a relative permittivity, of 3.55 and height of 0.305 mm. All metal will have a thickness of 0.035 mm and will be simulated as a PEC.

Once the substrate is chosen, the design follows as depicted in the section 2.7.3. The length of the patch should not affect the radiation pattern but is referred here to know the geometry of the antenna. It does affect, however, the efficiency but we are not taking it into account yet, as stated before. The results of these steps are $W = 3.55$ mm and $L = 2.72$ mm, a bit larger than a $\lambda/4$ dipole (2.68 mm).

To simulate in MATLAB an array of this antenna it is necessary to know how the radiation intensity changes with the orientation. To do so, the result from equation 2.116 is used, which is only valid for $270º > \phi > 90º$, since the ground is much larger than the patch. Towards others directions the antenna will not radiate, theoretically. In the figure 3.23 the directivity in each direction is shown. It can be seen that is very similar to the radiation pattern of a single dipole (figure 2) when $270º > \phi > 90º$, and the maximum directivity is 5dBi.

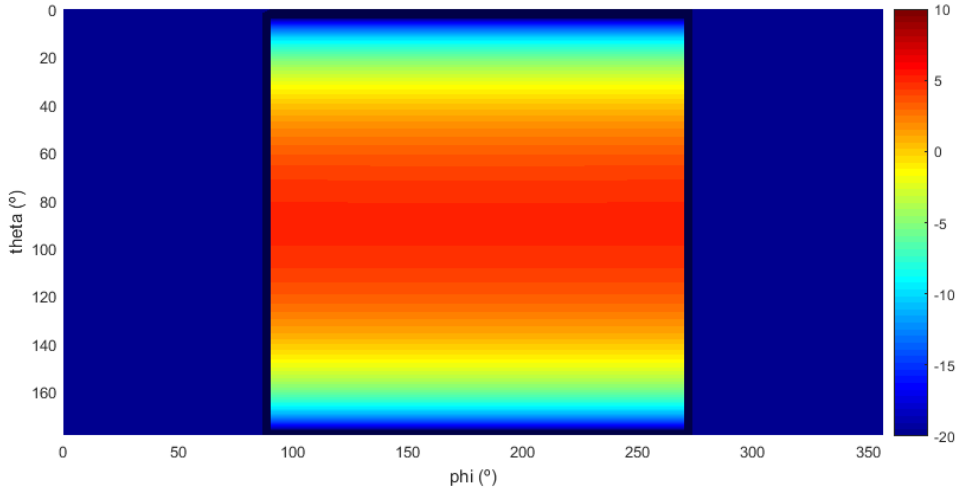

Figure 3.23: Directivity in each direction for a single rectangular patch in dBi.

Before we study the rectangular patch array, a CST simulation of a single patch has been done, so it is possible to see the differences between the radiation pattern of a ideal rectangular patch and the one that it could be implemented in the mobile terminal. The structure of this patch is shown in the figure 3.24. The ground plane has 4 mm of length and its width is $\lambda/2$, 5.65 mm. The feeding in this simple case is just a discrete port between the patch and the ground plane, situated in a way that the return losses are minimised at the desired frequency. The figure 3.25 shows the directivity for each

direction in this CST simulation. It can be seen that lobes appear and that the radiation pattern is not as uniform as in figure 3.23, using the expression from the cavity model method. The maximum directivity now it is higher, as expected, and its value is 6.7 dBi.

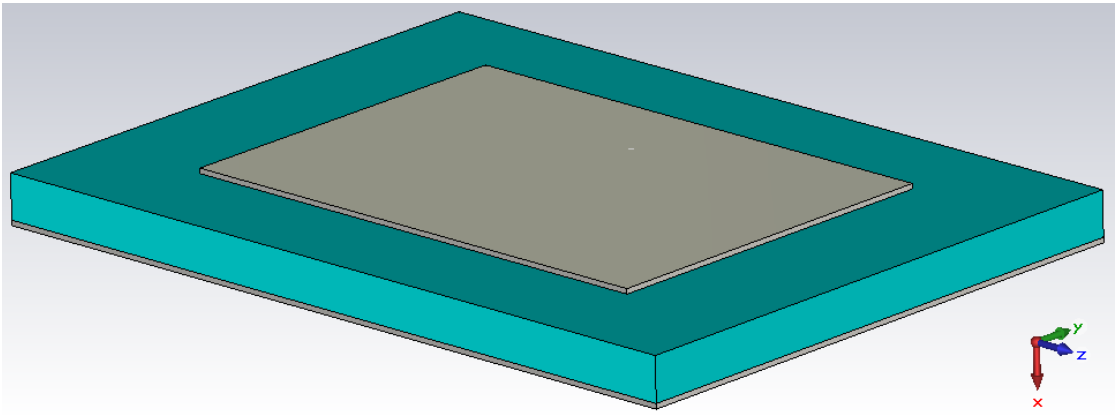

Figure 3.24: Geometry of a single patch in the CST simulation.

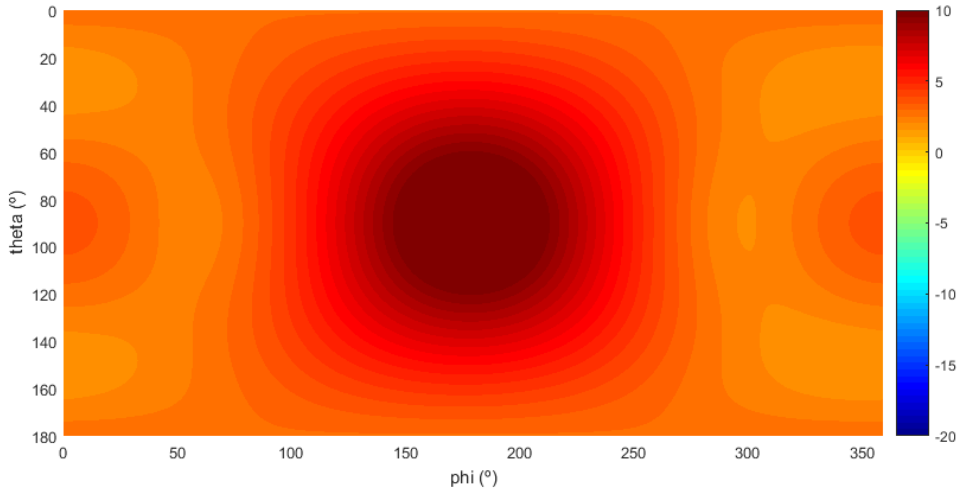

Figure 3.25: Directivity in each direction for a single rectangular patch in dBi using the CST simulation.

The next step is to use this patch to create a steerable array, as in the previous cases. To do that we need to compute the array factor, which is the same as before (the same spacing between elements is used, $\lambda/2$), and the expression of the directivity of the patch situated along the *x* axis,

$$D(\theta,\phi) = 4\pi \frac{F(\theta,\phi)^2}{\int_0^{2\pi}\int_0^{\pi} F(\theta,\phi)^2 \sin\theta \, d\theta d\phi},$$
$$with\ F(\theta,\phi) = \frac{\sqrt{1-\sin^2\theta\cos^2\phi}}{\cos\theta\sin\theta\cos\phi}\sin\left(\frac{k_0 h}{2}\cos\theta\right)\sin\left(\frac{k_0 W}{2}\sin\theta\cos\phi\right) \quad (3.3)$$

this way, the radiation pattern is computed for two arrays, one along the *z* axis and the other along the *x* axis, and then, the maximum achievable directivity in each direction changing the phase difference of the feed is calculated using MATLAB (the script can be seen in the Appendix A, section A.5), shown in figure 3.26, and using it, the coverage efficiency, shown in figure 3.29 (as a comparison with the other cases). In the figure 3.26 it is possible to see that there are two zones where is impossible to get any radiation. This happens because this patch with infinite ground plane do not radiates

downwards and the position of the arrays then leaves these two zones completely uncovered.

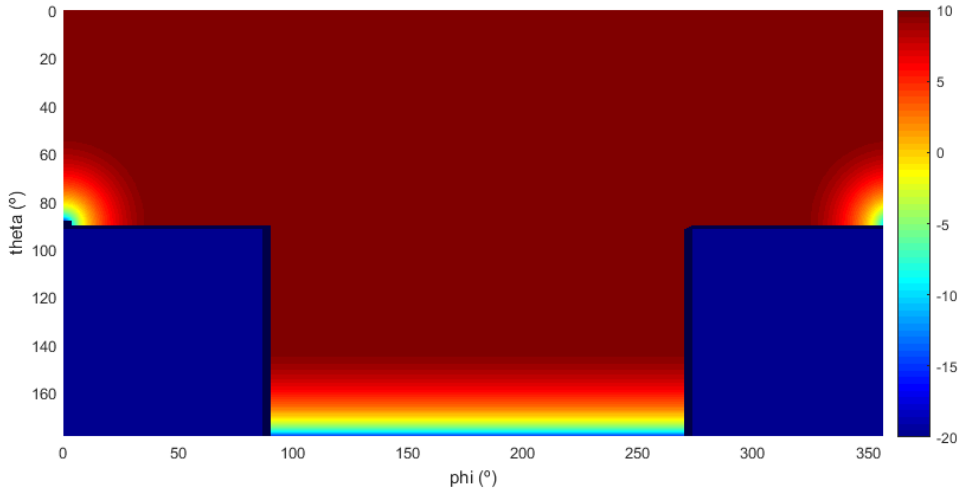

Figure 3.26: Maximum directivity in each direction using arrays of patches in the MATLAB simulation.

To conclude this section, a CST simulation of these arrays has been done so we can study the repercussion of the mobile terminal and the real rectangular patches. The geometry of the problem has been chosen in a way that the results could be comparable with the ones from the dipoles, so the distance between the mobile terminal and the arrays is $\lambda/4$ and, of course, the dimensions of the mobile terminal are also the same as before. A picture with this geometry is the figure 3.27. The results of the maximum directivity are shown in the figure 3.28 and the comparison of the coverage efficiency in the figure 3.29. The difference between the MATLAB and CST simulations is mainly caused by the imprecision of the cavity model and the radiation that goes through the ground plane, which is not zero in the real case.

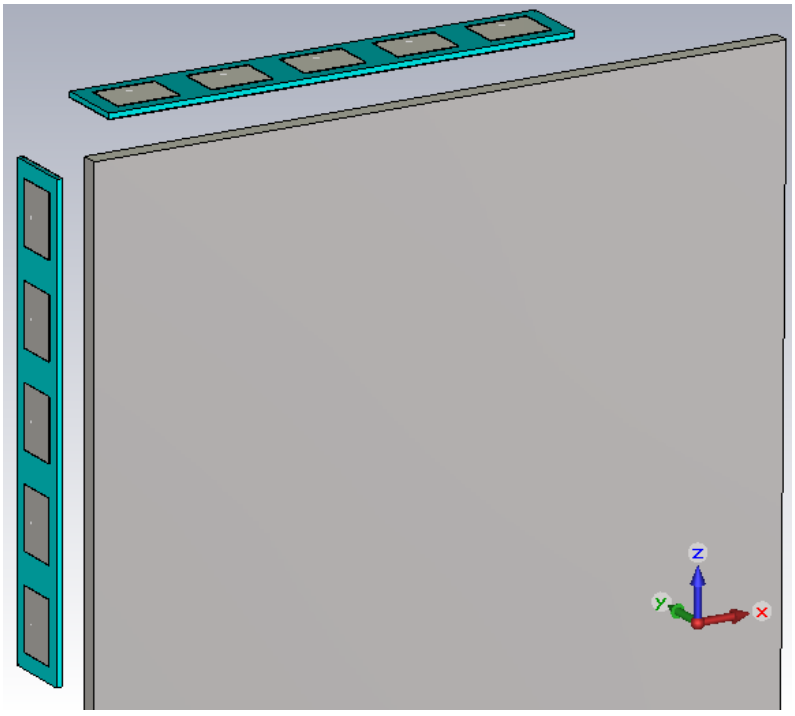

Figure 3.27: Chosen geometry of the patch arrays in the CST simulation.

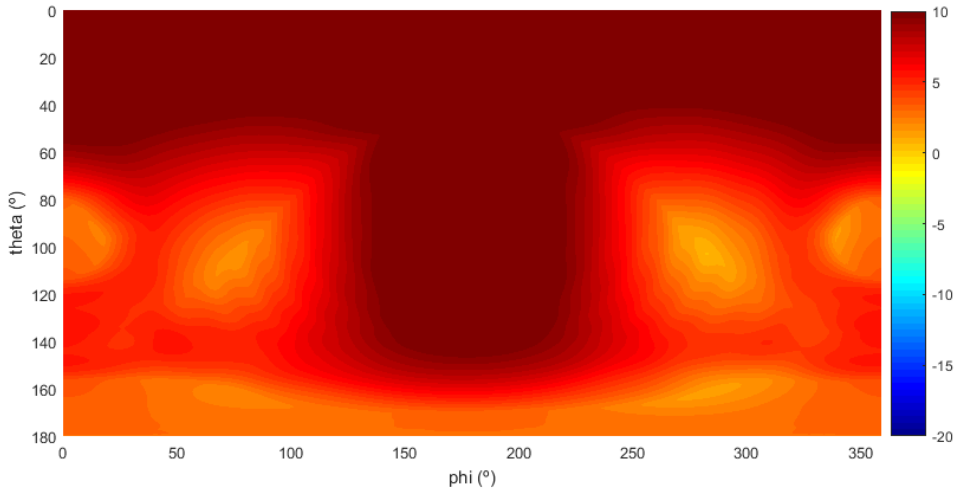

Figure 3.28: Maximum directivity in each direction using arrays of patches in the CST simulation.

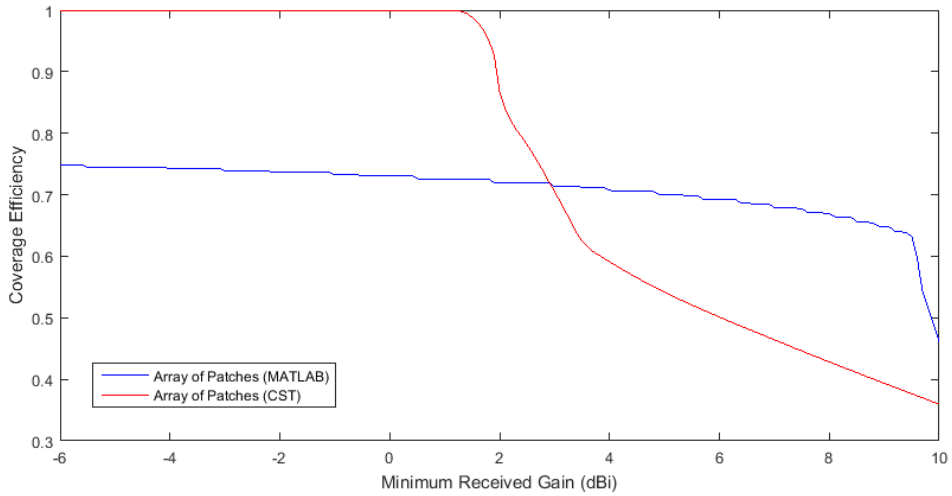

Figure 3.29: Comparison between the coverage efficiency as a function of the minimum received gain of the patch array.

3.3.6 Conclusions

As a summary, figure 3.30 shows the results of the CST simulations of all previous cases to discuss which types could be better than others. The monopole antenna and, especially, the IFA are very good when the coverage efficiency is high (> 85%), which may be the most interesting cases, however, the performance of these antennas are not very good compared to the others when the coverage efficiency is lower. The slot antenna may be the best of these options since has good performance overall, surpassing most of the other types of antennas along all the coverage efficiencies. The rotated dipoles offer similar performance to the slot but slightly lower. The patch antenna has too high directivity to give good coverage efficiency and the effect of the mobile terminal for the dipole antenna worsens excessively its performance, making these two types of antennas the worst options.

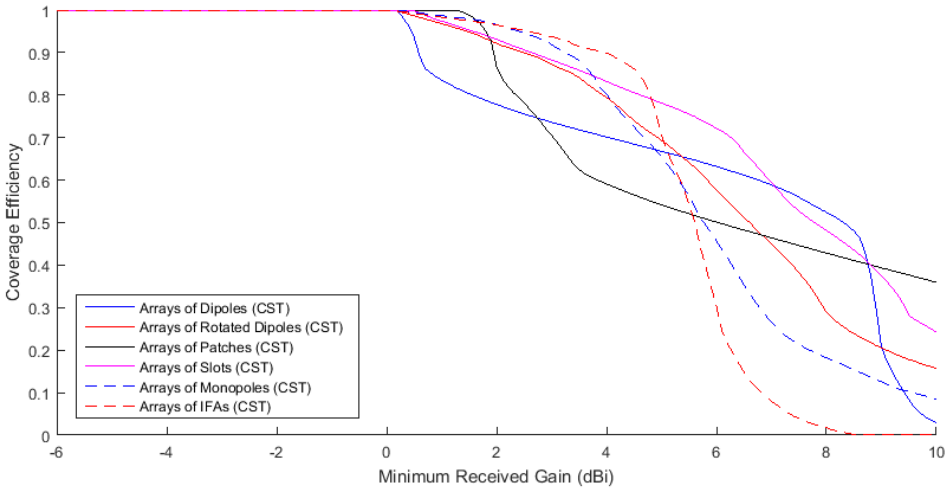

Figure 3.30: Comparison between the coverage efficiency as a function of the minimum received gain of all previous cases for the CST simulation.

3.4 Hybrid Arrays

In an attempt to improve the previous coverage efficiencies, two arrays of different types of antennas are going to be used in a way that the radiation patterns complement each other. To do this, it is not enough to pick the types of antennas with the best results obtained so far, but the ones that could lead to better results.

3.4.1 Dipole and Rotated Dipole Arrays

The dipole and rotated dipole types of antenna complement each other perfectly and thus are a simple and interesting case to start with the hybrid arrays. Using this two arrays there are two possible configurations, one where the array of dipoles is the horizontal array, at the top of the mobile terminal, and the array of the rotated dipoles is the vertical array, at the side of the terminal. The other configuration would be the reverse one, with the rotated dipole array at the top of the body of the terminal and the dipole array at the side of the terminal. The geometries of these two configurations are shown in the figures 3.31 and 3.32, respectively.

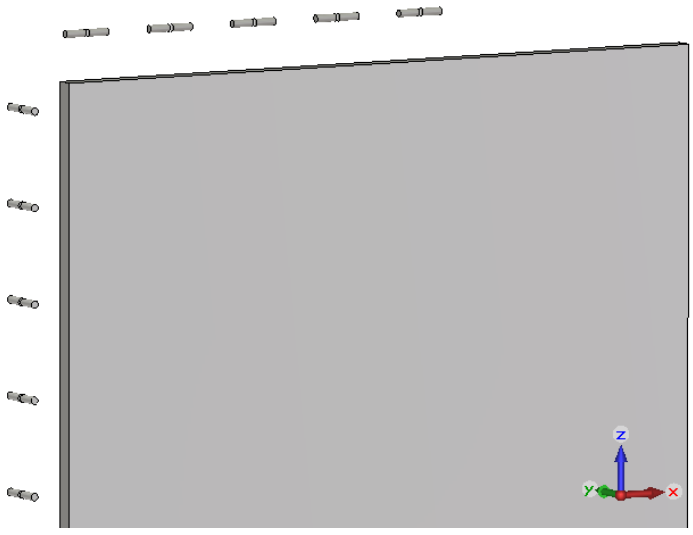

Figure 3.31: Geometry of the hybrid array configuration of dipole array (horizontal) and rotated dipole array (vertical) in CST.

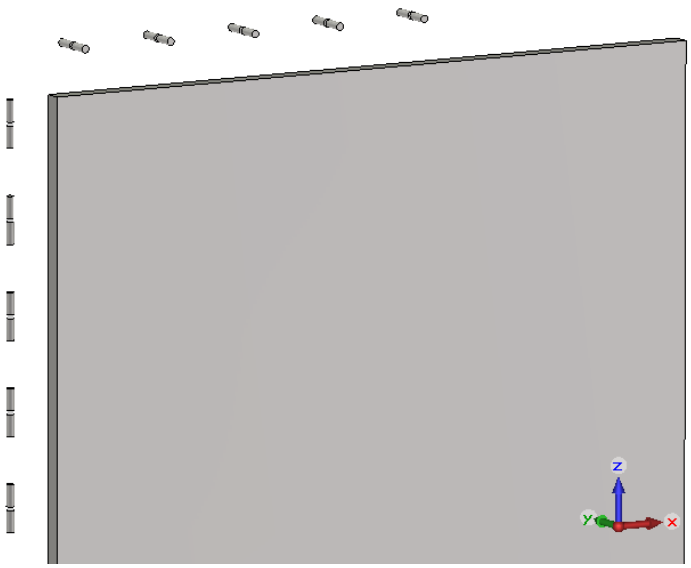

Figure 3.32: Geometry of the hybrid array configuration of rotated dipole array (horizontal) and dipole array (vertical) in CST.

Once these configurations are simulated using CST and in the same conditions as the previous ones, the directivity is shown in the figures 3.33 and 3.34. The coverage efficiency of both cases is compared to the results of non-hybrid dipoles configurations in figure 3.35.

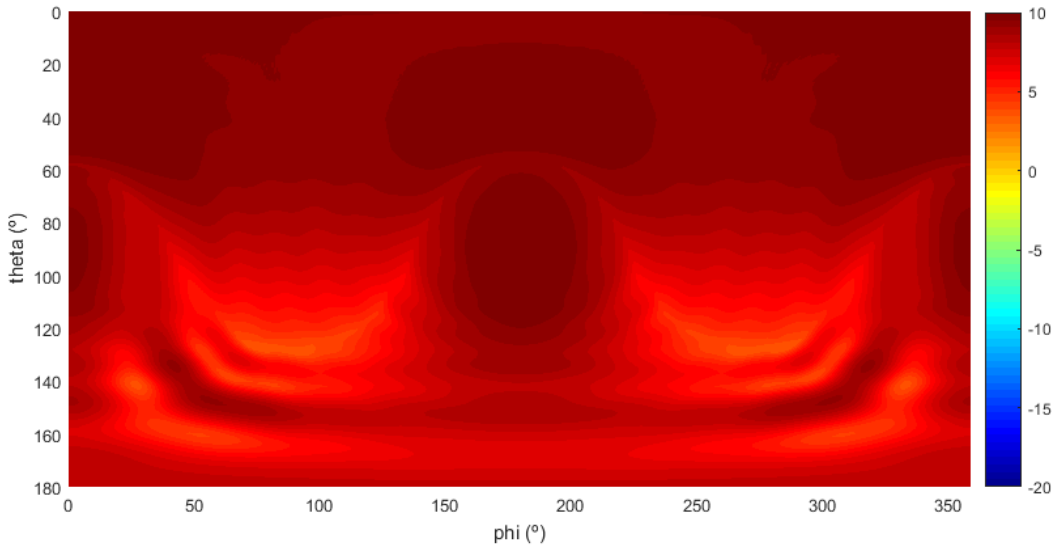

Figure 3.33: Maximum directivity in each direction using the hybrid array configuration of dipole array (horizontal) and rotated dipole array (vertical) in CST.

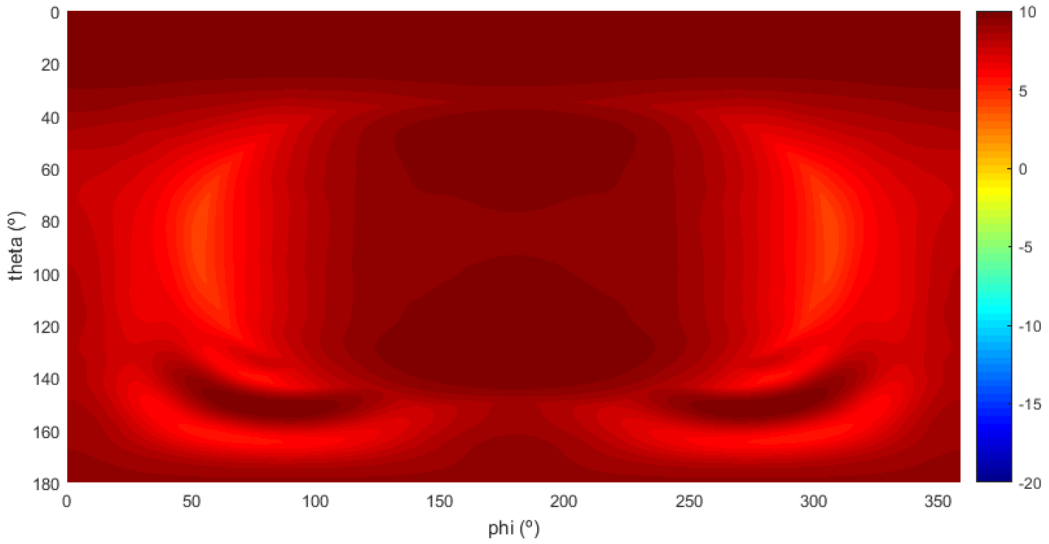

Figure 3.34: Maximum directivity in each direction using the hybrid array configuration of rotated dipole array (horizontal) and dipole array (vertical) in CST.

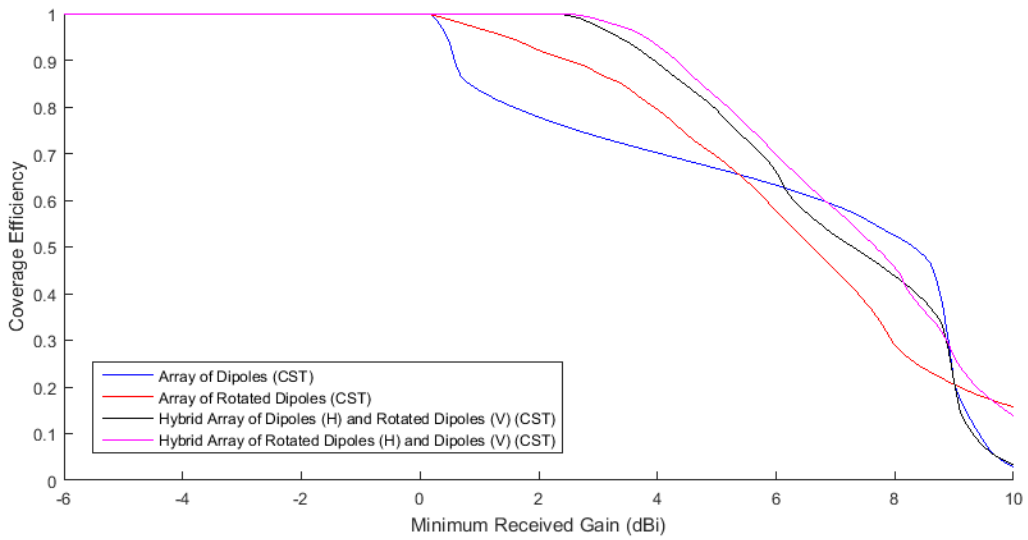

Figure 3.35: Comparison between the coverage efficiency as a function of the minimum received gain of the dipoles and hybrid dipoles cases.

3.4.2 Dipole and Slot Arrays

Since the slot antenna used here has a similar radiation pattern than the rotated dipole, the slot antenna and the dipole antenna make a good couple of antennas to use a hybrid array configuration. Again, there are two possible solutions: the slot as the horizontal array with the dipole as the vertical array and vice versa. These two configurations are shown in the following figures 3.36 and 3.37.

Figure 3.36: Geometry of the hybrid array configuration of slot array (horizontal) and dipole array (vertical) in CST.

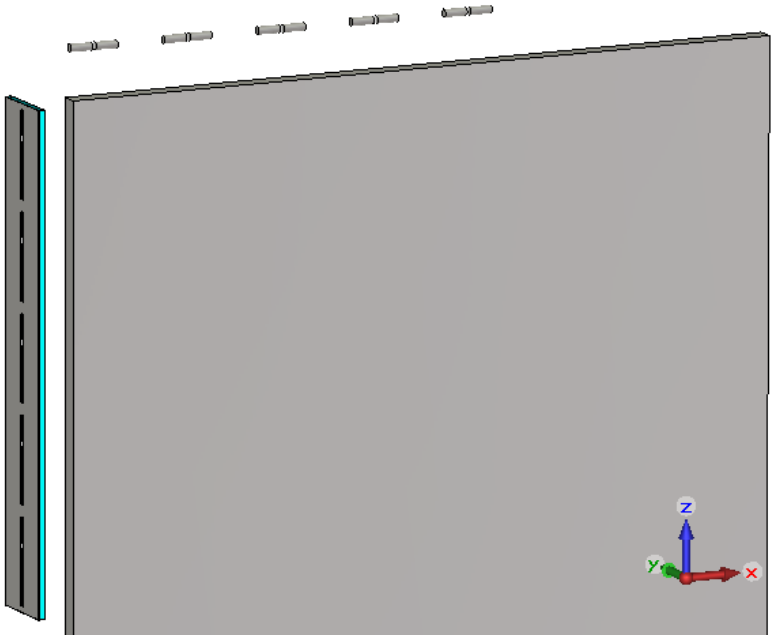

Figure 3.37: Geometry of the hybrid array configuration of dipole array (horizontal) and slot array (vertical) in CST.

After doing the CST simulation, computing the directivity and plotting the coverage efficiency in the figures 3.38, 3.39 and 3.40, it is possible to see that the first configuration (slots as the horizontal array and dipoles as the vertical array) is significantly better than the reverse one. This is caused by how the radiation pattern of the dipole and slot complement each other in a more effective way in the first case than in the later one.

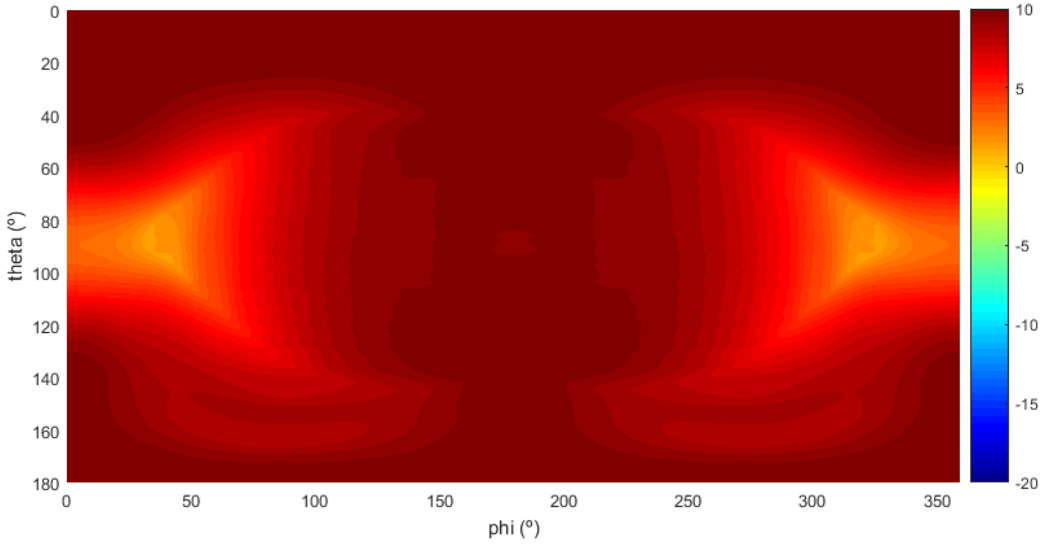

Figure 3.38: Maximum directivity in each direction using the hybrid array configuration of slot array (horizontal) and dipole array (vertical) in CST.

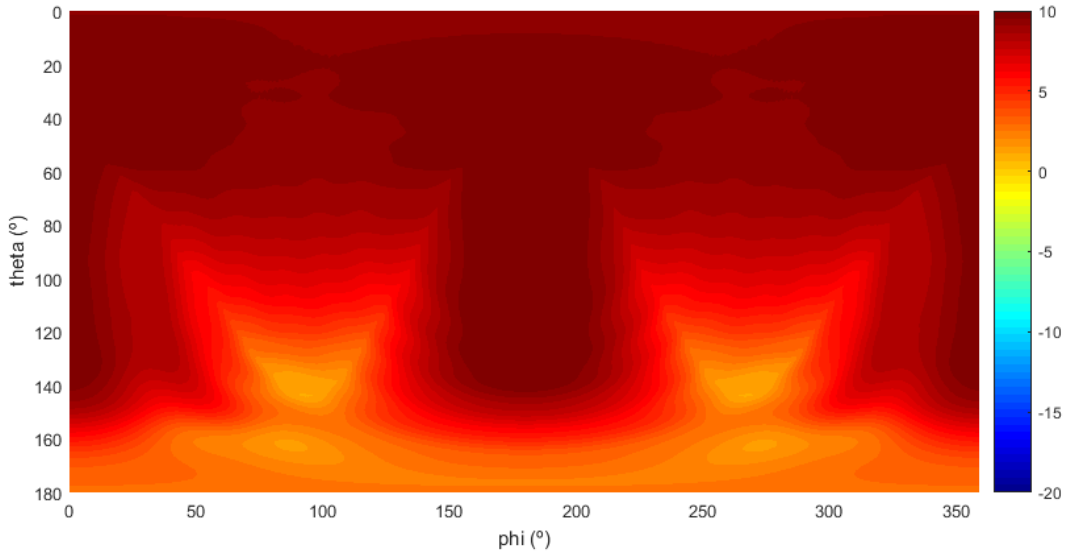

Figure 3.39: Maximum directivity in each direction using the hybrid array configuration of dipole array (horizontal) and slot array (vertical) in CST.

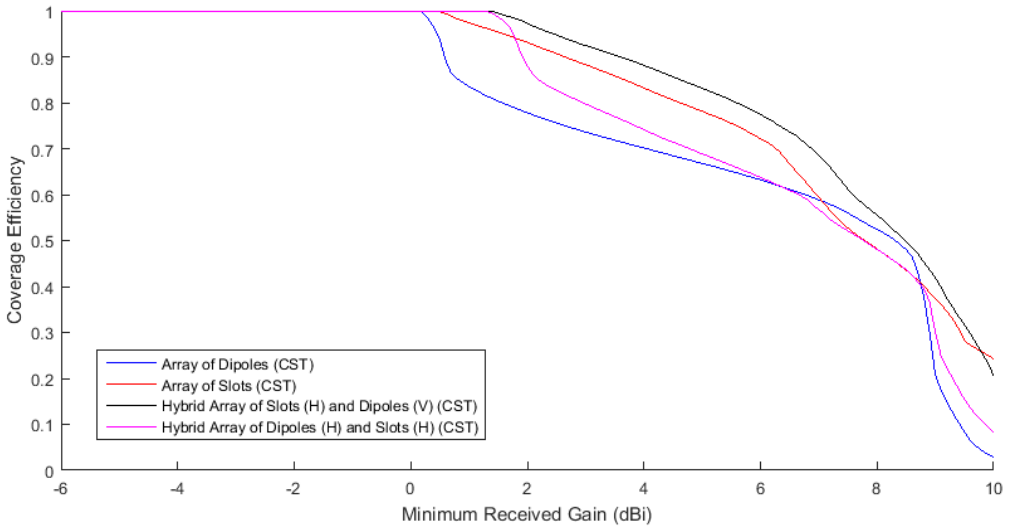

Figure 3.40: Comparison between the coverage efficiency as a function of the minimum received gain of the dipoles and slots and hybrid dipoles with slots cases.

3.4.3 Dipole and Patch Arrays

In an attempt to improve the performance of the patch array regarding coverage efficiency, in this section it is paired with the dipole array. They are placed in a way that complement each other as much as possible given the two geometries shown in the figures 3.41 and 3.42, being the first the one that uses the patch array as the horizontal array and the dipole array as the vertical array and the second using the dipole array as the horizontal array and the patch array as the vertical array. The results of the directivity from the CST simulation are shown in the figures 3.43 and 3.44 for each case, and the coverage efficiency can be seen in the figure 3.45.

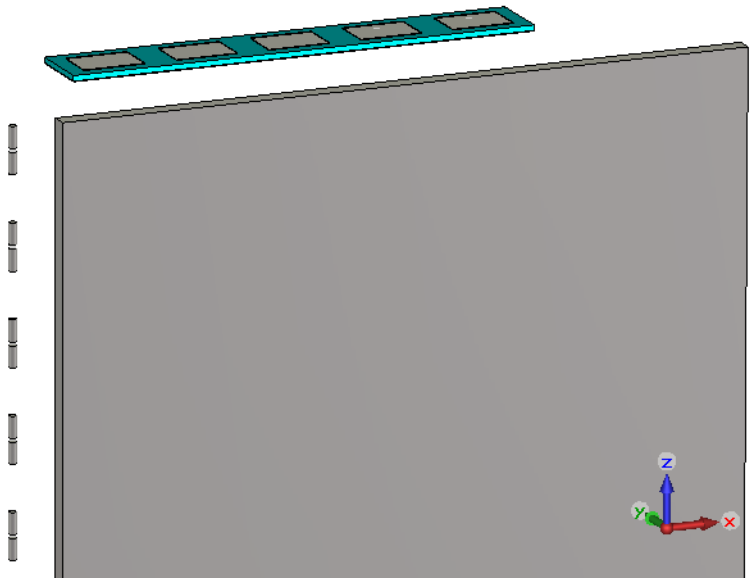

Figure 3.41: Geometry of the hybrid array configuration of patch array (horizontal) and dipole array (vertical) in CST.

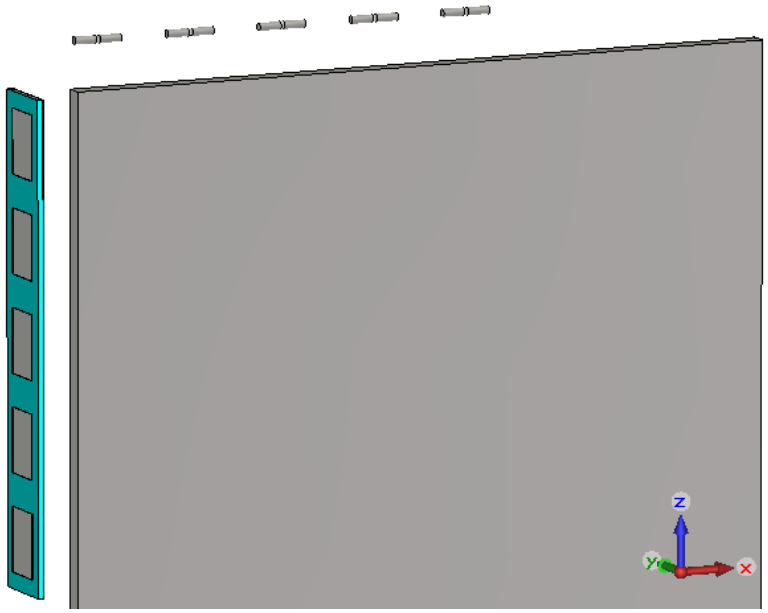

Figure 3.42: Geometry of the hybrid array configuration of dipole array (horizontal) and patch array (vertical) in CST.

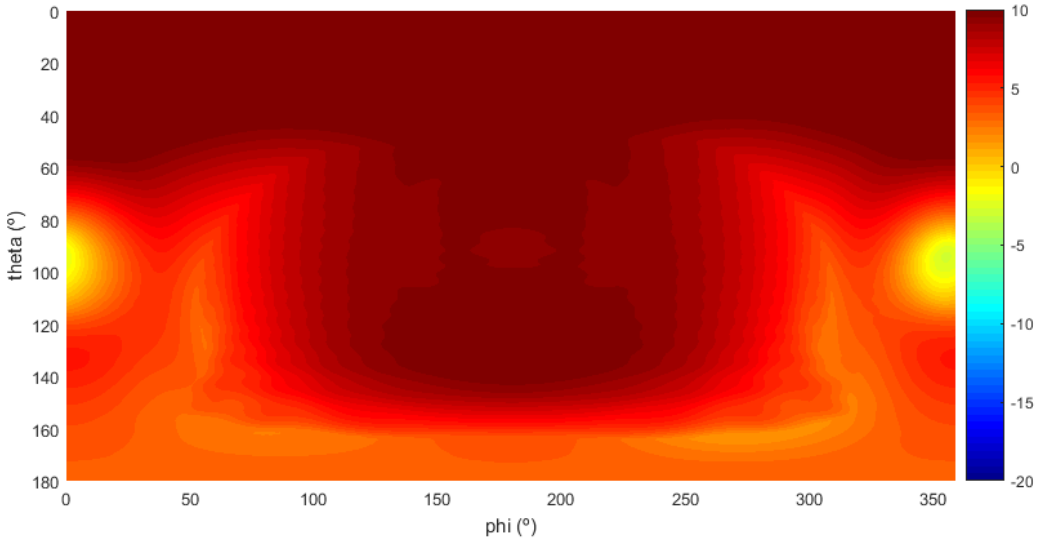

Figure 3.43: Maximum directivity in each direction using the hybrid array configuration of patch array (horizontal) and dipole array (vertical) in CST.

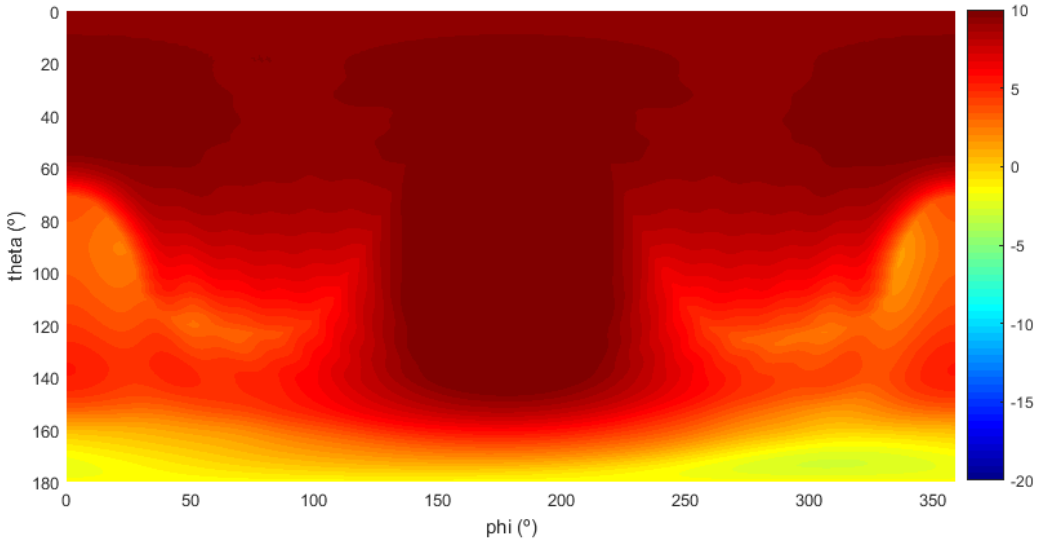

Figure 3.44: Maximum directivity in each direction using the hybrid array configuration of dipole array (horizontal) and patch array (vertical) in CST.

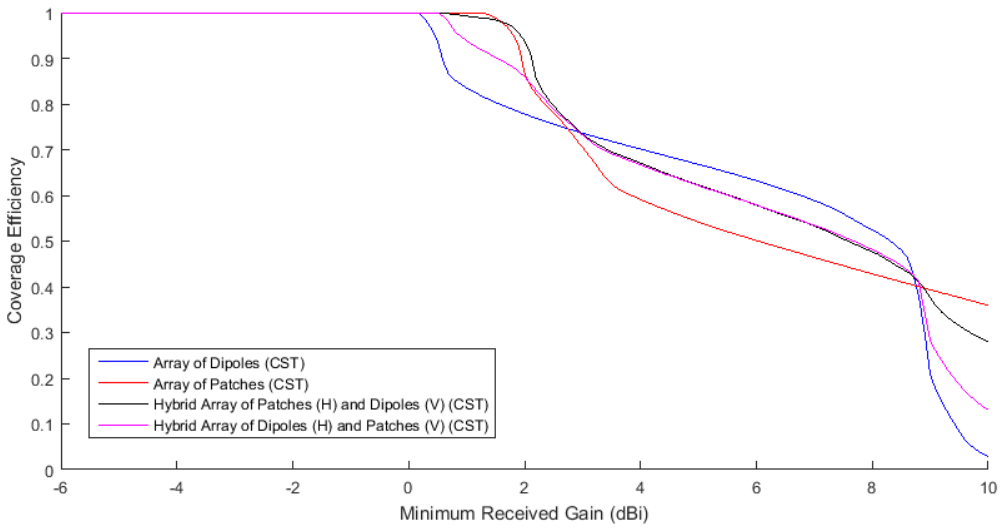

Figure 3.45: Comparison between the coverage efficiency as a function of the minimum received gain of the dipoles and patches and hybrid dipoles with patches cases.

3.4.4 Hybrid Array Conclusions

As a summary of this section, a comparison between all CST simulations is shown in figure 3.46. It has been shown in previous figures that the usage of hybrid array configurations can improve slightly the coverage efficiency. In figure 3.46 it is possible to see that the best overall coverage efficiency is achieved when the hybrid array configuration is composed of slots in the horizontal array and dipoles in the vertical one. However, the best configuration for higher coverage efficiency (85% and up) is the one using rotated dipoles and dipoles respectively.

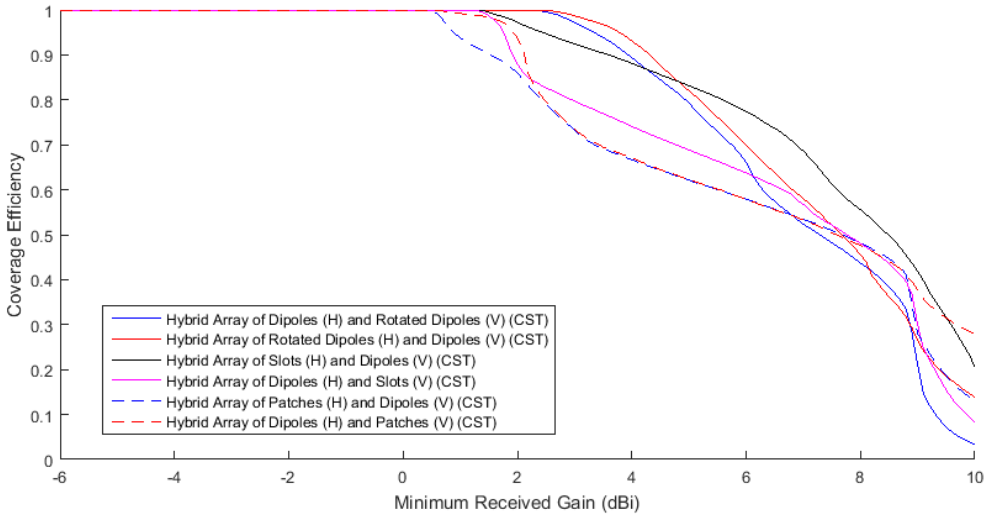

Figure 3.46: Comparison between the coverage efficiency as a function of the minimum received gain of all hybrid array configurations.

3.5 Final design

In order to provide a definite design and a physical realisation of the work of this chapter, a final design using the results above is attempted. To be able to measure the coverage efficiency of a physical antenna of these characteristics with the available equipment, the working frequency is going to be lowered to 5 GHz, increasing the size of the mobile terminal and antennas by a factor of 5.6 (which is 28/5), to emulate the behaviour that it would have at 28 GHz.

Also, to give a final value of the achievable gain of the prototype, all three arrays (top and both sides) are going to be used, where the side arrays 8 elements and the top array will have 12 elements. Although the hybrid array of slots and dipoles seems to have better results, the dipoles are easier to fabricate than the slots in the position studied here, so the type of antenna used is going to be the hybrid array of rotated dipoles (top side array) and dipoles (lateral sides arrays). Figure 3.47 shows the geometry of this final design where the placed dipoles can be seen.

At the time of writing this, the simulation of this last design is not done yet due to its longer duration (it has 28 elements in total). After the simulation, it is planned to fabricate a prototype and measure it.

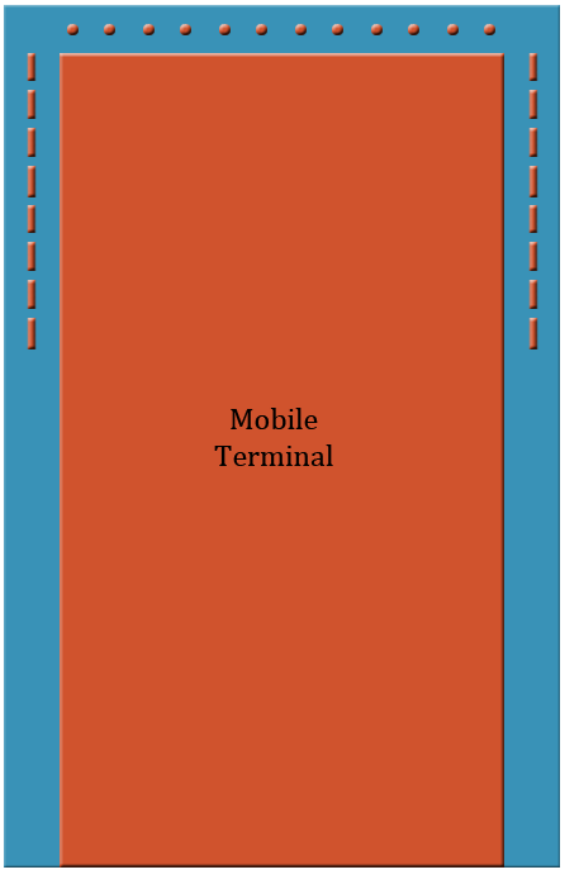

Figure 3.47: Schematic of the final design to measure coverage efficiency at 5 GHz.

Chapter 4

Losses

In the previous chapter different types of antennas were evaluated in function of its directivity to analyse its performance at 5G frequencies. This chapter evaluates the losses produced by the materials and the matching, and thus, the efficiency of the antennas at the target frequency. These results altogether with the previous ones let us evaluate the gain of the antennas, which is the main aim of this work. Later, some prototypes will be fabricated and measured to contrast the simulation results.

4.1 Introduction

To evaluate the losses, the body of the terminal used is going to be larger, so the antennas are included in the dimensions. These dimensions will be 60 mm x 120 mm, as shown in the figure 4.1. Furthermore, only one array will be evaluated to save simulation times without changing the results significantly. The number of elements of the array will be 8, which is expected as one of the possible numbers in real implementations due to the simplicity of the feeding network.

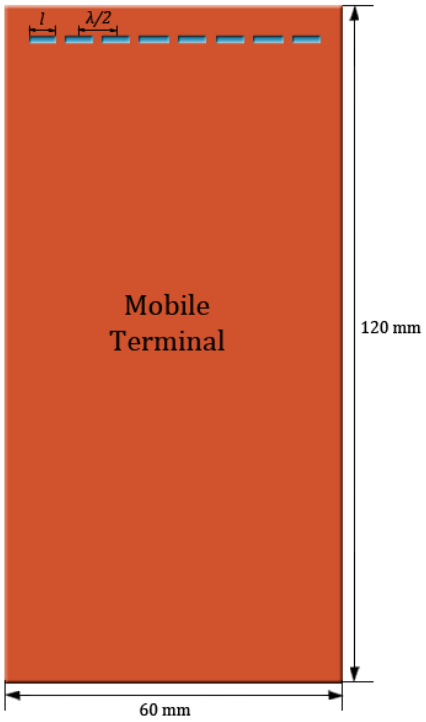

Figure 4.1: Geometry of the general case of study to evaluate losses.

Each antenna has its own design parameters. They must be designed and tuned to minimise the matching losses at the design frequency, which is 28 GHz. Once the return losses are -10 dB or less, the radiation and total efficiency are simulated using the CST simulator and plotted from 27 GHz to 29 GHz. Each case will be repeated for two different substrates: FR4 and RO3003, both with a height of 0.762 mm and a thickness of 0.05 mm. The conductor employed in these cases is annealed copper.

4.2 Slot Antenna Efficiency

As stated in section 3.3.6, the slot antenna provides the best coverage efficiency of the studied cases (except for hybrid arrays) so it has been chosen over the dipole array to be studied here. Also, it is easier to implement within a substrate and it has similar radiation properties. Two cases of slots will be designed and simulated, one of them with the slots orientated along the top side of the phone, and the other case with the slots orientated orthogonally to this side, as shown in figures 4.2 and 4.3.

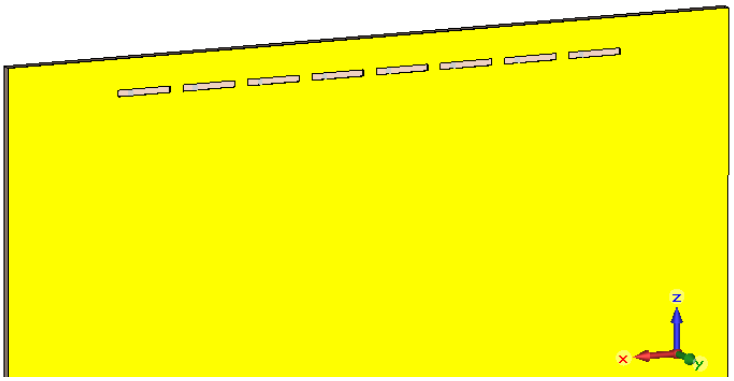

Figure 4.2: Geometry of the horizontal-oriented slot array to evaluate losses.

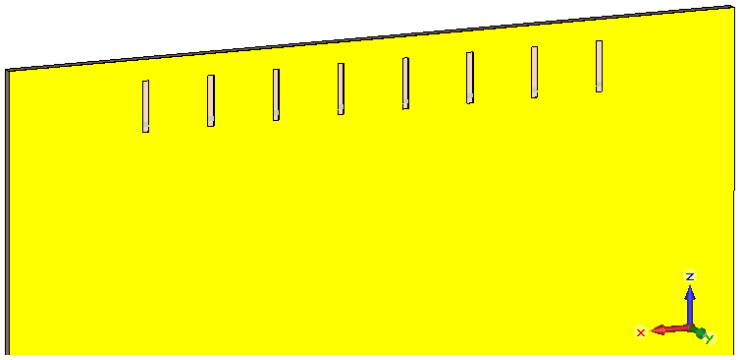

Figure 4.3: Geometry of the vertical-oriented slot array to evaluate losses.

4.2.1 Slot Antenna Design

The four cases follow the same design process but obviously with different results. The substrates have different dielectric permittivity and thus the lengths obtained will be different. Also, changing the orientation of the slots change the results since the distance between one slot and the other and the location of the side of the terminal causes the conductor plane to behave differently for both cases, leading to different solutions. The objective here is achieving a S_{11} parameter of less than -10 dB for the antennas in the centre of the array to reduce mismatch losses at 28 GHz.

The width of the slots in all cases is fixed to 0.5 mm, so they can be reproduced without problems here using the available technology. The distance between the array and the top side of the mobile terminal is fixed to 5.4 mm (λ/2) as well as the distance between elements which remain unchanged. This leads us to two design parameters: the length of the slots and the position of the ports. The length of the slots cannot be close or higher than 5.4 mm (λ/2) in order to avoid the superposition of the slots in the horizontal slot case and reaching the end of the body of the mobile terminal in the vertical slot case. After several parameter sweeps, the design parameters achieved are shown in the table 4.1.

Antenna Type	Substrate	Length of the slot (mm)	Width of the slot (mm)	Distance port to centre of the slot (mm)
Horizontal Slot	FR4	3.5	0.5	1
	RO3003	4.3	0.5	1.1
Vertical Slot	FR4	3.3	0.5	1.2
	RO3003	4	0.5	1.4

Table 4.1: Design results of the slot antennas to evaluate losses.

4.2.2 Horizontal Slot Antenna Results

In the next figures, the S-parameter of one of the middle elements of the arrays will be plotted and its radiation and total efficiencies. Since the middle element showed here is the number 4, the S_{44} is plotted with the S_{43} and S_{45} to evaluate the coupling between the element and its adjacent ones. Figure 4.4 shows the S-parameters when the substrate is FR4 and figure 4.6 when it is RO3003. Figure 4.5 shows the radiation and total efficiencies for FR4 substrate and figure 4.7 for RO3003 substrate.

In the pictures it is possible to appreciate that the S_{44} is always less than -10 dB at 28 GHz. The coupling is even lower, so little power is leaked to other antennas. Furthermore, the superior material, RO3003, has fewer losses than the FR4, as expected. However, the FR4 behaviour is not especially bad, given how high is the studied frequency.

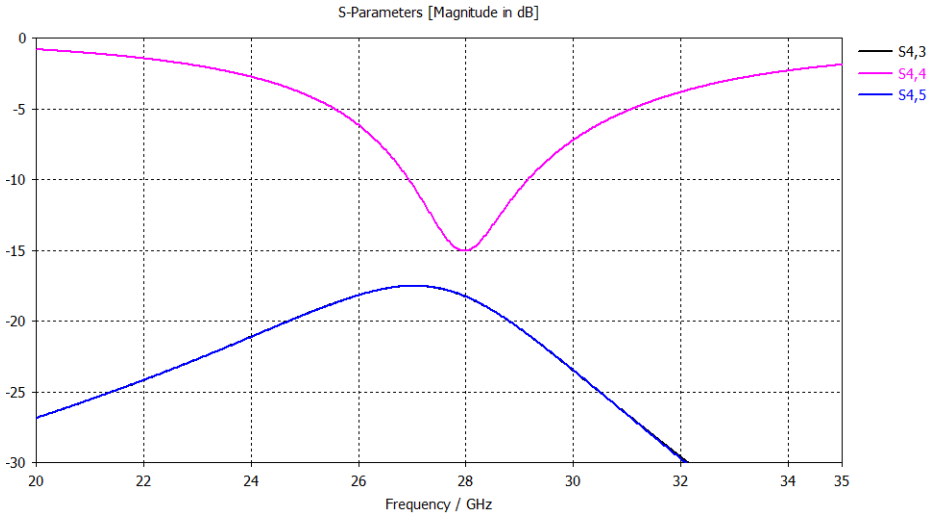

Figure 4.4: S-parameters obtained after simulation of the horizontal slot array when the substrate is FR4 to evaluate losses.

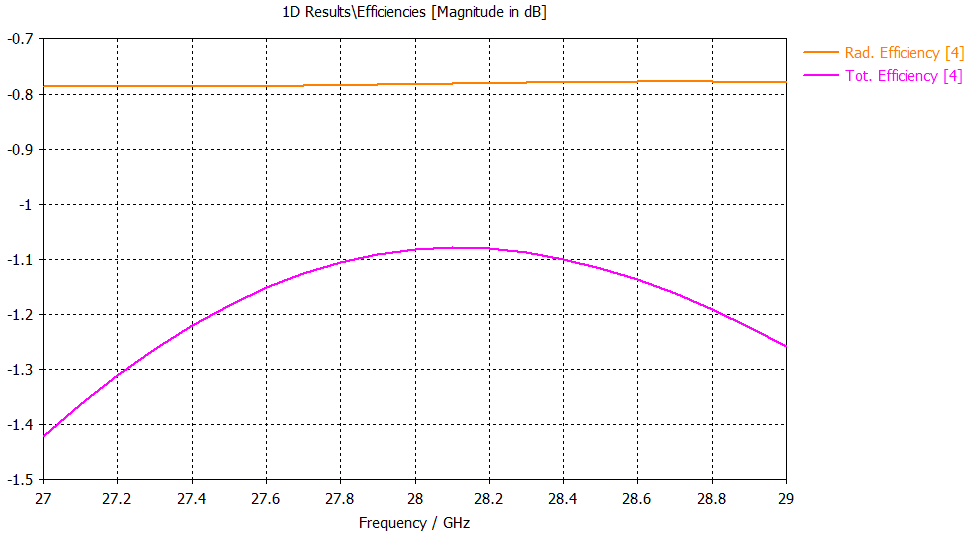

Figure 4.5: Radiation and total efficiency obtained after simulation of the horizontal slot array when the substrate is FR4 to evaluate losses.

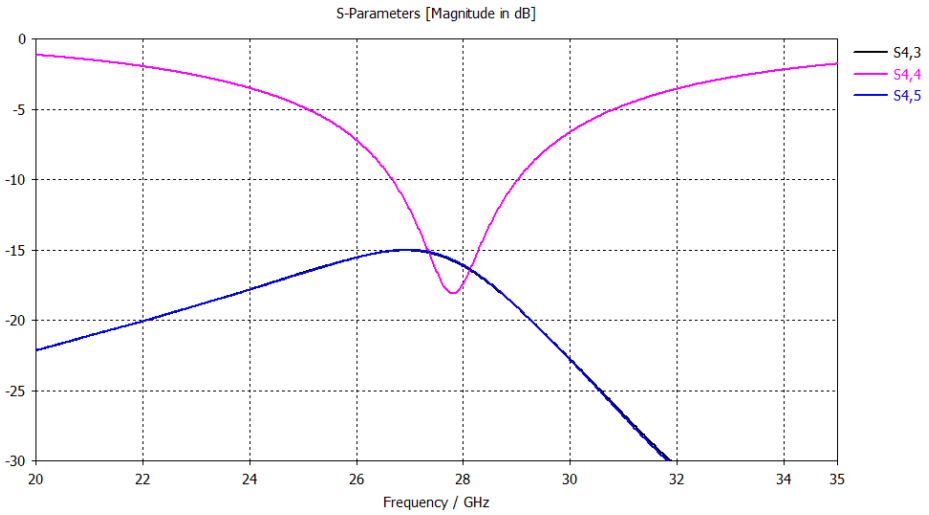

Figure 4.6: S-parameters obtained after simulation of the horizontal slot array when the substrate is RO3003 to evaluate losses.

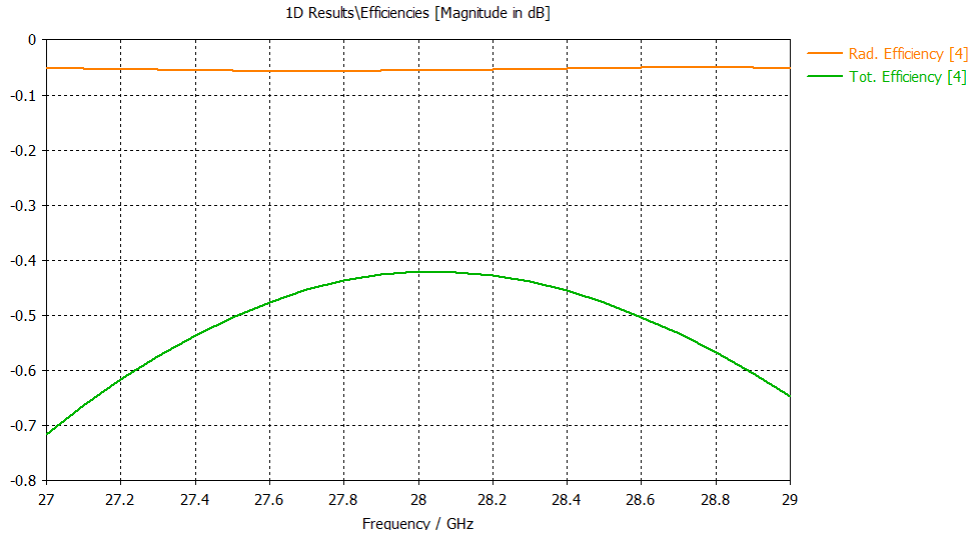

Figure 4.7: Radiation and total efficiency obtained after simulation of the horizontal slot array when the substrate is RO3003 to evaluate losses.

4.2.3 Vertical Slot Antenna Results

Same as above, the results of the S-parameters and efficiencies are plotted for the different substrates in figures 4.8, 4.9, 4.10 and 4.11. Note that the results are very similar to the ones from the horizontal slots.

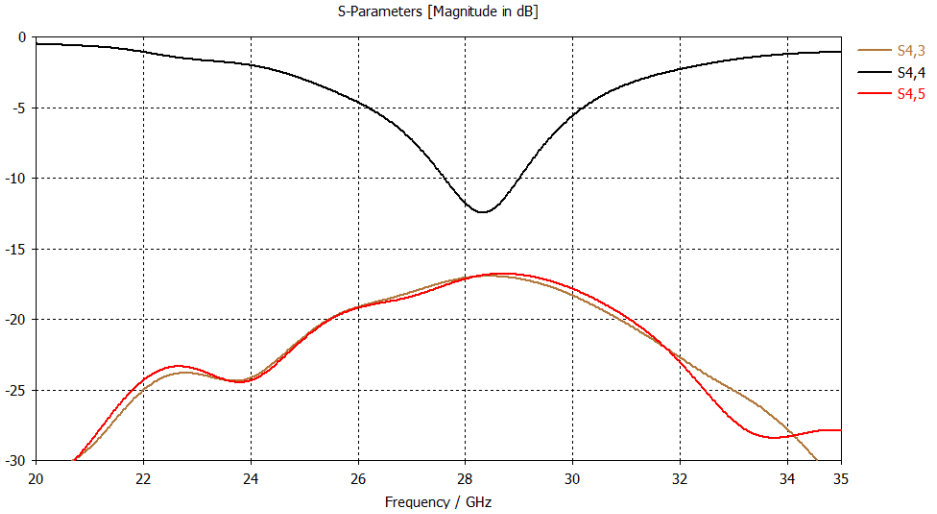

Figure 4.8: S-parameters obtained after simulation of the vertical slot array when the substrate is FR4 to evaluate losses.

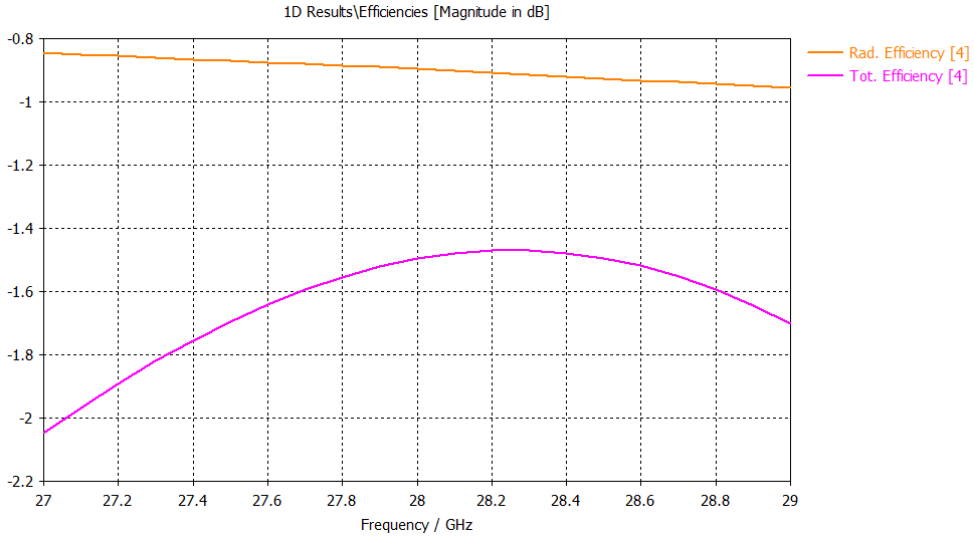

Figure 4.9: Radiation and total efficiency obtained after simulation of the vertical slot array when the substrate is FR4 to evaluate losses.

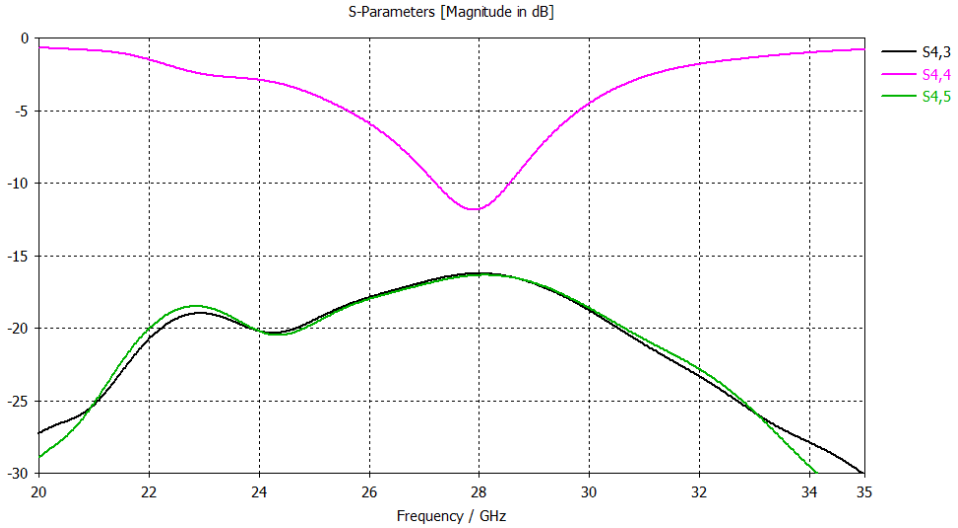

Figure 4.10: S-parameters obtained after simulation of the vertical slot array when the substrate is RO3003 to evaluate losses.

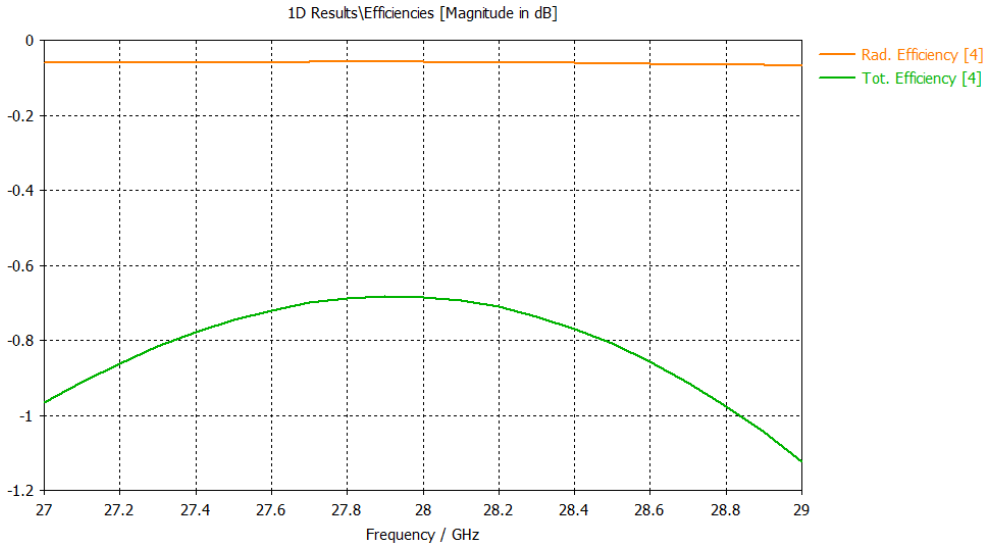

Figure 4.11: Radiation and total efficiency obtained after simulation of the vertical slot array when the substrate is RO3003 to evaluate losses.

4.3 Monopole Antenna Efficiency

The next type of antenna whose losses are going to be evaluated is the monopole antenna. The monopole is integrated into the substrate by making a thin line on it. The geometry and design of this antenna is very straightforward, as can be seen in figure 4.12.

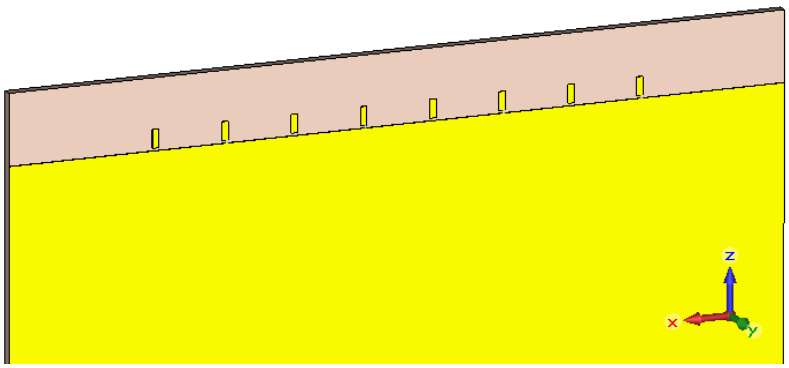

Figure 4.12: Geometry of the monopole array to evaluate losses.

4.3.1 Monopole Antenna Design

Following the same goal as the previous case, the antenna elements must be designed to reduce mismatch losses. The widths of the monopoles are fixed to 0.5 mm as were the widths of the slots before. The distance between the monopoles and the top copper plane is fixed to 0.2 mm. This leaves the length of the monopole as the only design parameter. Doing a parameter sweep we obtain the values shown in the table 4.2 for each different substrate:

Antenna Type	Substrate	Length of the monopole (mm)	Width of the line (mm)	Distance monopole to plane (mm)
Monopole	FR4	1.5	0.5	0.2
	RO3003	1.6	0.5	0.2

Table 4.2: Design results of the monopole antennas to evaluate losses.

4.3.2 Monopole Antenna Results

The following figures 4.13, 4.14, 4.15 and 4.16 show the S-parameters and efficiencies of one of the middle elements for each substrate. In both substrates it is possible to appreciate that the S_{44} parameter is low at more frequencies than 28GHz but, the main problem presented is the high coupling that this antenna present which decreases the total efficiency significantly.

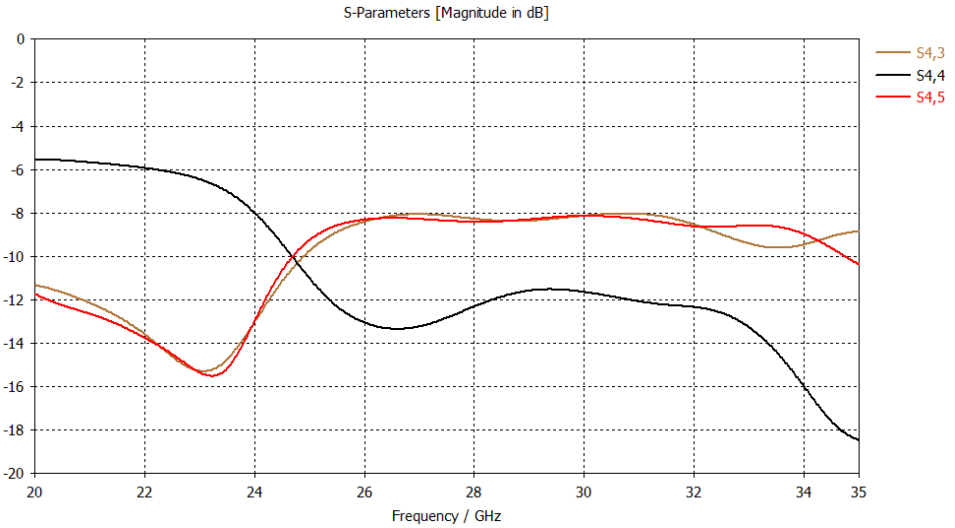

Figure 4.13: S-parameters obtained after simulation of the monopole array when the substrate is FR4 to evaluate losses.

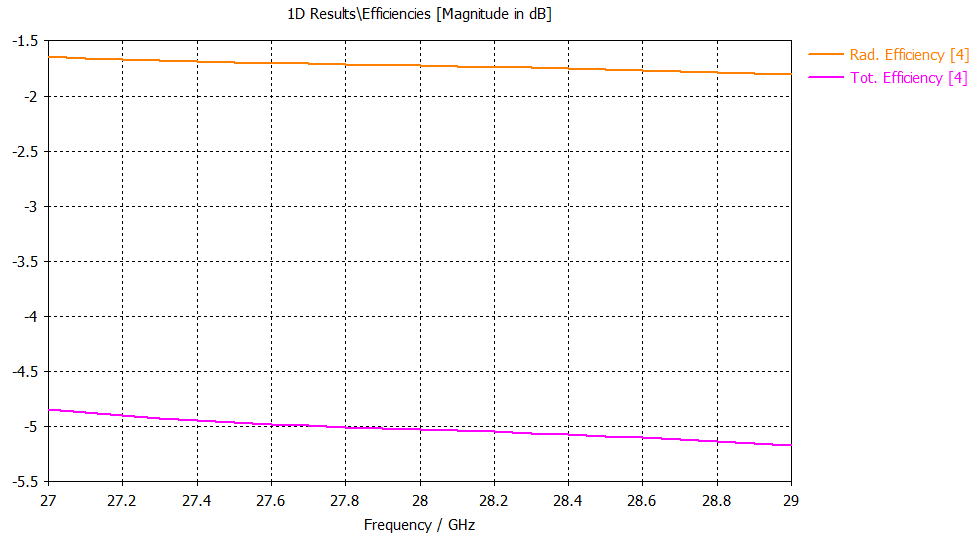

Figure 4.14: Radiation and total efficiency obtained after simulation of the monopole array when the substrate is FR4 to evaluate losses.

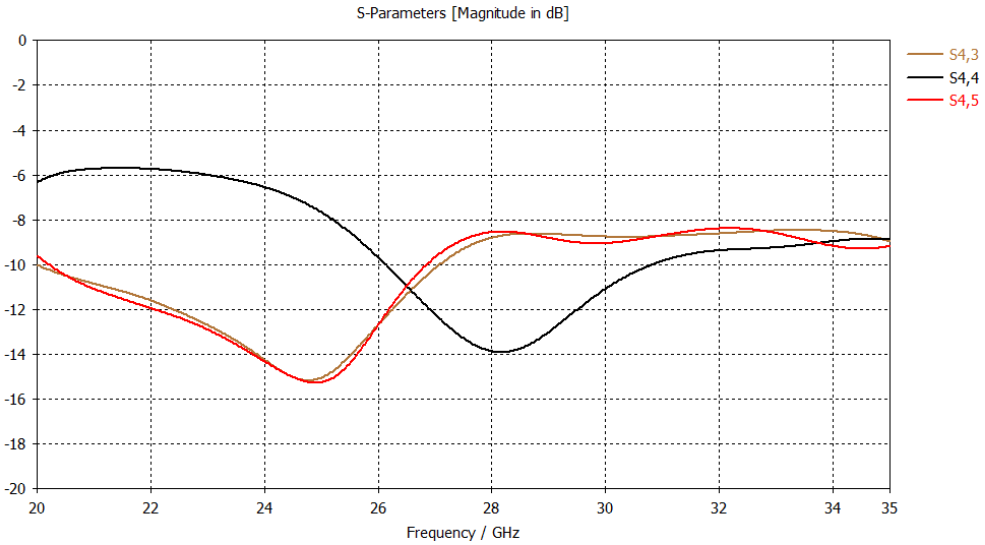

Figure 4.15: S-parameters obtained after simulation of the monopole array when the substrate is RO3003 to evaluate losses.

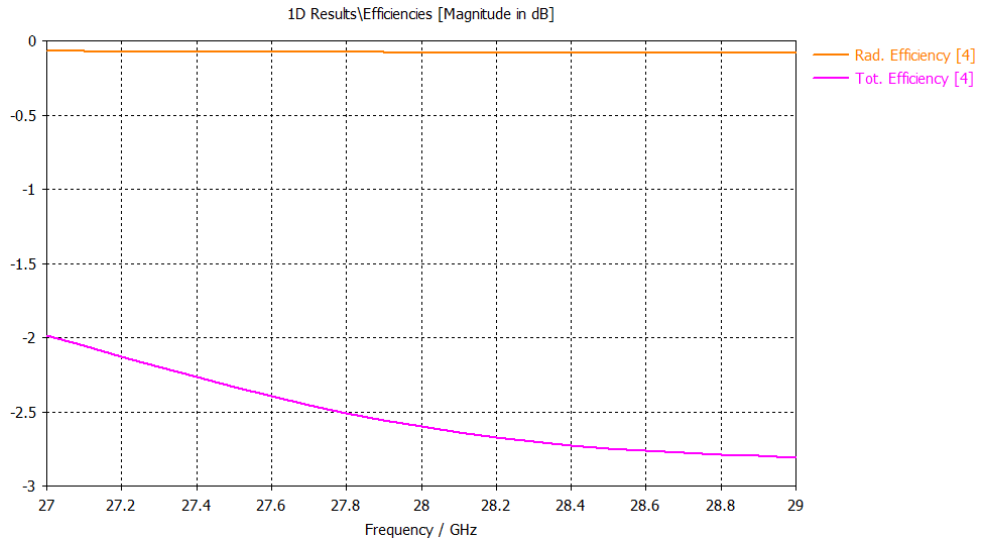

Figure 4.16: Radiation and total efficiency obtained after simulation of the monopole array when the substrate is RO3003 to evaluate losses.

4.4 IFA Antenna Efficiency

The IFA antenna has similar characteristics to the monopole antenna although it seems to have better performance, at least in terms of coverage efficiency, as shown in section 3.3.6. The implementation in a substrate is analogue to the monopole, as can be seen in the figure 4.17.

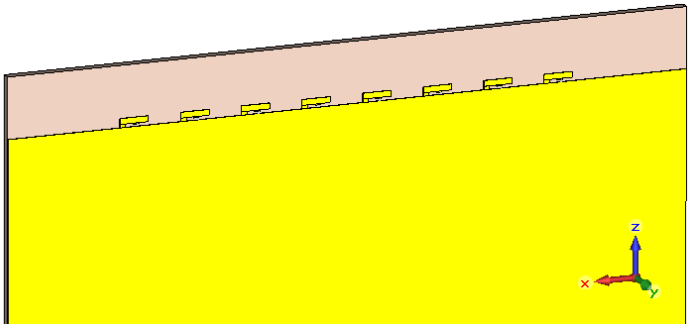

Figure 4.17: Geometry of the IFA array to evaluate losses.

4.4.1 IFA Antenna Design

The IFA antenna has more design parameters than the monopole antenna, thus, making the design process more elaborated. Instructions for its design can be found in [4], and, following them, the values of the designed parameters are shown in the table 4.3. Figure 4.18 explains how the distances are taken. Note that the width of the line and the distance with the copper layer is fixed to 0.5 mm and 0.2 mm respectively, as the monopole case.

Antenna Type	Substrate	L (mm)	W (mm)	D (mm)	H (mm)	S (mm)
IFA	FR4	0.8	0.5	0.2	0.8	1.2
	RO3003	1.1	0.5	0.2	0.8	1.4

Table 4.3: Design results of the IFA antennas to evaluate losses.

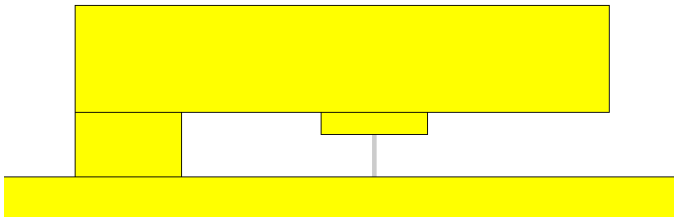

Figure 4.18: Indications of how are the design parameters of the IFA antenna measured.

4.4.2 IFA Antenna Results

Figures 4.19, 4.20, 4.21 and 4.22 show the results of the S-parameters and total and radiation efficiencies for both substrates for the IFA antenna. The same phenomena produced with the monopole antenna array are manifested this time too: high coupling and, thus, lower total efficiency.

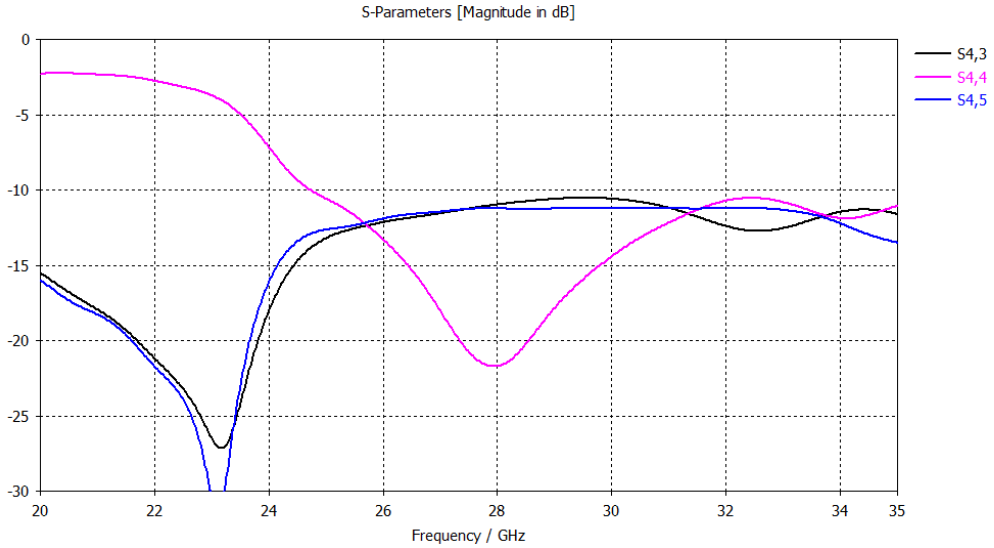

Figure 4.19: S-parameters obtained after simulation of the IFA array when the substrate is FR4 to evaluate losses.

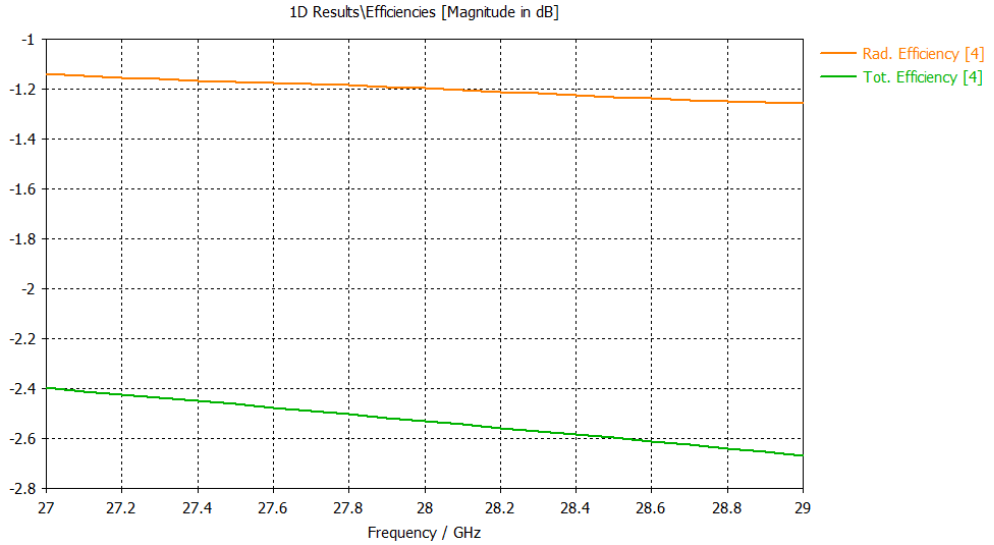

Figure 4.20: Radiation and total efficiency obtained after simulation of the IFA array when the substrate is FR4 to evaluate losses.

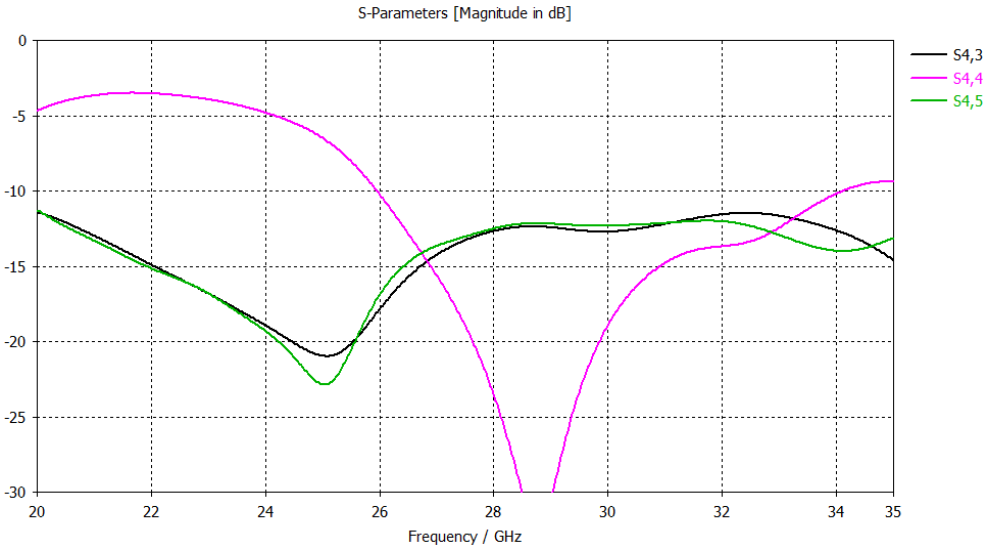

Figure 4.21: S-parameters obtained after simulation of the IFA array when the substrate is RO3003 to evaluate losses.

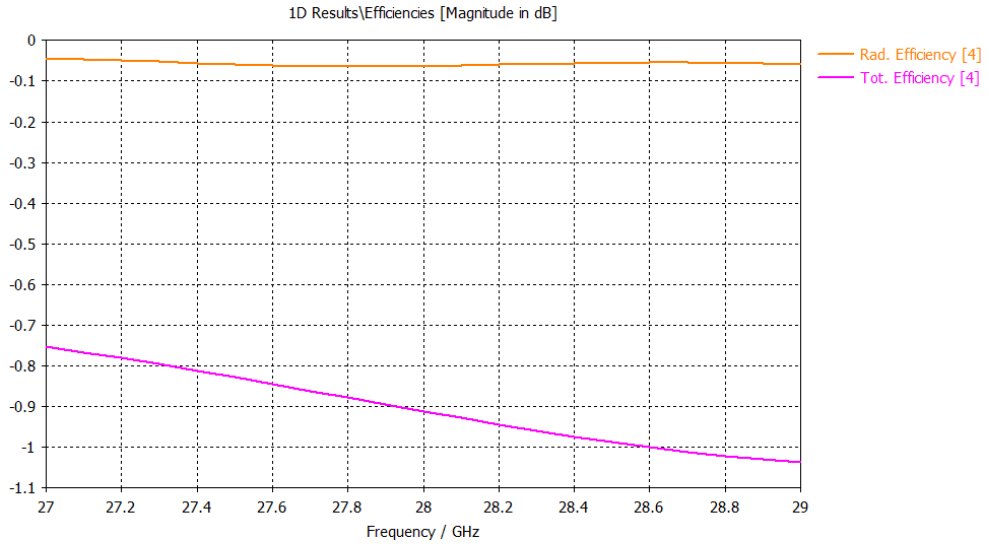

Figure 4.22: Radiation and total efficiency obtained after simulation of the IFA array when the substrate is FR4 to evaluate losses.

4.5 Patch Antenna Efficiency

Lastly, the process is repeated for the patch antenna. In this case, the patches are within the same plane as the top copper layer of the mobile terminal, as can be seen in figure 4.23. Note that this case has a ground plane on the back of the mobile terminal as well and are fed by a coaxial cable, as shown in figure 4.24.

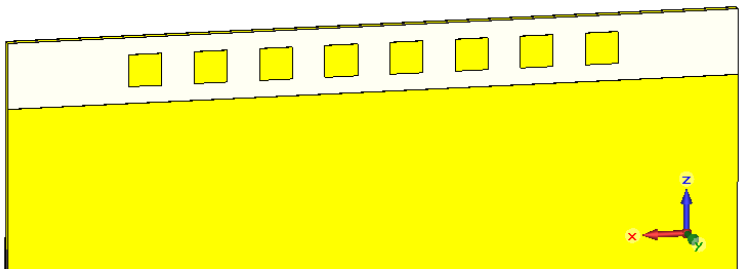

Figure 4.23: Geometry of the patch antenna array to evaluate losses.

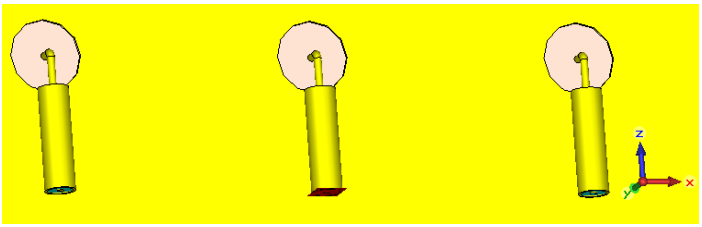

Figure 4.24: Geometry of the back of the patch antenna array to evaluate losses.

4.5.1 Patch Antenna Design

The patch antenna design process is depicted in section 2.7.3, which has been the guideline to obtain the results of this section. The coaxial cable used to feed the patches has a diameter of 0.5 mm and the conductor inside has a diameter of 0.15 mm. The relative permittivity of the dielectric inside the coaxial cable is 2.1. The gap in the ground plane where the coaxial is introduced is a new design parameter which must be tuned together with the length and width of the patch. The obtained results are shown in the table 4.4.

Antenna Type	Substrate	Length of the patch (mm)	Width of the patch (mm)	Feeding gap diameter (mm)
Patch	FR4	2.6	2.7	0.7
	RO3003	2.2	2.3	1.4

Table 4.4: Design results of the patch antennas to evaluate losses.

4.5.2 Patch Antenna Results

The obtained results are shown in the figures 4.25, 4.26, 4.27 and 4.28. In this case only one port is analysed to reduce simulation times and thus coupling could not be evaluated. Even so, the simulation of the substrate from Rogers did not finish properly due to long simulation time, which is why the results shown are less smooth than the others.

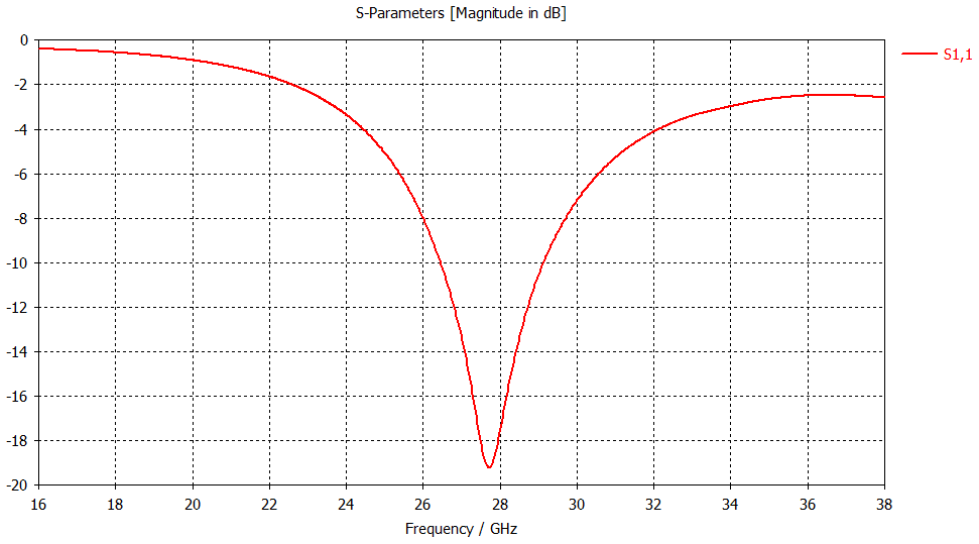

Figure 4.25: S-parameters obtained after simulation of the patch array when the substrate is FR4 to evaluate losses.

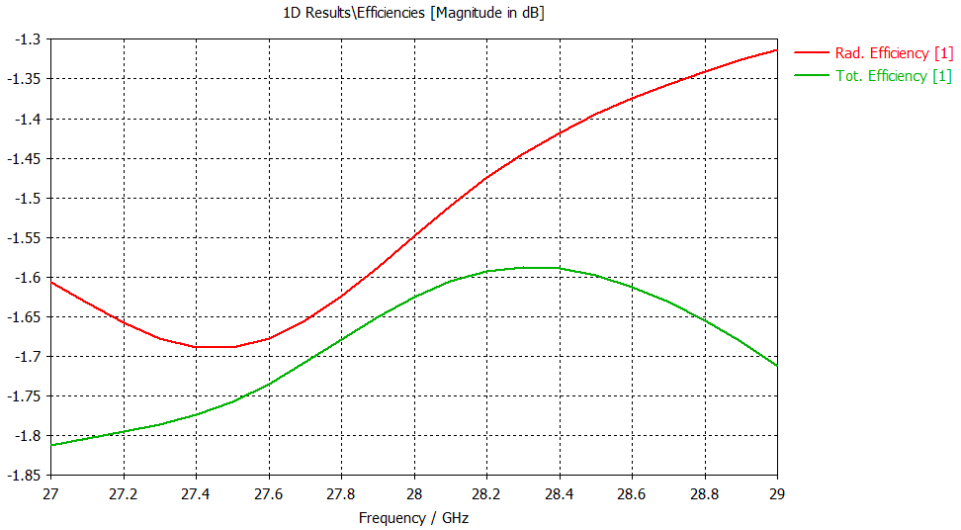

Figure 4.26: Radiation and total efficiency obtained after simulation of the patch array when the substrate is FR4 to evaluate losses.

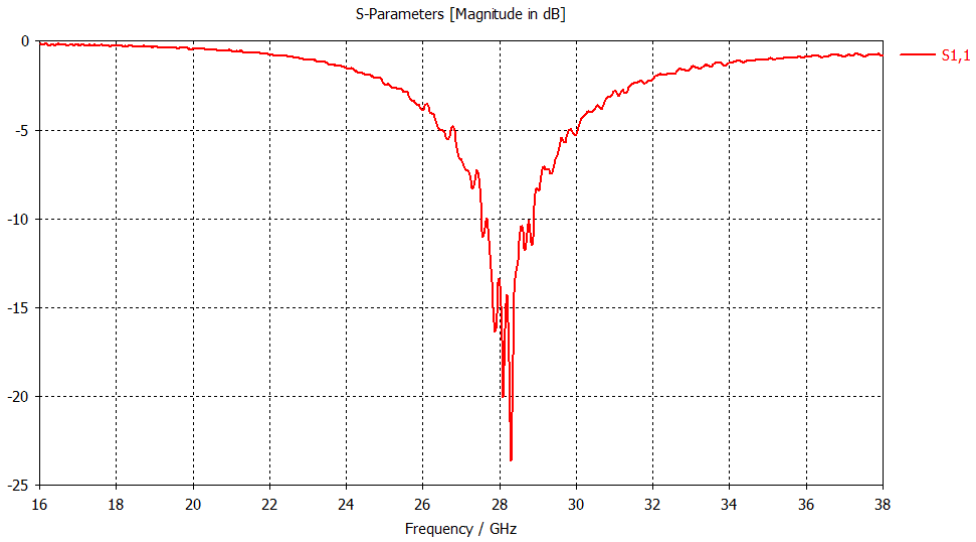

Figure 4.27: S-parameters obtained after simulation of the patch array when the substrate is RO3003 to evaluate losses.

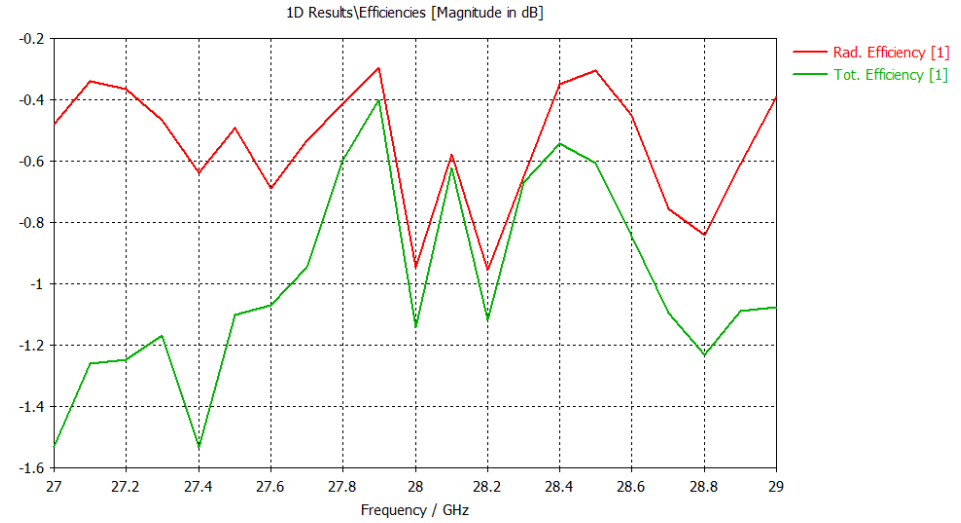

Figure 4.28: Radiation and total efficiency obtained after simulation of the patch array when the substrate is RO3003 to evaluate losses.

4.6 Prototypes fabrication, measurement and results

To finalise the evaluation of the losses, several prototypes have been fabricated and measured so it is possible to compare the previous results of this chapter with the ones from a physical realisation.

4.6.1 Layout and fabrication

The layout of the antennas and terminal were exported from the CST simulator and printed using the substrates mentioned previously, FR4 and RO3003 with 0.762 mm of height and 0.05 mm of thickness both of them. After the PCBs were fabricated, they needed to be fed properly and thus cables and connectors were soldered to them. Figure 4.29 shows the results after these steps.

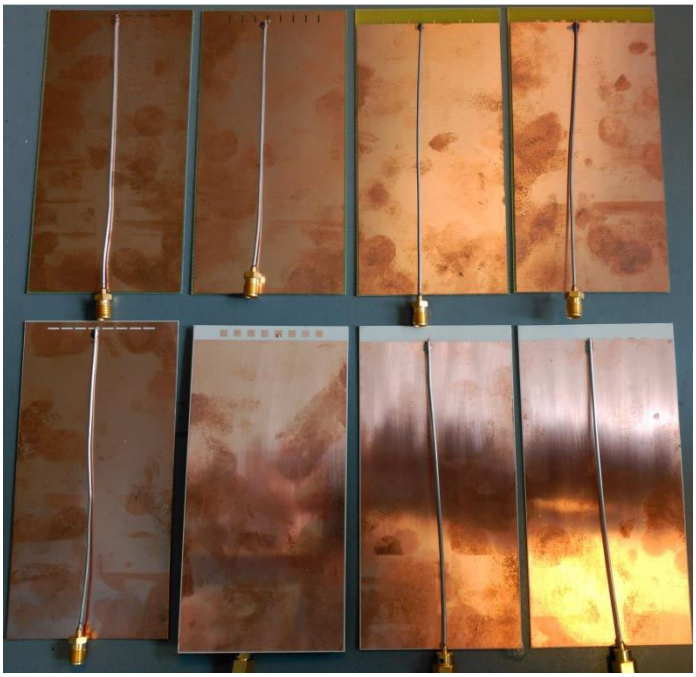

Figure 4.29: Picture of the different fabricated prototypes with soldered connections.

4.6.2 Measurement equipment and process

After the PCBs were ready, the power radiated in each direction was measured using the anechoic chamber here from Aalborg University which is shown in the figures 4.30 and 4.31. The chamber is supported by two devices: one of them, shown in figure 4.32, is the network analyser which collects the measurements and the other is charge of controlling the movement of the pedestals to do the measurement in different angles and it is shown in figure 4.33.

Figure 4.30: Picture of the entrance of the anechoic chamber.

Figure 4.31: Picture from the entrance of the anechoic chamber where the main area is seen.

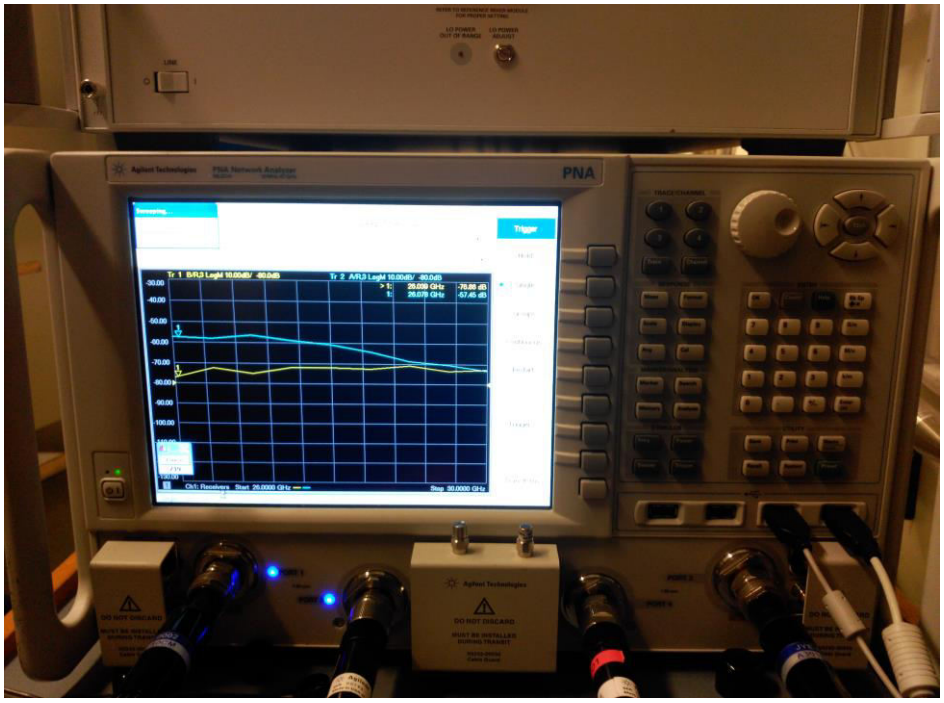

Figure 4.32: Picture of the network analyser used to take measures from the anechoic chamber.

Figure 4.33: Picture of the device used to control the movement of the pedestals in the anechoic chamber.

The measurement process consists of two parts. First, the S_{11}-parameter is measured using only the network analyser for each prototype. After this, one of them is placed on top of the mechanical pedestal in the anechoic chamber and connected, as shown in figure 4.34. The network analysed is then programmed to take measurements as the pedestals move, which is set up lastly with the device shown previously in figure 4.33. One picture of this process is shown in figure 4.35. This is then repeated for each PCB. To make the measurement process shorter and since there are too many prototypes, the measurements are taken with steps of 10º in vertical angle and 2.5º of horizontal angle, from 0º to 140º and 0º to 357.5º respectively, thus, 2160 directions are measured. Furthermore, the measurements are taken for 26 GHz, 26.5 GHz, 27 GHz, 27.5 GHz, 28 GHz, 28.5 GHz, 29 GHz, 29.5 GHz and 30 GHz. That makes 19440 measurements for each prototype.

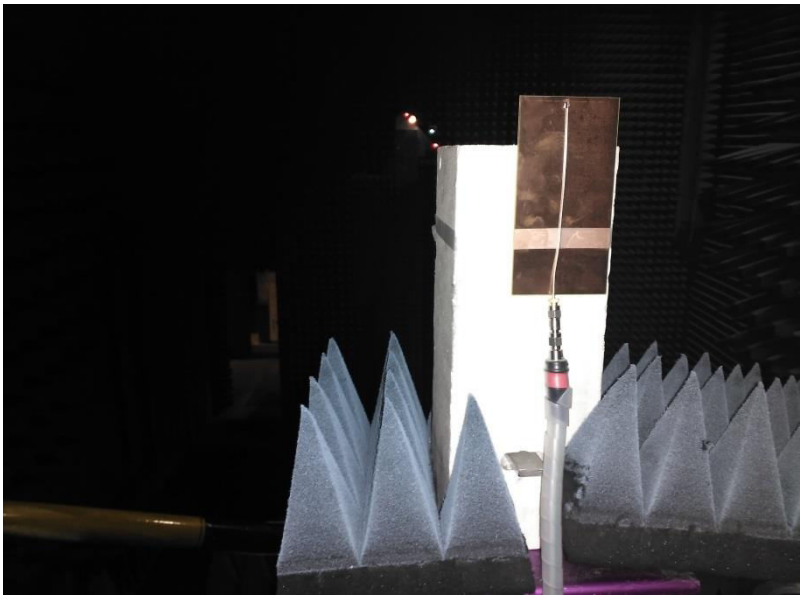

Figure 4.34: Picture of one of the prototypes connected on top of the mechanical pedestal in the anechoic chamber.

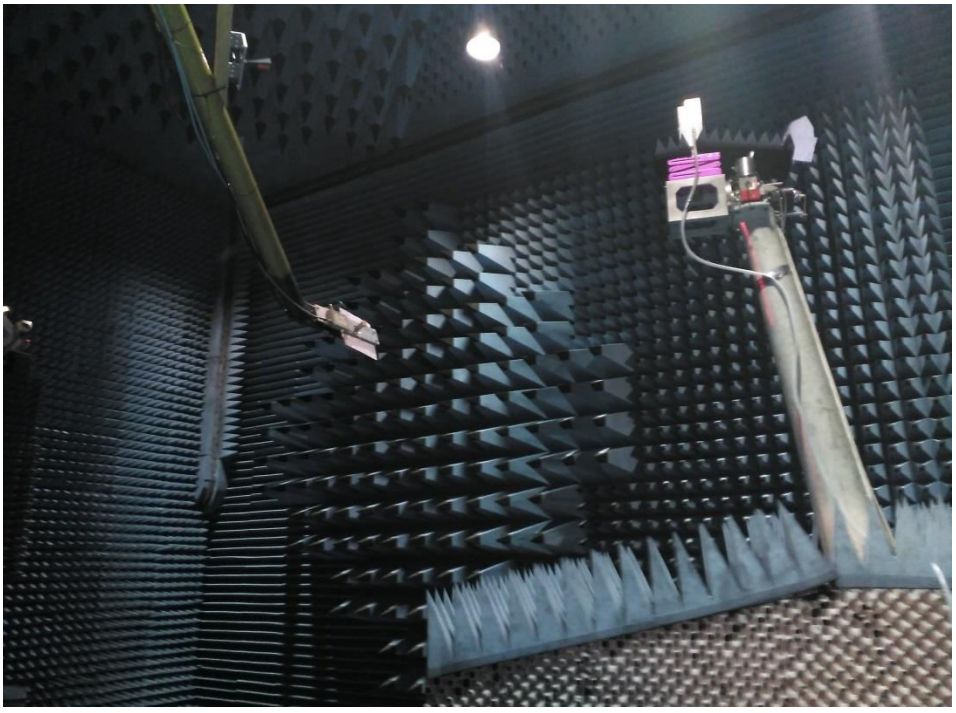

Figure 4.35: Picture of one of the prototypes being measured in the anechoic chamber.

4.6.3 Data analysis and results

With the measurements taken in the previous step, it was possible to compute the radiated power by every antenna and thus the efficiency of them. However, since the calibration data of the equipment was not available, only relative results are meaningful. A MATLAB code was necessary to manipulate all the data properly and compute the radiated power using the obtained measurements. Results are then compared with the ones from the previous simulations and shown in table 4.5.

Antenna Type		Simulated (dB)	Measured (dB)
Horizontal Slot	Difference between radiation efficiency: FR4 and RO3003	-0.73	-1.7
	Absolute values for radiation efficiency using FR4	-0.78	---
	Absolute values for radiation efficiency using RO3003	-0.05	---
Vertical Slot	Difference between radiation efficiency: FR4 and RO3003	-0.85	---
	Absolute values for radiation efficiency using FR4	-0.9	---
	Absolute values for radiation efficiency using RO3003	-0.05	---
Monopole	Difference between radiation efficiency: FR4 and RO3003	-1.65	-1.4
	Absolute values for radiation efficiency using FR4	-1.7	---
	Absolute values for radiation efficiency using RO3003	-0.05	---
IFA	Difference between radiation efficiency: FR4 and RO3003	-1.15	-1.5
	Absolute values for radiation efficiency using FR4	-1.2	---
	Absolute values for radiation efficiency using RO3003	-0.05	---
Patch	Difference between radiation efficiency: FR4 and RO3003	---	---
	Absolute values for radiation efficiency using FR4	-1.55	---
	Absolute values for radiation efficiency using RO3003	---	---

Table 4.5: Relative results from measurements and comparison with simulation results.

From the results it is possible to conclude that the monopole and IFA antennas behave similar to the simulation, and that the behaviours of the slots are not very similar. The substrate from Rogers do have less losses than FR4 as expected but between two different antennas using both this substrate there is more difference than expected, so the absolute losses must be higher than simulated.

Chapter 5

Conclusion

This project studied the different design possibilities of antennas for the fifth generation of mobile communications. These antennas differ from the previous ones in the higher frequencies employed and the high gain needed to compensate the propagation losses. Using higher frequencies allow the mobile terminal to include more antennas, since they are smaller, and thus, arrays of antennas which will provide the gain needed. To have the flexibility of an isotropic antenna in a situation where the receiving and transmitting direction are unknown, the main lobe of the radiation pattern of a 5G antenna must be able to orientate himself, which can be done by changing the phase of the feeding between the elements of the antenna array. To be able to cover more possible directions, the radiation pattern of each element of the array should be close to an isotropic one and in a way that it interact with the physical body of the mobile terminal properly.

The antenna types used in this work were the dipole, the monopole, the slot, the IFA and the patch antenna, which were depicted after the background of the antenna theory. After, a study of the coverage efficiency using arrays of these antennas was done. The simulation results pointed to the slot antenna to one of the best solutions and, after using two arrays of different types of elements, hybrid arrays, the dipole antenna employed with the slot looked slightly better than using only slot antennas. The patch antenna, however, does not seem like a good 5G antenna due to the high maximum directivity that presents as a single element, being unable to cover many angles.

Finally, after the analysis of the coverage efficiency, a study of the losses was done using two substrates: FR4 and RO3003. The slot antenna had better results in the simulation and, between both substrates the FR4 did not behave as bad as expected since it only introduced losses of less than 1 dB compared to RO3003. The monopole and IFA antennas were greatly affected by coupling issues, which would need to be solved before using them. Physical fabrication and measurements were also done to verify the simulation of the losses. However, several small discrepancies in results were found. The monopole and IFA antennas presented fewer losses than the slot and the gap in performance between both substrates seemed to increase.

As future work, there is much still to be done in mobile antennas for 5G. This work only studied the performance of five types of antenna, but many others less known antennas should be studied too. Also, this is a great opportunity to modify the antennas to adapt them to this new situation or to use less conventional antennas. Not only antenna types, but number of arrays placed and their location could be discussed too. Apart from these and other parameters which could have been studied too, the

measurement of a prototype to test the coverage efficiency would have probed valuable data, and that is why the 5 GHz design is underway.

Although it is out of the scope of this project, it is worth mentioning that the feeding network and the transmitting and receiving system present new problem, and so the possible MIMO system. All of these, when joined, make the fifth generation of mobile communications a new and beautiful challenge for the telecommunication engineering.

Bibliography

[1] NTT Docomo, "Docomo 5G White Paper," Jul. 2014 [Online]. Available: https://www.nttdocomo.co.jp/english/corporate/technology/whitepaper_5g/

[2] Tianyang Bai and Robert W. Heath, "Coverage and rate analysis for millimeter wave cellular networks," *IEEE Transactions on Wireless Communications*, vol. 14, no. 2, pp. 1100–1114, Feb. 2015.

[3] Constantine A. Balanis, *Antenna theory: Analysis and Design.* 3 rd. Ed. New York, USA: John Wiley & Sons, Inc, 1997.

[4] Zhijun Zhang, *Antenna Design for Mobile Devices.* 1 st. Ed. Singapore: John Wiley & Sons (Asia) Pte Ltd, Inc, 2011.

[5] Jakob Helander, Kun Zhao, Zhinong Ying, and Daniel Sjöberg, "Performance Analysis of Millimeter-Wave Phased Array Antennas in Cellular Handsets", *IEEE Antennas and wireless propagation letters*, vol. 15, pp. 504-507, 2016

Appendix A

MATLAB Scripts

A.1 Main script to compute the theoretical coverage efficiency

This script is used with two of the next scripts, which determine the type of the individual elements of the vertical and horizontal arrays.

```
%Initialisation of parameters
f = 28e9;
c = 299792458;
lambda = c/f;
acc = 50; %Precision
l = lambda/4;
k = 2*pi/lambda;
d = lambda/2;
N = 5;
Gminref = -6:0.1:10; %Minimum gain to calculate the coverage efficiency

%dipolesv runs the computation of the directivity for each beta when the
%individual elements is a vertical placed dipole
dipolesv;
%Store the directivity and optimum beta in new variables
DdBv = DdB;
DTbetadBv = DTbetadB;
optbetav = optbeta;

%Same with the horizontal dipoles
dipolesh;
DdBh = DdB;
DTbetadBh = DTbetadB;
optbetah = optbeta;

%Compare both vertical array and horizontal array directivity to get the
%biggest. Get which array and beta is used for each direction.
antenna = DTbetadBh>=DTbetadBv;
DTbetadB(DTbetadBh>=DTbetadBv) = DTbetadBh(DTbetadBh>=DTbetadBv);
DTbetadB(DTbetadBv>DTbetadBh) = DTbetadBv(DTbetadBv>DTbetadBh);
optbeta = optbetah.*(DTbetadBh>=DTbetadBv) + optbetav.*(DTbetadBh<DTbetadBv);

%Compute coverage efficiecy
etac=[];
for Gmin=Gminref
```

```
    etac = [etac sum(sum(DTbetadB>Gmin))/numel(DTbetadB)];
end

%Plot results
figure (1);
hold on
plot(Gminref,etac, 'b')
xlabel('Minimum Received Gain (dBi)')
ylabel('Coverage Efficiency')

figure;
pcolor(180*phi/pi,180*teta/pi,DTbetadB)
shading INTERP
colorbar
colormap('jet')
caxis([-20 10])
set(gca,'YDir','Reverse')
xlabel('phi (º)')
ylabel('theta (º)')
```

A.2 Scripts to compute the directivity of dipoles

A.2.1 Script to compute the directivity of the horizontal dipole array

```
%Initialisation and prealocation
teta = 0:pi/acc/2:pi-pi/acc/2;
F = zeros(length(teta),length(teta));
Fsin = zeros(length(teta),length(teta));
AF = zeros(length(teta),length(teta));
AFsin = zeros(length(teta),length(teta));
DTbetadB = -Inf*ones(length(teta),length(teta));
optbeta = NaN*ones(length(teta),length(teta));

%Computing maximum directivity for each beta using theoretical expressions
for beta = k*d:-k*d/acc:-k*d

    iteration = 0;
    for phi = 0:pi/acc:2*pi-pi/acc
        iteration = iteration + 1;
        F(:,iteration) = ((cos(k.*l.*sin(teta)*cos(phi)./2) - cos(k.*l/2))./sqrt(1-
sin(teta).^2*cos(phi).^2)).^2;
        Fsin(:,iteration) = ((cos(k.*l.*sin(teta)*cos(phi)./2) - cos(k.*l/2))./sqrt(1-
sin(teta).^2*cos(phi).^2)).^2.*sin(teta);
        AF(:,iteration) = abs((1/N).*(exp(1i.*N.*(k.*d*sin(teta)*cos(phi)+beta))-
1)./(exp(1i.*(k.*d.*sin(teta)*cos(phi)+beta))-1)).^2;
        AFsin(:,iteration) =
sin(teta).*abs((1/N).*(exp(1i.*N.*(k.*d*sin(teta)*cos(phi)+beta))-
1)./(exp(1i.*(k.*d.*sin(teta)*cos(phi)+beta))-1)).^2;
    end

    phi = 0:pi/acc:2*pi-pi/acc;

    F(isnan(F))=0;
    Fsin(isnan(Fsin))=0;
```

```
    AF(isnan(AF))=1;
    AFsin(isnan(AFsin))=0;
    D = F*2/pi/sum(sum(Fsin))*length(phi)*length(teta);
    DdB = 10*log10(D);
    AF_D = AF*2/pi/sum(sum(AFsin))*length(phi)*length(teta);
    AF_DdB=10*log10(AF_D);
    DT = F.*AF*2/pi/sum(sum(AF.*Fsin))*length(phi)*length(teta);
    DTdB = 10*log10(DT);

    optbeta(DTdB>=DTbetadB) = beta;
    DTbetadB(DTdB>DTbetadB) = DTdB(DTdB>DTbetadB);
end
```

A.2.2 Script to compute the directivity of the vertical dipole array

```
%Initialisation and prealocation
teta = 0:pi/acc/2:pi-pi/acc/2;
F = zeros(length(teta),length(teta));
Fsin = zeros(length(teta),length(teta));
AF = zeros(length(teta),length(teta));
AFsin = zeros(length(teta),length(teta));
DTbetadB = -Inf*ones(length(teta),length(teta));
optbeta = NaN*ones(length(teta),length(teta));

%Computing maximum directivity for each beta using theoretical expressions
for beta = k*d:-k*d/acc:-k*d

    iteration = 0;
    for phi = 0:pi/acc:2*pi-pi/acc
        iteration = iteration + 1;
        F(:,iteration) = ((cos(k.*l.*cos(teta)./2) - cos(k.*l/2))./sin(teta)).^2;
        Fsin(:,iteration) = ((cos(k.*l.*cos(teta)./2) -
cos(k.*l/2))./sin(teta)).^2.*sin(teta);
        AF(:,iteration) = abs((1/N).*(exp(1i.*N.*(k.*d*cos(teta)+beta))-
1)./(exp(1i.*(k.*d.*cos(teta)+beta))-1)).^2;
        AFsin(:,iteration) = sin(teta).*abs((1/N).*(exp(1i.*N.*(k.*d*cos(teta)+beta))-
1)./(exp(1i.*(k.*d.*cos(teta)+beta))-1)).^2;
    end

    phi = 0:pi/acc:2*pi-pi/acc;

    F(isnan(F))=0;
    Fsin(isnan(Fsin))=0;
    AF(isnan(AF))=1;
    AFsin(isnan(AFsin))=0;
    D = F*2/pi/sum(sum(Fsin))*length(phi)*length(teta);
    DdB = 10*log10(D);
    AF_D = AF*2/pi/sum(sum(AFsin))*length(phi)*length(teta);
    AF_DdB=10*log10(AF_D);
    DT = F.*AF*2/pi/sum(sum(AF.*Fsin))*length(phi)*length(teta);
    DTdB = 10*log10(DT);

    optbeta(DTdB>=DTbetadB) = beta;
    DTbetadB(DTdB>DTbetadB) = DTdB(DTdB>DTbetadB);
end
```

A.3 Scripts to compute the directivity of rotated dipoles

A.3.1 Script to compute the directivity of the rotated horizontal dipole array

```
%Initialisation and prealocation
teta = 0:pi/acc/2:pi-pi/acc/2;
F = zeros(length(teta),length(teta));
Fsin = zeros(length(teta),length(teta));
AF = zeros(length(teta),length(teta));
AFsin = zeros(length(teta),length(teta));
DTbetadB = -Inf*ones(length(teta),length(teta));
optbeta = NaN*ones(length(teta),length(teta));

%Computing maximum directivity for each beta using theoretical expressions
for beta = k*d:-k*d/acc:-k*d

    iteration = 0;
    for phi = 0:pi/acc:2*pi-pi/acc
        iteration = iteration + 1;
        F(:,iteration) = ((cos(k.*l.*sin(teta)*sin(phi)./2) - cos(k.*l/2))./sqrt(1-
sin(teta).^2*sin(phi).^2)).^2;
        Fsin(:,iteration) = ((cos(k.*l.*sin(teta)*sin(phi)./2) - cos(k.*l/2))./sqrt(1-
sin(teta).^2*sin(phi).^2)).^2.*sin(teta);
        AF(:,iteration) = abs((1/N).*(exp(1i.*N.*(k.*d*sin(teta)*cos(phi)+beta))-
1)./(exp(1i.*(k.*d.*sin(teta)*cos(phi)+beta))-1)).^2;
        AFsin(:,iteration) =
sin(teta).*abs((1/N).*(exp(1i.*N.*(k.*d*sin(teta)*cos(phi)+beta))-
1)./(exp(1i.*(k.*d.*sin(teta)*cos(phi)+beta))-1)).^2;
    end

    phi = 0:pi/acc:2*pi-pi/acc;

    F(isnan(F))=0;
    Fsin(isnan(Fsin))=0;
    AF(isnan(AF))=1;
    AFsin(isnan(AFsin))=0;
    D = F*2/pi/sum(sum(Fsin))*length(phi)*length(teta);
    DdB = 10*log10(D);
    AF_D = AF*2/pi/sum(sum(AFsin))*length(phi)*length(teta);
    AF_DdB=10*log10(AF_D);
    DT = F.*AF*2/pi/sum(sum(AF.*Fsin))*length(phi)*length(teta);
    DTdB = 10*log10(DT);

    optbeta(DTdB>=DTbetadB) = beta;
    DTbetadB(DTdB>DTbetadB) = DTdB(DTdB>DTbetadB);
end
```

A.3.2 Script to compute the directivity of the rotated vertical dipole array

```
%Initialisation and prealocation
teta = 0:pi/acc/2:pi-pi/acc/2;
F = zeros(length(teta),length(teta));
Fsin = zeros(length(teta),length(teta));
AF = zeros(length(teta),length(teta));
```

```
AFsin = zeros(length(teta),length(teta));
DTbetadB = -Inf*ones(length(teta),length(teta));
optbeta = NaN*ones(length(teta),length(teta));

%Computing maximum directivity for each beta using theoretical expressions
for beta = k*d:-k*d/acc:-k*d

    iteration = 0;
    for phi = 0:pi/acc:2*pi-pi/acc
        iteration = iteration + 1;
        F(:,iteration) = ((cos(k.*l.*sin(teta)*sin(phi)./2) - cos(k.*l/2))./sqrt(1-
sin(teta).^2*sin(phi).^2)).^2;
        Fsin(:,iteration) = ((cos(k.*l.*sin(teta)*sin(phi)./2) - cos(k.*l/2))./sqrt(1-
sin(teta).^2*sin(phi).^2)).^2.*sin(teta);
        AF(:,iteration) = abs((1/N).*(exp(1i.*N.*(k.*d*cos(teta)+beta))-
1)./(exp(1i.*(k.*d.*cos(teta)+beta))-1)).^2;
        AFsin(:,iteration) = sin(teta).*abs((1/N).*(exp(1i.*N.*(k.*d*cos(teta)+beta))-
1)./(exp(1i.*(k.*d.*cos(teta)+beta))-1)).^2;
    end

    phi = 0:pi/acc:2*pi-pi/acc;

    F(isnan(F))=0;
    Fsin(isnan(Fsin))=0;
    AF(isnan(AF))=1;
    AFsin(isnan(AFsin))=0;
    D = F*2/pi/sum(sum(Fsin))*length(phi)*length(teta);
    DdB = 10*log10(D);
    AF_D = AF*2/pi/sum(sum(AFsin))*length(phi)*length(teta);
    AF_DdB=10*log10(AF_D);
    DT = F.*AF*2/pi/sum(sum(AF.*Fsin))*length(phi)*length(teta);
    DTdB = 10*log10(DT);

    optbeta(DTdB>=DTbetadB) = beta;
    DTbetadB(DTdB>DTbetadB) = DTdB(DTdB>DTbetadB);
end
```

A.4 Scripts to compute the directivity of monopoles

A.4.1 Script to compute the directivity of the horizontal monopole array

```
%Initialisation and prealocation
teta = 0:pi/acc/2:pi-pi/acc/2;
F = zeros(length(teta),length(teta));
Fsin = zeros(length(teta),length(teta));
AF = zeros(length(teta),length(teta));
AFsin = zeros(length(teta),length(teta));
DTbetadB = -Inf*ones(length(teta),length(teta));
optbeta = NaN*ones(length(teta),length(teta));

%Computing maximum directivity for each beta using theoretical expressions
for beta = k*d:-k*d/acc:-k*d

    iteration = 0;
```

```
    for phi = 0:pi/acc:2*pi-pi/acc
        iteration = iteration + 1;
        if (phi >= pi/2 && phi <= 3*pi/2)
            F(:,iteration) = ((cos(k.*l.*sin(teta)*cos(phi)./2) - cos(k.*l/2))./sqrt(1-
sin(teta).^2*cos(phi).^2)).^2;
            Fsin(:,iteration) = ((cos(k.*l.*sin(teta)*cos(phi)./2) -
cos(k.*l/2))./sqrt(1-sin(teta).^2*cos(phi).^2)).^2.*sin(teta);
        else
            F(:,iteration) = 0;
            Fsin(:,iteration) = 0;
        end
        AF(:,iteration) = abs((1/N).*(exp(1i.*N.*(k.*d*sin(teta)*cos(phi)+beta))-
1)./(exp(1i.*(k.*d.*sin(teta)*cos(phi)+beta))-1)).^2;
        AFsin(:,iteration) =
sin(teta).*abs((1/N).*(exp(1i.*N.*(k.*d*sin(teta)*cos(phi)+beta))-
1)./(exp(1i.*(k.*d.*sin(teta)*cos(phi)+beta))-1)).^2;
    end

    phi = 0:pi/acc:2*pi-pi/acc;

    F(isnan(F))=0;
    Fsin(isnan(Fsin))=0;
    AF(isnan(AF))=1;
    AFsin(isnan(AFsin))=0;
    D = F*2/pi/sum(sum(Fsin))*length(phi)*length(teta);
    DdB = 10*log10(D);
    AF_D = AF*2/pi/sum(sum(AFsin))*length(phi)*length(teta);
    AF_DdB=10*log10(AF_D);
    DT = F.*AF*2/pi/sum(sum(AF.*Fsin))*length(phi)*length(teta);
    DTdB = 10*log10(DT);

    optbeta(DTdB>=DTbetadB) = beta;
    DTbetadB(DTdB>DTbetadB) = DTdB(DTdB>DTbetadB);
end
```

A.4.2 Script to compute the directivity of the vertical monopole array

```
%Initialisation and prealocation
teta = 0:pi/acc/2:pi-pi/acc/2;
F = zeros(length(teta),length(teta));
Fsin = zeros(length(teta),length(teta));
AF = zeros(length(teta),length(teta));
AFsin = zeros(length(teta),length(teta));
DTbetadB = -Inf*ones(length(teta),length(teta));
optbeta = NaN*ones(length(teta),length(teta));

%Computing maximum directivity for each beta using theoretical expressions
for beta = k*d:-k*d/acc:-k*d

    iteration = 0;
    for phi = 0:pi/acc:2*pi-pi/acc
        iteration = iteration + 1;
        F(:,iteration) = ((cos(k.*l.*cos(teta)./2) - cos(k.*l/2))./sin(teta)).^2;
        Fsin(:,iteration) = ((cos(k.*l.*cos(teta)./2) -
cos(k.*l/2))./sin(teta)).^2.*sin(teta);
```

```
        AF(:,iteration) = abs((1/N).*(exp(1i.*N.*(k.*d*cos(teta)+beta))-
1)./(exp(1i.*(k.*d.*cos(teta)+beta))-1)).^2;
        AFsin(:,iteration) = sin(teta).*abs((1/N).*(exp(1i.*N.*(k.*d*cos(teta)+beta))-
1)./(exp(1i.*(k.*d.*cos(teta)+beta))-1)).^2;
    end

    F(teta > pi/2, :) = 0;
    Fsin(teta > pi/2, :) = 0;

    phi = 0:pi/acc:2*pi-pi/acc;

    F(isnan(F))=0;
    Fsin(isnan(Fsin))=0;
    AF(isnan(AF))=1;
    AFsin(isnan(AFsin))=0;
    D = F*2/pi/sum(sum(Fsin))*length(phi)*length(teta);
    DdB = 10*log10(D);
    AF_D = AF*2/pi/sum(sum(AFsin))*length(phi)*length(teta);
    AF_DdB=10*log10(AF_D);
    DT = F.*AF*2/pi/sum(sum(AF.*Fsin))*length(phi)*length(teta);
    DTdB = 10*log10(DT);

    optbeta(DTdB>=DTbetadB) = beta;
    DTbetadB(DTdB>DTbetadB) = DTdB(DTdB>DTbetadB);
end
```

A.5 Scripts to compute the directivity of patches

A.5.1 Script to compute the directivity of the horizontal patch array

```
%Initialisation and prealocation
teta = 0:pi/acc/2:pi-pi/acc/2;
F = zeros(length(teta),length(teta));
Fsin = zeros(length(teta),length(teta));
AF = zeros(length(teta),length(teta));
AFsin = zeros(length(teta),length(teta));
DTbetadB = -Inf*ones(length(teta),length(teta));
optbeta = NaN*ones(length(teta),length(teta));

%Computing maximum directivity for each beta using theoretical expressions
for beta = k*d:-k*d/acc:-k*d

    iteration = 0;
    for phi = 0:pi/acc:2*pi-pi/acc
        iteration = iteration + 1;
        F(:,iteration) = (sqrt(1-
sin(teta).^2*cos(phi).^2).*sin(k.*h./2.*cos(teta))./(k.*h./2.*cos(teta))...
            .*sin(k.*W./2.*sin(teta).*cos(phi))./(k.*W./2.*sin(teta).*cos(phi))).^2;
        Fsin(:,iteration) = (sqrt(1-
sin(teta).^2*cos(phi).^2).*sin(k.*h./2.*cos(teta))./(k.*h./2.*cos(teta))...

.*sin(k.*W./2.*sin(teta).*cos(phi))./(k.*W./2.*sin(teta).*cos(phi))).^2.*sin(teta);
        AF(:,iteration) = abs((1/N).*(exp(1i.*N.*(k.*d*sin(teta)*cos(phi)+beta))-
1)./(exp(1i.*(k.*d.*sin(teta)*cos(phi)+beta))-1)).^2;
```

```
        AFsin(:,iteration) =
sin(teta).*abs((1/N).*(exp(1i.*N.*(k.*d*sin(teta)*cos(phi)+beta))-
1)./(exp(1i.*(k.*d.*sin(teta)*cos(phi)+beta))-1)).^2;
    end

    F(teta > pi/2, :) = 0;
    Fsin(teta > pi/2, :) = 0;

    phi = 0:pi/acc:2*pi-pi/acc;

    F(isnan(F))=1;
    Fsin(isnan(Fsin))=1;
    AF(isnan(AF))=1;
    AFsin(isnan(AFsin))=0;
    D = F*2/pi/sum(sum(Fsin))*length(phi)*length(teta);
    DdB = 10*log10(D);
    AF_D = AF*2/pi/sum(sum(AFsin))*length(phi)*length(teta);
    AF_DdB=10*log10(AF_D);
    DT = F.*AF*2/pi/sum(sum(AF.*Fsin))*length(phi)*length(teta);
    DTdB = 10*log10(DT);

    optbeta(DTdB>=DTbetadB) = beta;
    DTbetadB(DTdB>DTbetadB) = DTdB(DTdB>DTbetadB);
end
```

A.5.2 Script to compute the directivity of the horizontal patch array

```
%Initialisation and prealocation
teta = 0:pi/acc/2:pi-pi/acc/2;
F = zeros(length(teta),length(teta));
Fsin = zeros(length(teta),length(teta));
AF = zeros(length(teta),length(teta));
AFsin = zeros(length(teta),length(teta));
DTbetadB = -Inf*ones(length(teta),length(teta));
optbeta = NaN*ones(length(teta),length(teta));

%Computing maximum directivity for each beta using theoretical expressions
for beta = k*d:-k*d/acc:-k*d

    iteration = 0;
    for phi = 0:pi/acc:2*pi-pi/acc
        iteration = iteration + 1;
        if (phi >= pi/2 && phi <= 3*pi/2)
            F(:,iteration) =
(sin(teta).*sin(k.*h./2.*sin(teta).*cos(phi))./(k.*h./2.*sin(teta).*cos(phi))...
                .*sin(k.*W./2.*cos(teta))./(k.*W./2.*cos(teta))).^2;
            Fsin(:,iteration) =
(sin(teta).*sin(k.*h./2.*sin(teta).*cos(phi))./(k.*h./2.*sin(teta).*cos(phi))...
                .*sin(k.*W./2.*cos(teta))./(k.*W./2.*cos(teta))).^2.*sin(teta);
        else
            F(:,iteration) = 0;
            Fsin(:,iteration) = 0;
        end
        AF(:,iteration) = abs((1/N).*(exp(1i.*N.*(k.*d*cos(teta)+beta))-
1)./(exp(1i.*(k.*d.*cos(teta)+beta))-1)).^2;
```

```
        AFsin(:,iteration) = sin(teta).*abs((1/N).*(exp(1i.*N.*(k.*d*cos(teta)+beta))-
1)./(exp(1i.*(k.*d.*cos(teta)+beta))-1)).^2;
    end

    phi = 0:pi/acc:2*pi-pi/acc;

    F(isnan(F))=0;
    Fsin(isnan(Fsin))=0;
    AF(isnan(AF))=1;
    AFsin(isnan(AFsin))=0;
    D = F*2/pi/sum(sum(Fsin))*length(phi)*length(teta);
    DdB = 10*log10(D);
    AF_D = AF*2/pi/sum(sum(AFsin))*length(phi)*length(teta);
    AF_DdB=10*log10(AF_D);
    DT = F.*AF*2/pi/sum(sum(AF.*Fsin))*length(phi)*length(teta);
    DTdB = 10*log10(DT);

    optbeta(DTdB>=DTbetadB) = beta;
    DTbetadB(DTdB>DTbetadB) = DTdB(DTdB>DTbetadB);
end
```

A.6 Scripts to compute the coverage efficiency using CST results

```
%Initialisation and prealocation
f = 28e9;
c = 299792458;
lambda = c/f;
k = 2*pi/lambda;
d = lambda/2;
acc = 1; %Precision of 1°
Gminref = -6:0.1:10;
theta = 0:acc:180;
phi = 0:acc:360-acc;
optbetax = k*d*ones(length(theta),length(phi));
optbetaz = k*d*ones(length(theta),length(phi));
Dxopt = -Inf*ones(length(theta),length(phi));
Dzopt = -Inf*ones(length(theta),length(phi));

%Load radiation E pattern from CST simulation for each element
load 1x.txt
load 2x.txt
load 3x.txt
load 4x.txt
load 5x.txt

load 1z.txt
load 2z.txt
load 3z.txt
load 4z.txt
load 5z.txt

%Computing the directivity in each direction for each beta using the loaded
%data from CST
for beta = k*d:-k*d*acc*pi/180:-k*d;
    ExCST = X1x(:,3)...
```

```
        +X2x(:,3).*exp(1*1i*(k*d*sin(X2x(:,1)*pi/180).*cos(X2x(:,2)*pi/180)+beta))...
        +X3x(:,3).*exp(2*1i*(k*d*sin(X3x(:,1)*pi/180).*cos(X3x(:,2)*pi/180)+beta))...
        +X4x(:,3).*exp(3*1i*(k*d*sin(X4x(:,1)*pi/180).*cos(X4x(:,2)*pi/180)+beta))...
        +X5x(:,3).*exp(4*1i*(k*d*sin(X5x(:,1)*pi/180).*cos(X5x(:,2)*pi/180)+beta));
    EzCST = X1z(:,3)...
        +X2z(:,3).*exp(1*1i*(k*d*cos(X2z(:,1)*pi/180)+beta))...
        +X3z(:,3).*exp(2*1i*(k*d*cos(X3z(:,1)*pi/180)+beta))...
        +X4z(:,3).*exp(3*1i*(k*d*cos(X4z(:,1)*pi/180)+beta))...
        +X5z(:,3).*exp(4*1i*(k*d*cos(X5z(:,1)*pi/180)+beta));

    Ez = [];
    Ex = [];
    p = 180/acc+1;
    for q = 1:p:(p*(p-1)*2-p+1)
        Ez = [Ez EzCST(q:(q+p-1))];
        Ex = [Ex ExCST(q:(q+p-1))];
    end

    Ux = abs(Ex).^2;
    Uz = abs(Ez).^2;

    Uxsin = Ux;
    Uzsin = Uz;
    for thetaf = 0:acc:180
        Uxsin(thetaf+1,:) = Ux(thetaf+1,:)*sin(thetaf*pi/180);
        Uzsin(thetaf+1,:) = Uz(thetaf+1,:)*sin(thetaf*pi/180);
    end
    Px = 2*pi*pi*sum(sum(Uxsin))/length(Uxsin(:,1))/length(Uxsin(1,:));
    Pz = 2*pi*pi*sum(sum(Uzsin))/length(Uzsin(:,1))/length(Uzsin(1,:));

    Dx = 4*pi*Ux/Px;
    Dz = 4*pi*Uz/Pz;

    optbetax(Dx>Dxopt) = beta;
    optbetaz(Dz>Dzopt) = beta;
    Dxopt(Dx>Dxopt) = Dx(Dx>Dxopt);
    Dzopt(Dz>Dzopt) = Dz(Dz>Dzopt);
end

%Selecting the best directivity in each direction between the two arrays
optbeta = optbetaz;
Dopt = Dzopt;
optbeta(Dxopt>Dzopt) = optbetax(Dxopt>Dzopt);
Dopt(Dxopt>Dzopt) = Dxopt(Dxopt>Dzopt);

%Compute coverage efficiecy
etac = [];
for Gmin=Gminref
    etac = [etac sum(sum(Dopt>Gmin))/numel(Dopt)];
end

%Plot the results
figure (1);
hold on
plot(Gminref,etac, 'r')
xlabel('Minimum Received Gain (dBi)')
ylabel('Coverage Efficiency')
```

```
figure;
pcolor(phi,theta,(10*log10(Dopt)))
shading INTERP
colorbar
caxis([-20 10])
colormap('jet')
set(gca,'YDir','Reverse')
xlabel('phi (º)')
ylabel('theta (º)')
```